Developing *In Vitro* Multi Co-Culture Models and Analysis Tools for Muscle Regeneration

by

Colin Venter

Submitted in fulfilment of the academic requirements of

Doctor of Philosophy

In Biochemistry

School of Life Sciences

College of Agriculture, Engineering and Science

University of KwaZulu-Natal

Pietermaritzburg

South Africa

August 2019

PREFACE

The research contained in this thesis was completed by the candidate while based in the Discipline of Biochemistry, School of Life Sciences of the College of Agriculture, Engineering and Science, University of KwaZulu-Natal, Pietermaritzburg, South Africa. The research was financially supported by the National Research Foundation.

The contents of this work have not been submitted in any form to another university and, except where the work of others is acknowledged in the text, the results reported are due to investigations by the candidate.

_____

Signed: Prof. C. U. Niesler

Date: 29/08/2019

DECLARATION 1: PLAGIARISM

I, Colin Venter, declare that:

(i) the research reported in this thesis, except where otherwise indicated or acknowledged, is my original work;

(ii) this thesis has not been submitted in full or in part for any degree or examination to any other university;

(iii) this thesis does not contain other persons' data, pictures, graphs or other information, unless specifically acknowledged as being sourced from other persons;

(iv) this thesis does not contain other persons' writing, unless specifically acknowledged as being sourced from other researchers. Where other written sources have been quoted, then:

a) their words have been re-written but the general information attributed to them has been referenced;

b) where their exact words have been used, their writing has been placed inside quotation marks, and referenced;

(v) where I have used material for which publications followed, I have indicated in detail my role in the work;

(vi) this thesis is primarily a collection of material, prepared by myself, published as journal articles or presented as a poster and oral presentations at conferences. In some cases, additional material has been included;

(vii) this thesis does not contain text, graphics or tables copied and pasted from the Internet, unless specifically acknowledged, and the source being detailed in the thesis and in the References sections.

Signed: Colin Venter

Date: 29/08/2019

DECLARATION 2: PUBLICATIONS

The * indicates corresponding author.

1. Venter and Niesler* (2019). Rapid quantification of cellular proliferation and migration using ImageJ. *BioTechniques* 66 (2), 99-102
2. Venter and Niesler* (2018). A triple co-culture method to investigate the effect of macrophages and fibroblasts on myoblast proliferation and migration. *BioTechniques* 64, 52-58
3. Venter and Niesler* (2018). Cellular alignment and fusion: Quantifying the effect of macrophages and fibroblasts on myoblast terminal differentiation. *Experimental Cell Research* 370 (2), 542-550

Colin Venter designed the experiments, executed the laboratory work as well as compiled and revised the manuscript.

Prof. Niesler advised on experimental design and data analysis, provided funding and revised the manuscript during its preparation

Signed: Colin Venter

Date: 29/08/2019

ABSTRACT

Skeletal muscle regeneration represents a complex process mediated by non-myogenic cell types. These cells, such as macrophages and fibroblasts, display a range of interactions with muscle stem cells (myoblasts) during myogenesis (the differentiation and fusion of myoblasts into muscle fibres). Our knowledge of these interactions has been elucidated using *in vivo* and *in vitro* skeletal muscle models. Although *in vivo* models are more physiologically relevant, *in vitro* models, such as co-culture, offer a simpler and cost-effective means to study muscle regeneration. We therefore developed a novel and inexpensive co-culture method using three different cells types, which closely resembled the *in vivo* microenvironment by permitting a range of cellular interactions. Once this method was established, cellular behaviour in response to various experimental conditions could be evaluated. A second challenge we encountered was that the strategies available to us for assessing myogenesis *in vitro* were suboptimal in terms of speed and accuracy. We therefore sought to optimize image processing methods to rapidly and accurately quantify cellular numbers (proliferation), wound area (migration) and orientation (alignment) in our co-culture model. We then used these methods to evaluate the roles of macrophages and/or fibroblasts during the early (proliferation and migration) and late (alignment and fusion) stages of myogenesis.

We observed a significant increase in myoblast proliferation and migration in response to co-culture with either unstimulated macrophages or fibroblasts. In triple co-culture, macrophages continued to promote myoblast proliferation in the presence of fibroblasts. However, the presence of macrophages abrogated the positive effect of fibroblasts on myoblast migration; qualitative analysis also suggested a decrease in fibroblast number. Following analysis of later differentiation, we found that macrophages significantly promoted alignment, but prevented fusion, in a cell density-dependent manner. Fibroblasts, on the other hand, had no significant effect on myoblast alignment, but either promoted (at low fibroblast numbers) or inhibited (at higher fibroblast numbers) fusion. In triple co-culture, the effect of macrophages on myoblast alignment and fusion was unaltered by the additional presence of fibroblasts.

In order to determine whether pro-macrophages have a direct quantitative effect on fibroblast number, M1 macrophages were generated following incubation with LPS and then co-cultured with a fibroblast population. The latter population was characterised as containing both fibroblasts and their differentiated counterpart, myofibroblasts. A significant decrease in

the size of this population (potentially as a result of cell death) was observed in response to M1 macrophages; this decrease was prevented by the addition of LY294002, a phosphoinositide 3-kinase (PI3K) inhibitor. Subsequent analysis demonstrated that LY294002 decreases macrophage numbers, suggesting a potential mechanism for the rescue of the fibroblast population by this inhibitor. Dexamethasone, on the other hand, caused the fibroblast population to acquire a rounder myofibroblast morphology, but the implications of this morphological change requires further investigation.

In this thesis, we presented optimized and novel methods which were used to study skeletal muscle regeneration *in vitro*. The findings provided new insights into the temporal regulation of myogenesis by non-myogenic cells. During the early stages of myogenesis, macrophages need to increase in number to promote myoblast proliferation, but subsequently resolve with an increase in fibroblast numbers to promote myoblast migration into the wound. During the later stages of myogenesis, macrophage and fibroblast numbers need to subside to promote myoblast alignment and fusion, respectively. The communication between these non-myogenic cells and the phenotypes they acquire can also indirectly influence myogenesis. The fibroblast population is important for promoting myoblast fusion, but macrophages with an M1 phenotype resulted in death of myofibroblasts. This makes it imperative that the population of M1 macrophages timeously subsides. However, M1 macrophage-mediated death of myofibroblasts was prevented by inhibition of the PI3K pathway which resulted in macrophage, but not myofibroblast, death. This suggests a potential therapeutic target for the treatment of muscle diseases, such as myositis, caused by the dysregulated presence of macrophages.

ACKNOWLEDGMENTS

I'd like to give special thanks to some of the people in my life that I wouldn't have been able to do this mountain of work without:

Prof. Niesler, thank you for providing me with guidance and keeping me centred in my moments of panic. This was a long and difficult journey and I couldn't have done it without you.

Papa en Julie, you still may not know exactly what I do, but I couldn't have gotten this far without you. Baie dankie vir alles.

Mom, Brian and Chané, thank you for keeping me sane during all the hard work and making me take breaks to relax.

Cait and the Strydom family (including Brent), I cannot express how thankful I am for welcoming me into your home. A great deal of this work was done with your support.

Tracey, thank you for providing me with the means and encouragement to cross the finish line. Your pep talks helped so much in those difficult moments.

TABLE OF CONTENTS

Page

LIST OF TABLES

Table **Page**

LIST OF FIGURES

Figure **Page**

CHAPTER 1: INTRODUCTION

Rationale for the Research

Skeletal muscle tissue is responsible for all voluntary movement in the body, but the contractile functionality is periodically impaired by damage as a result of injury and disease [1,2]. Regeneration occurs to restore the wounded tissue; this represents a complex process involving a myriad of cellular and molecular events in the muscle microenvironment, but the precise mechanisms require elucidation [3]. Gaining a comprehensive understanding of these mechanisms is essential for developing therapeutic strategies, such as regenerative medicine and tissue engineering, to effectively mediate muscle wound repair and treat muscle disease [4,5].

Successful regeneration is dependent on the coordinated interactions between non-myogenic and myogenic cells via an array of interactions [6]. Non-myogenic cells, such macrophages and fibroblasts, have been shown to be essential for wound repair, but it is unclear exactly how these cells affect and mediate muscle cell behaviour during regeneration [7,8]. Several *in vitro* methods have been developed and used to model *in vivo* muscle regeneration; these methods largely differ in the range of interactions, such as cell-cell, cell-soluble factor and cell-matrix factor, which they permit. However, since *in vitro* models aim to mimic the *in vivo* microenvironment as closely as possible, it is important to establish *in vitro* models which permit the range of interactions observed *in vivo*.

During normal wound repair, macrophages and fibroblasts typically acquire regulated phenotypical changes which exhibit different effects on muscle cells. Macrophages initially acquire a pro-inflammatory (M1) phenotype which promotes myoblast proliferation and inhibits apoptosis, but later acquire an anti-inflammatory (M2) phenotype to promote myoblast differentiation and fusion [9,10]. Fibroblasts are initially present as quiescent cells which become activated by M2 macrophages to differentiate into myofibroblasts that reform the extracellular matrix (ECM) surrounding myofibers and promote myoblast fusion [11]. In muscle diseases, however, aberrant communication results in dysregulated phenotypes. Pathophysiological fibrosis, for example, is a consequence of a sustained presence of M2 macrophages upregulating the deposition of matrix factors by myofibroblasts [11,12]. Other diseases, such as myositis, are characterized by an upregulated presence of pro-inflammatory

cells and impaired muscle regeneration, but the effect on the fibroblast population remains unclear [13,14].

Aims and Objectives

Skeletal muscle regeneration is mediated by an array of non-myogenic cells, such as macrophages and fibroblasts, which interact with myogenic cells during muscle regeneration [6]. In the current study, we first aimed to evaluate the effect of macrophages and/or fibroblasts on the behaviour of myoblasts *in vitro*. Within this aim, our first objective was to optimize methods to rapidly and accurately quantify cell numbers and wound area. The second objective was to develop a novel *in vitro* co-culture assay that closely mimicked the *in vivo* microenvironment by permitting cell-cell contact and signalling via soluble factors. The third objective was to optimize a method to rapidly quantify myoblast/myotube alignment. The final objective was to determine the effects of macrophages and/or fibroblasts on myoblast proliferation, migration, alignment and fusion.

Incorrect communication between non-myogenic cells, such as macrophages and fibroblasts, often results in muscle disease [12]. The effect of a pro-inflammatory microenvironment on the population fibroblasts in muscle disease, such as myositis, is less understood compared to anti-inflammatory conditions. Therefore, our second aim was to evaluate the effect of pro-inflammatory (M1) macrophages on the population of fibroblasts/myofibroblasts in a muscle regenerative *in vitro* microenvironment. Here, the first objective was to phenotypically characterize the population of fibroblasts and macrophages under standardized culture conditions. The second objective was then to evaluate the effect of M1 macrophages on fibroblast/myofibroblast numbers. The final objective was to determine the mechanism of action of M1 macrophage-mediated cell death on this fibroblast population.

Outline of Thesis Structure

Chapter 2 is a review which focuses on known interactions between non-myogenic cells, particularly macrophages and fibroblasts, and myogenic cells. This chapter also focuses on the available methods to generate *in vitro* muscle models using various mono-culture and co-culture systems as wells as methods to study cellular behaviours and signalling during myogenesis.

Chapter 3 is a benchmark paper that addresses the first objective of the first aim. This paper describes optimized methods we have developed to rapidly and accurately quantify cell numbers and wound area using ImageJ.

Chapter 4 is a research article that addresses the second and fourth objective of the first aim. This paper describes a novel *in vitro* co-culture method that we used to evaluate the effect of macrophages and/or fibroblasts on myoblast proliferation and migration.

Chapter 5 is a research article that addresses the third and fourth aim. This paper describes an optimized method to determine myoblast/myotube orientation to quantify alignment which we used, in conjunction with our novel co-culture method, to evaluate the effect of macrophages and/or fibroblasts on myoblast alignment and fusion.

Chapter 6 address the objectives in the second aim. This chapter focuses on the characterization of macrophages and (myo)fibroblasts, the effect of M1 macrophages on proto-myofibroblasts, and the mechanism of M1 macrophage-mediated proto-myofibroblast cell death.

Chapter 7 provides concluding remarks and recommendations for future work.

References

1. Bentzinger CF, Wang YX, Rudnicki MA. Building muscle: molecular regulation of myogenesis. *Cold Spring Harb Perspect Biol*, 4(2), pii: a008342 (2012).
2. Frontera WR, Ochala J. Skeletal muscle: a brief review of structure and function. *Calcif Tissue Int*, 96(3), 183-195 (2015).
3. Karalaki M, Fili S, Philippou A, Koutsilieris M. Muscle regeneration: cellular and molecular events. *In Vivo*, 23(5), 779-796 (2009).
4. Ostrovidov S, Hosseini V, Ahadian S *et al.* Skeletal muscle tissue engineering: methods to form skeletal myotubes and their applications. *Tissue Eng Part B Rev*, 20(5), 403-436 (2014).
5. Baoge L, Van Den Steen E, Rimbaut S *et al.* Treatment of skeletal muscle injury: a review. *ISRN Orthop*, 2012, 689012 (2012).
6. Bentzinger CF, Wang YX, Dumont NA, Rudnicki MA. Cellular dynamics in the muscle satellite cell niche. *EMBO Rep*, 14(12), 1062-1072 (2013).
7. Liu X, Liu Y, Zhao L, Zeng Z, Xiao W, Chen P. Macrophage depletion impairs skeletal muscle regeneration: The roles of regulatory factors for muscle regeneration. *Cell Biol Int*, 41(3), 228-238 (2017).
8. Murphy MM, Lawson JA, Mathew SJ, Hutcheson DA, Kardon G. Satellite cells, connective tissue fibroblasts and their interactions are crucial for muscle regeneration. *Development*, 138(17), 3625-3637 (2011).

9. Arnold L, Henry A, Poron F *et al.* Inflammatory monocytes recruited after skeletal muscle injury switch into antiinflammatory macrophages to support myogenesis. *J Exp Med*, 204(5), 1057-1069 (2007).
10. Sonnet C, Lafuste P, Arnold L *et al.* Human macrophages rescue myoblasts and myotubes from apoptosis through a set of adhesion molecular systems. *J Cell Sci*, 119(Pt 12), 2497-2507 (2006).
11. Chapman MA, Meza R, Lieber RL. Skeletal muscle fibroblasts in health and disease. *Differentiation*, 92(3), 108-115 (2016).
12. Mann CJ, Perdiguero E, Kharraz Y *et al.* Aberrant repair and fibrosis development in skeletal muscle. *Skelet Muscle*, 1(1), 21 (2011).
13. Villalta SA, Nguyen HX, Deng B, Gotoh T, Tidball JG. Shifts in macrophage phenotypes and macrophage competition for arginine metabolism affect the severity of muscle pathology in muscular dystrophy. *Hum Mol Genet*, 18(3), 482-496 (2009).
14. Loell I, Lundberg IE. Can muscle regeneration fail in chronic inflammation: a weakness in inflammatory myopathies? *J Intern Med*, 269(3), 243-257 (2011).

CHAPTER 2: MYOGENESIS IN A DISH: A GUIDE TO GENERATING *IN VITRO* SKELETAL MUSCLE MODELS AND STUDYING MYOGENESIS

Venter C, Niesler CU*

Discipline of Biochemistry, School of Life Sciences, University of KwaZulu-Natal, Private Bag X01, Scottsville 3209, South Africa

**Corresponding author: Prof C.U. Niesler, Tel: (033) 260 5465, Fax: (033) 260 6127, email: niesler@ukzn.ac.za*

In preparation for submission to: *BioTechniques*

Abstract

Following severe muscle injury, muscle stem cells (myoblasts) are stimulated to repair the damaged tissue. This process, known as myogenesis, is regulated by non-myogenic cells, such as macrophages and fibroblasts, which initially promote the proliferation and migration of myoblasts into the wound and subsequently promote the alignment and fusion of these muscle cells into regenerated muscle fibres. Regulation of myogenesis has previously been evaluated using various *in vivo* and *in vitro* experimental models. While *in vivo* models are more physiologically relevant, *in vitro* models have been useful to understand the precise regulatory mechanisms of non-myogenic cells on myogenesis. In this review, we describe the methods used to model the cellular interactions *in vitro* as well as the methods used to assess cellular behaviours and mechanisms during myogenesis.

Keywords: myogenesis, myoblasts, non-myogenic cells, *in vitro* models

Introduction

Skeletal muscle wound repair is a well-coordinated process regulated by non-myogenic cells, such as macrophages and fibroblasts, which modulate the behaviour of muscle cells [1]. Macrophages are crucial during wound repair as they secrete factors which mediate the myogenic process in muscle precursor cells. Fibroblasts also regulate satellite cell behaviour, but additionally form and maintain the surrounding connective tissue which supports muscle contraction and regenerating muscle fibres [1,2]. It is necessary to better understand the communication between non-myogenic and myogenic cells in order to improve wound repair strategies following muscle injury [2].

Much of our understanding of these relationships is derived from *in vivo* experimental models [3,4]. *In vivo* studies typically use small animal models to emulate disease, injury and repair processes observed in humans in order to study cellular interactions [5,6]. The crucial role of specific cells in muscle wound repair is commonly demonstrated using depletion methods. For instance, the ablation of satellite cells leads to a complete loss in regenerative capability of skeletal muscle following injury, while the depletion of macrophages or fibroblasts impairs regeneration in this tissue [7-10]. Transplantation of satellite cells *in vivo* has, despite poor survival and migration, been shown to promote regeneration when injected in dystrophic muscle [11-13]. This regenerative capacity is further enhanced when co-transplanted with macrophages which may be related to their promotion of myoblast survival, expansion and migration [14,15]. The interaction of satellite cells, macrophages and fibroblasts is therefore essential for effective skeletal muscle wound repair; however, the mechanism of intercellular communication is unclear.

In vivo models have also provided significant insight and offer an accurate and a relevant means to study the interactions between cell types, but they are often subject to ethical constraints, complex methodology and multi-parameter variables [16,17]. *In vitro* systems overcome the challenges of *in vivo* models by offering a simpler, cost-effective and high-throughput approach to not only mimic the *in vivo* environment, but also to pinpoint precise interactions between cell types, free from the complexity associated with *in vivo* experimentation [4,16]. Although *in vitro* models risk over-simplification by examining a limited scope of interactions and less accurately representing the in vivo environment, their advantages mean that they are extensively used [16].

Numerous *in vitro* systems have previously been developed to represent an isolated model to study the physiology, pathology and regeneration of skeletal muscle. Here, we review these systems used to model myogenesis and describe commonly used techniques to study the interaction of non-myogenic cells (such as macrophages and fibroblasts) with myogenic progenitor cells during key regenerative processes.

Skeletal Muscle Wound Repair

Skeletal muscle wound repair represents a complex process involving the sequential and overlapping stages of degeneration, inflammation and regeneration, and includes multiple cell types (Figure 1) [18,19]. Upon severe muscle injury, degeneration occurs as proteases, released by damaged cells into the wound, necrotize the surrounding tissue; this stimulates an inflammatory response [18]. During inflammation, cells such as neutrophils, monocytes and macrophages initially remove cellular debris by phagocytosis [20]. Macrophages then become activated to acquire a pro-inflammatory (M1) phenotype, via T-helper (Th) 1 cells, to promote the activation of quiescent satellite cells to myoblasts and the subsequent expansion of these muscle stem cells [21-23]. As wound repair progresses to regeneration, the Th2 cells stimulate M1 macrophages to acquire an anti-inflammatory (M2) phenotype; the M2 macrophages stimulate the migration, alignment and subsequent fusion of myoblasts into multinucleated myofibres [23,24]. Anti-inflammatory macrophages also stimulate the differentiation of fibroblasts into proliferative myofibroblasts which deposit and remodel the surrounding extracellular matrix (ECM) [25-28].

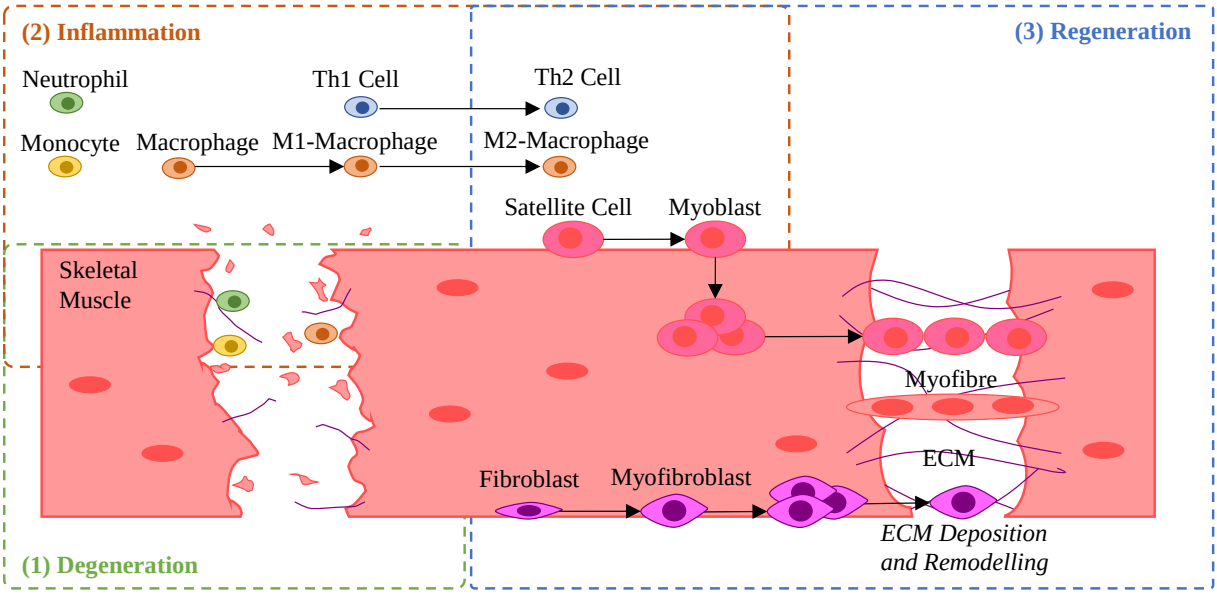

Figure 1: Overview of skeletal muscle wound healing. (1) Degeneration occurs upon severe muscle injury and results in necrosis of the surrounding tissue. (2) Inflammation follows where neutrophils, monocytes and macrophages enter the wound and phagocytose necrotic the tissue; T-helper (Th) 1 cells stimulate macrophages to acquire a pro-inflammatory (M1) phenotype which activate quiescent satellite cells to myoblasts and promote their expansion. (3) Regeneration ensues and Th2 cells stimulate M1 macrophages to acquire an anti-inflammatory (M2) phenotype which subsequently stimulate myoblast migration and alignment in the wound followed by fusion into multinucleated myofibres. M2 macrophages also stimulate the differentiation of fibroblasts into myofibroblasts which proliferate to deposit and remodel the extracellular matrix (ECM) [Constructed with reference to Forbes and Rosenthal, 2014].

Intercellular communication between the various cell types during muscle wound repair involves a multitude of signalling interactions (Table 1). Macrophages are activated by Th1 cell-secreted cytokines (e.g. tumour necrosis factor (TNF)-α and interferon (IFN)-γ) to acquire the M1 phenotype [21,22]. Pro-inflammatory macrophages express and secrete enzymes, such as inducible nitric oxide synthase (iNOS) (which catalyses the production of nitric oxide (NO)) and matrix-degrading matrix metalloproteinases (MMPs) [30,31]. These enzymes release matrix-bound hepatocyte growth factor (HGF), a crucial factor for the activation of quiescent satellite cells to myoblasts [19]. Pro-inflammatory macrophages also secrete a myriad of growth factors and cytokines, such as TNF-α, interleukin (IL)-1β and IL-6, which regulate myoblast proliferation, migration and differentiation [23,32,33]. Moreover, M1 macrophages mediate anti-apoptotic effects on myoblasts and their differentiated myofibres through direct cell-cell contacts via vascular cell adhesion molecule/ very late antigen-4 (VCAM-1/VLA-4), intercellular cell adhesion molecule-1/ leukocyte function

associated molecule-1 (ICAM-1/LFA-1), CXCL1/CX3CR1 and platelet-endothelial cell adhesion molecule-1 (PECAM-1)/ PECAM-1. These cell-cell interactions potentially activate survival signalling pathways, such as mitogen-activated protein kinases (MAPK), phosphatidylinositol 3-kinase (PI3K) and serine/threonine protein kinase (PKB/Akt) [34].

Table 1: Intercellular communication between activating and target cells.

Activating Cell	Known Mediator(s)	Target Cell	Effect on Target Cell	Reference
Th1 Cells	TNF-α; IFN-γ	M0 Macrophages	Activated to M1 macrophage	[21, 22]
M1 Macrophages	iNOS/NO/HGF; MMP/HGF	Satellite Cells	Activated to myoblasts	[19, 30, 31]
	TNF-α; IL-1β; IL-6	Myoblasts	↑ Proliferation; ↓ Migration; ↓ Differentiation	[23, 32, 33]
	VCAM-1/VLA-4; ICAM-1/LFA-1; CXCL1/CXCR1; PECAM-1/PECAM-1	Myoblasts and Myotubes	↓ Apoptosis	[34]
	Unknown	Fibroblasts	↑ IL-6, CCL2, MMPs; ↓ Collagen	[35]
Th2 Cells	IL-4, -10, -13	M1 Macrophages	Activation to M2 macrophages	[39, 40]
M2 Macrophages	TGF-β; IL-10	Myoblasts	↑ Migration, alignment, fusion	[23, 24, 45]
	TGF-β	Fibroblasts	Differentiation to myofibroblasts	[25-37]
Fibroblasts	COX-2/PGE_2	M1 Macrophages	↓ TNF-α and MIP-1α	[37, 38]
Myofibroblasts	Unknown FGF-2	Myoblasts	↑ Migration; ↓ Apoptosis; ↓ & ↑ Fusion; ↑ Alignment	[44-48]

Activating cells are recruited during wound repair and facilitate regeneration by signalling to target cells. Known signalling mediators are listed as well as the effects, such as the up- (↑) or down-regulation (↓), on various cell behaviours.

Pro-inflammatory macrophages also interact with fibroblasts and regulate their matrix-degrading behaviour by secreting factors which upregulate fibroblast expression of pro-

inflammatory genes (e.g. IL-6 and chemokine ligand 2 (CCL2)) and the production of MMPs (e.g. MMP-1 and -3), while decreasing the production of collagen (e.g. collagen I and III) [35]. Unstimulated (M0) macrophages have been shown to directly interact with fibroblasts via ICAM-1 to increase the production of the pro-inflammatory chemokine macrophage inflammatory protein (MIP)-1α [36]. In contrast, fibroblast-secreted factors (e.g. prostaglandin E_2 (PGE_2)) have been shown to decrease the production of pro-inflammatory factors (e.g. TNF-α and MIP-1α) by M1 macrophages in a cyclooxygenase (COX)-2 dependent manner [37,38].

As wound repair progresses, M1 macrophages phagocytose apoptotic neutrophils, which stimulates the switch to an M2 phenotype; this is augmented by Th2 secreted cytokines (e.g. IL-4, IL-10 and IL-13) [39,40]. Anti-inflammatory macrophages attenuate the initial pro-inflammatory response by secreting factors, such as transforming growth factor (TGF)-β and IL-10. These cells and cytokines regulate migration, alignment, and fusion of mono-nucleated myoblasts to form multinucleated myofibres [23,24,41]. Anti-inflammatory macrophages also stimulate the differentiation of fibroblasts into myofibroblasts in a TGF-β-dependent manner [25-27].

Myofibroblasts are primarily involved in the remodelling and maintenance of connective tissue surrounding skeletal muscle [28]. These cells secrete growth and ECM factors (such as fibroblast growth factor (FGF-2), collagen, fibronectin and laminin) which provide various cues that mediate muscle cell behaviour [42-44]. Myofibroblast-secreted factors have been shown to promote myoblast migration and prevent apoptosis of differentiating myoblasts [45-47], but have also displayed opposing effects on myoblast fusion depending on their density [44,48]. These connective tissue cells have been shown to promote the alignment of myoblasts in both a cell contact-dependent and FGF-2-dependent manner; in contrast, our studies suggest that they do not significantly influence myoblast alignment [41,44]. This may have been due to differences in the *in vitro* models, such as the cell lines used. Myofibroblasts also deposit the ECM that surrounds and physically supports muscle fibres. Fibrous scaffolds (e.g. collagen) exhibit mechanical and physical features, such as orientation and rigidity, that influence myogenesis: rigid fibres promote myoblast proliferation, while softer fibres promote fusion; organized fibres promote the alignment and subsequent fusion of other myoblasts [49].

Generating *In Vitro* Skeletal Muscle Models

In vitro muscle models have extensively been used to study intercellular relationships and are aimed at delineating specific interactions that occur *in vivo*. *In vitro* models typically include the use of co-culture methods (to study paracrine and juxtacrine signalling), conditioned media (to study paracrine signalling) or cell-derived matrices (to study the effect of signalling via deposited matrix factors) [50-52]. However, there are several considerations to be made when selecting a system; these include expense, ease of operation, degree to which they mimic the *in vivo* environment, and the range of cellular interactions permitted [50].

Cell Selection

Cell selection is often the first and most crucial consideration when generating an *in vitro* model since the cell types establish the microenvironment. Species (e.g. animals versus humans), tissue type (e.g. skeletal and cardiac muscle) and pathology (e.g. normal or dystrophic muscle) must be considered. The origin and phenotype of cells are also crucial: cells can be derived from tissues (primary cells), while some are available as cell lines [53]; it is important to keep in mind that cells, particularly primary cultures, can acquire different phenotypes over time depending on the experimental conditions [54-56].

Primary cells are derived from disaggregated tissue explants, which make them somewhat similar to cells *in vivo*; they are preferred to cell lines as they may provide more accurate and relevant data during experimentation [53]. However, isolation of primary cells requires ethical approval, while reproducibility can be hampered by donor-to-donor variation and is limited by lower proliferative abilities than cell lines, therefore requiring multiple isolations [57,58]. Secondary cells (cell lines) are immortalized (via genetic manipulation or through long-term cell culture) which permits easy and indefinite cell culture (usually without special culture conditions e.g. added cytokines) to inexpensively to produce large cell numbers [53]. Numerous cell lines are commercially available from cell banks such as American Type Culture Collection (ATCC)® (www.atcc.org). Macrophages (e.g. J774a.1 and RAW 264.7 cells), fibroblasts (e.g. NIH/3T3, NOR-10 and LMTK cells) and myoblasts (e.g. C2C12 and L6 cells) have been used in muscle models *in vitro* [32,44,45,56,59]. Cell lines represent a pure population and are therefore able to yield reproducible results; however, phenotypic and genotypic variations between cell lines and primary cells may result in disparate experimental results [16,58,60].

In vitro phenotypes can be regulated by modifying the culture conditions of cells. For instance, macrophages ($F4/80^+$ and $CD11b^+$) can be stimulated to acquire a pro-inflammatory phenotype ($CD64^+CD80^+$) via the addition of lipopolysaccharide (LPS), TNF-α and/or IFN-γ, while an M2 phenotype ($CD209^+$) can be achieved via addition of IL-4, IL-10 and/or dexamethasone [23,54,61]. Myofibroblasts and fibroblasts (both $Tcf4^+$) represent an interchangeable population of cells: fibroblasts (α-smooth muscle actin $(SMA)^-$) differentiate to myofibroblasts (α-SMA^+) in response to serum or TGF-β and have been reported to de-differentiate back to fibroblasts in the absence of these stimuli [10,62]. However, studies often do not distinguish between the two phenotypes; the term "fibroblast" is used indiscriminately to describe both populations. This represents a challenge when interpreting the literature as each phenotype behaves differently and provides a distinct contribution during wound repair [46,48,55,59]. Lastly, mononucleated myoblasts ($Myf5^+MyoD^+$) can be switched from conditions which promote proliferation, such as high serum and/or FGF-2, and then switched from conditions which promote proliferation, such as high serum and/or FGF-2, to conditions that promote differentiation and fusion, such as low serum, into multinucleated myotubes which are myosin heavy chain $(MHC)^+$ and muscle creatine kinase $(MCK)^+$ [56,63,64].

Mono-Culture Systems

Individual cell types can be plated as a mono-culture to evaluate the effects of various proteins on cell behaviour (Figure 2A). Numerous signalling and matrix proteins are available as commercial products, such as recombinantly expressed TGF-β or purified tail collagen isolates. The advantage of using such commercial products is that they can be used to accurately study the effects of single proteins on cell behaviour. These isolates are therefore useful in understanding the *in vitro* mechanism of action on cell behaviour, but may not be a true reflection of the environment due to discrepancy between *in vivo* and *in vitro* concentrations [17].

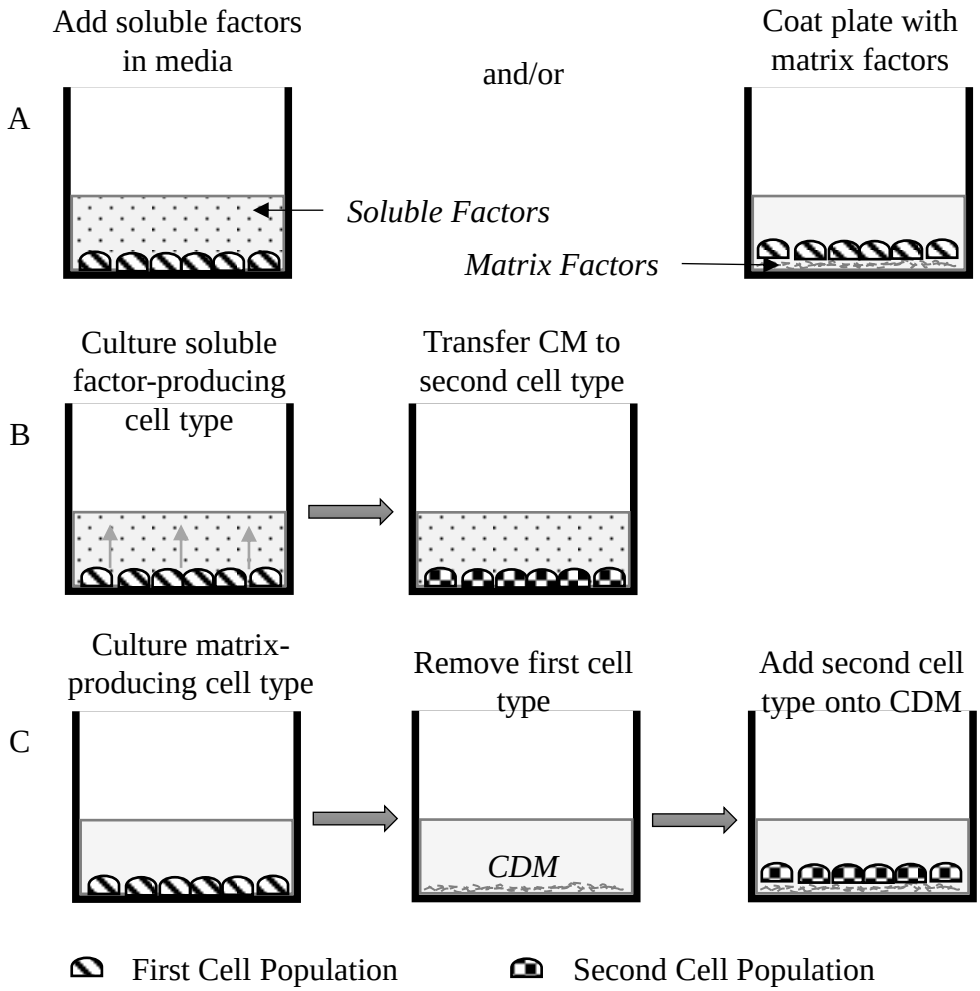

Figure 2: Methods to generate mono-culture systems.
(A) commercial products of recombinant soluble factors can be added to the culture media and/or purified matrix factors can be coated onto a multi-well plate. (B) Conditioned media (CM) is generated by culturing cells in media and transferring the CM to a second cell type. (C) Cell-derived matrices (CDM) are generated by culturing cells on a multi-well plate and subsequently removing the cells prior to adding another cell type on top of the CDM.

Cells produce a myriad of proteins and these profiles vary depending on the cell type and its role in wound repair. Therefore, it becomes more physiologically relevant to collectively assess the effects of all factors on cell behaviour. Conditioned media (CM) and cell-derived matrices (CDM) can be generated to study the roles of secreted soluble and deposited insoluble factors, respectively. Conditioned media (Figure 2B) is generated by culturing a cell type in media which becomes "conditioned" with the cell secretome which includes various soluble growth factors, cytokines, chemokines and enzymes. The second cell type is then cultured in the presence of the CM [51,65]. Conditioned media is typically generated under

serum-free conditions to prevent masking of any effects by the myriad of proteins present in serum [65]. However, the absence of serum may impair cell growth and therefore such media may need supplementation [51]. Finally, proteins are often secreted at very low levels and may need to be concentrated [66].

Cell-derived matrices (Figure 2C) are created by culturing a confluent monolayer of matrix-producing cells, such as fibroblasts or endothelial cells, in flasks or multi-well plates for an extended period. Cells are then removed (via physical, chemical or enzymatic methods) leaving behind the CDM on which other cell populations can subsequently be cultured on [52]. The physical and chemical properties of CDMs can be customized as the matrix generated depends on the cell type and the conditions they are cultured in. For example, culturing cells under shear stress conditions results in the deposition of more organized and aligned matrices [67]; while adding factors such as ascorbic acid increases collagen levels, and epidermal growth factor (EGF) or FGF-2 increases matrix production and thickness [68].

Co-Culture Systems

Co-culture systems represent an *in vitro* model where two or more distinct cell types are cultured together in a common environment in order to study intercellular communication [50]. Co-culture systems are utilized in two forms: those that allow direct contact between cell types (direct co-culture) and those that physically separate cells but permit paracrine signalling (indirect co-culture) [45,46,69]. Direct co-culture is often easier to perform and permits a range of interactions present *in vivo*; indirect co-culture systems often require additional equipment and are dependent on the diffusion rates of secreted factors [50]. Despite the inherent advantages and disadvantages of direct versus indirect co-culture, simultaneous use of both systems may elucidate whether or not direct cell contacts between cell types regulate behaviour [16,69,70].

The simplest method of direct co-culture is to plate different cell types together as a mixed cell population (Figure 3Ai) or plate one cell type over a confluent layer of another (Figure 3Aii) [33,48,51]. This approach of mixing or layering cell populations (at different ratios) is an easy and inexpensive method of co-culture that does not require any specialized equipment and maximizes intercellular communication [51]. However, it is difficult to distinguish between cell types during analysis. Analysing the effects of one cell type on the behaviour of

another (e.g. apoptosis, proliferation and differentiation) therefore requires specific antibodies coupled with confocal microscopy and/or flow cytometry when using this approach [48,70,71].

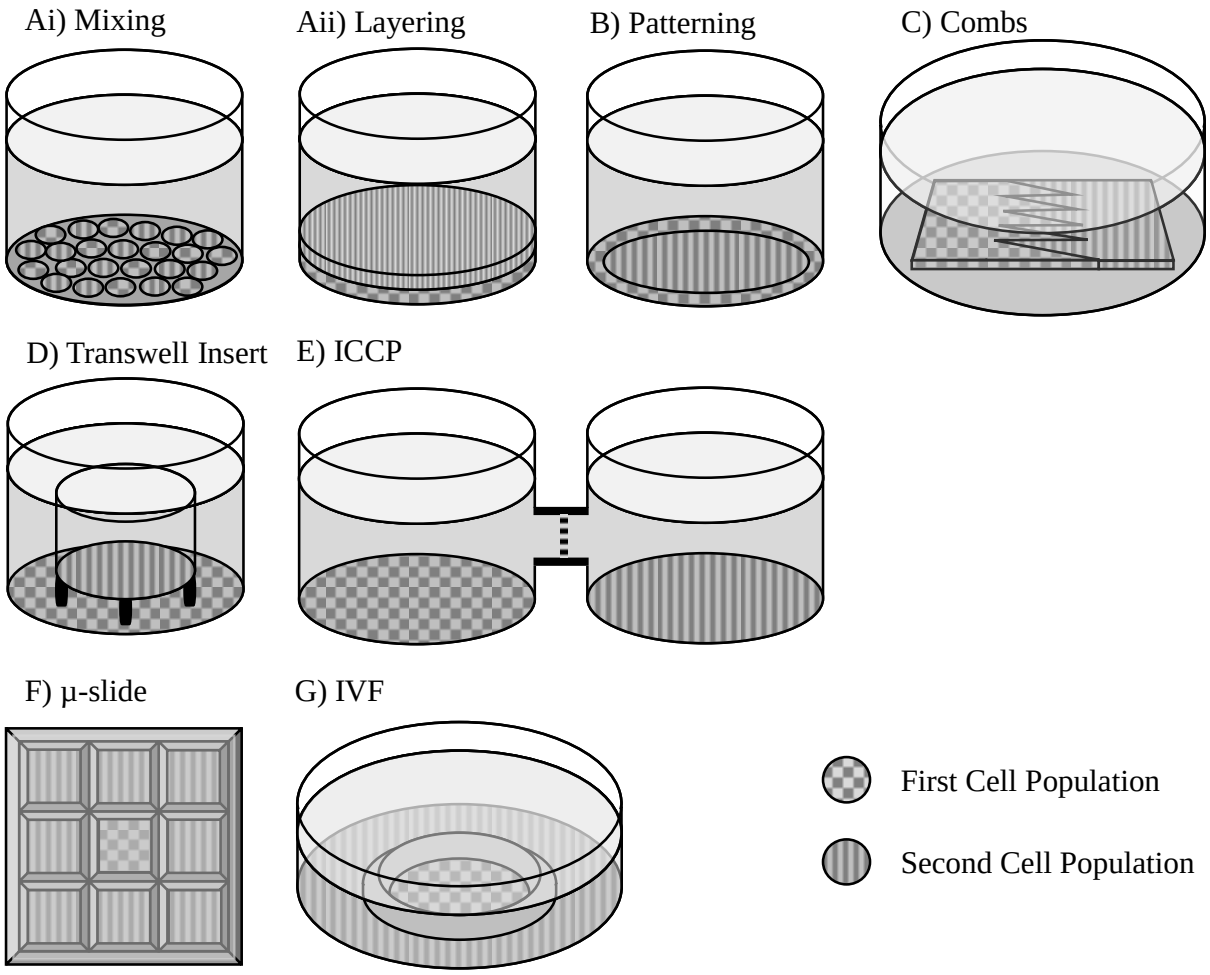

Figure 3: Methods to generate co-culture systems.
Cells can be cultured together by (A) mixing/layering cells, (B) cellular patterning, (C) interlocking combs, (D) transwell inserts, (D) interactive co-culture plate (ICCP), (F) µ-slide co-culture wells and (G) *in vitro* fertilization (IVF) plates.

Cellular patterning can be used to spatially control the adherence of different cell types [50]. Several patterning techniques are available such as using physical (e.g. stencils [72]) or chemical (e.g. bovine serum albumin (BSA) [73]) barriers to exclude cells from a certain area and prevent attachment. The first cell type adheres to the area surrounding the barrier, the barrier is then removed (by physical removal or by coating the cell repellent area with an adhesive matrix factor), and the second cell type is added which adheres to the remaining space. We have created a cellular patterning co-culture technique (Figure 3B) without the

need of barriers and corresponding additional reagents/equipment [45]. This method is simply performed by plating the first cell type on the outer edge of a culture well followed by incubation to promote adherence; the second cell type is added which then adheres to the centre. Cells are therefore separate but are still permitted to interact by cell-cell contact to some extent. Co-culture by patterning does usually not need specialized equipment and creating distinct cell populations makes it easier to analyse cell behaviours without the need to identify cell types.

Hui and Bhatia (2006) have previously developed a co-culture system to mechanically control cell-cell interactions; this method employs a pair of interlocking silicon combs (Figure 2C), where one cell type is plated on the female half and another on the male half [74]. The combs can be completely interlocked for direct cell-cell contact between the cell types or slightly separated to prevent direct contact and only permit paracrine signalling via indirect co-culture. The disadvantages of this method include: the combs (which are currently not commercially available) need to be coated with matrix proteins (e.g. collagen); there is no control on the ratio of cell numbers and requires confluence to effectively allow direct cell-cell contacts.

The most common method of indirect co-culture is the use of a Corning® Transwell® insert (www.corning.com) (or other commercially available transwell inserts) (Figure 3D) containing a microporous membrane (ranging from 0.4 and 8μm in diameter) that allows soluble factors, but not cells, to pass through it. One cell type is plated in the lower culture well while a second cell type is plated directly onto the membrane. A shortcoming of these inserts, however, is that adherent cells above the membrane often migrate through the pores onto the underside of the membrane [24].

The Interactive Co-Culture Plate (ICCP) (http://arb-ls.com/en/iccp) (Figure 3E) is a newly developed alternative to the transwell co-culture system and consists of two side-by-side culture wells joined by a microporous membrane. This system enables both cell types to easily be observed and analysed at the same time; this is a distinct advantage since both cell types may directly influence each other but requires more specialized and unconventional equipment. Moreover, due to the relative newness of the technology, limited studies have been performed using this method [75].

ibidi® µ-slide 2-well co-culture plate (https://ibidi.com) (Figure 2F) consists of chambers separated by dividers. Individual cell types are plated into each chamber and, once they have adhered, the slide is flooded with media to extend above the physical divisions to enable communication via soluble factors. Similarly, our laboratory has previously adapted *in vitro* fertilization (IVF) culture plates (Figure 3G) for co-culture [46]. In this method, one cell type is plated on the outer ring of the culture plate while another is plated in the centre well. Once the cells have adhered, the plate is flooded with culture media and cells are able to communicate via secreted soluble factors. The advantage of these "overflow" co-culture plates is that both cell types are on the same two-dimensional (2D) plane and can be simultaneously observed; however, communication between cell types is reliant on the amount of media used and the timeous diffusion rates of secreted factors.

Studying Myogenesis *In Vitro*

Myogenesis can be emulated *in vitro* to study the effects of specific experimental conditions on cell behaviours, such as proliferation, apoptosis, motility, alignment and fusion. There are numerous methods to study *in vitro* myogenesis but these techniques have been extensively reviewed elsewhere. Therefore, we only describe the methodological procedures (Table 2) of some of the simplest and/or popular techniques to study *in vitro* cell behaviours during myogenesis below.

Table 2: Summary of methods used to evaluate cellular behaviours of non-myogenic and myogenic cells during myogenesis.

Behaviour	Method	Reference
Proliferation & Apoptosis	Direct Cell Counts	
	• Haemocytometer/Automated Cell Counter	[76]
	• Image Counts (Brightfield/Confocal Microscopy)	[35, 77]
	• Flow Cytometer	[23, 34]
	Indirect Cell Counts	
	• Colorimetric Assay	[78, 79]
	• Chemiluminescent Assay	[34]
Motility	Scratch Assay	[77, 80]
	Chemotactic Attraction Assay	[70, 81]
Alignment	Fast Fourier Transform	[84]
	Local Intensity Gradient	[85]
	Binarization-based Extraction of Alignment Score	[86]
	ct-FIRE & Alignment Index	[45]
Fusion	Myotube Morphological Characteristics	[88]
	Fusion Index	[89]
	Myotube Density	[90, 91]

The simplest and most accessible methods used to assess proliferation, apoptosis, motility, alignment and fusion during *in vitro* myogenesis are shown.

Proliferation and Apoptosis

Proliferation is the increase in cell number as a result of growth and mitosis while apoptosis results in a decrease in cell number. Therefore, enumeration of living and/or dead cells is a useful tool to evaluate the effect of experimental conditions on these behaviours. Cell quantification may be performed using direct cell counts or approximated using colorimetric/chemiluminescent assays. Cell counts can be easily performed on suspension cells stained with trypan blue to distinguish between living (colourless) and dead (blue) cells using haemocytometers or automated cell counters [76]. Live cells can also be more accurately evaluated using the LIVE/DEAD® Viability/Cytotoxicity Kit (available https://www.thermofisher.com) which measures esterase activity and an intact plasma

membrane. Adherent cells can be resuspended and similarly counted or simply fixed, stained with histological dyes (e.g. crystal violet) and counted from brightfield microscope images [77]. However, more advanced and accurate methods, such as flow cytometry and confocal microscopy, are also available to identify cells that are fluorescently labelled for the expression of specific markers, such as Ki-67 (proliferation) or annexin V (apoptosis) [23,34,35].

Colorimetric and chemiluminescent assays can be used to approximate proliferation and apoptosis by assessing cell number, metabolism or enzyme activity. These assays generate a soluble colour (colorimetric) or fluorescent (chemiluminescent) product and the concentration of this product (which is proportional to the degree of proliferation or apoptosis) is quantified using spectrophotometry at specific absorbance or excitation/emission wavelengths. The colorimetric crystal violet assay is used to quantify DNA content of adherent cells stained with crystal violet which is then solubilized and assessed via spectrophotometry [78]. The colorimetric tetrazolium assay is used to quantify metabolism of viable cells; a tetrazolium compound (e.g. MTT) is reduced to formazan by living cells [79]. The chemiluminescent caspase-3 activity assay is used to quantify apoptosis by measuring the proteolytic cleaving ability of caspase-3 (a marker for apoptosis) for a fluorogenic substrate (e.g. Ac-DEVD-AFC) to generate a fluorescent product [34].

Motility

Motility assays, such as migration and chemotactic attraction assays, are often used to assess directional cell movement. Although there are numerous methods to model and study 2D migration *in vitro* [80], the wound healing assay (or scratch assay) is favoured owing to its simplicity, cost effectiveness and ease of analysis [81]. In this assay, a confluent layer of cells is mechanically wounded (usually with a pipette tip) to scrape cells and create a cell-free area (i.e. wound) that the surrounding cells migrate into. Microscope images of the wound are acquired at various time points, the wound area can be manually or automatically measured, and the percentage wound closure (relative to the initial wound size) calculated [77]. Wound closure is often inaccurately affected by cell proliferation, but the migration period may be limited (≤7 hours) to prevent proliferation from being a contributing factor [81].

Chemotactic attraction is the directed movement of cells towards a solubilized attractant gradient and this process is often mimicked using a transwell insert (or Boyden chamber) [80]. In this chemotactic attraction assay, like the transwell co-culture assay, a cell type is plated on top of the porous membrane while a chemoattractant or chemoattractant-producing cell is plated below the membrane. The cells are then incubated for an appropriate period (e.g. 3 hours), the cells fixed and stained, and the cells adhering to the underside of the membrane counted; the number of cells being proportional to the degree of chemotactic attraction [70].

Mechanical attraction (durotaxis) is the directed movement of cells towards a stiff substrate region from a softer region [82]. Durotaxis is typically a consequence of changes in the ECM stiffness that cells migrate along *in vivo*. To study mechanical attraction *in vitro*, hydrogels are created with different degrees of stiffness; this is determined by the concentration of the hydrogel monomers and the extent of crosslinking [82,83].

Alignment

Cellular alignment is the oriented organization of cells and is quantified by first determining cell orientation and then calculating the degree of alignment. Several methods have previously been developed to analyse collagen and/or cell alignment. The Fast Fourier Transform (FFT) [84] applies the Fourier transform algorithm to images to identify recurring patterns of collagen/cells and determines their orientation. The local intensity gradient [85] method identifies the edges of collagen/cells in images and determines their orientation. The Binarization-based Extraction of Alignment Score (BEAS) [86] distinguishes the background from the foreground (i.e. collagen/cells) from which orientation data can be extracted. However, we have recently developed a simpler method to quantify alignment. In this method, we optimized the program ct-FIRE to automatically extract orientation information from binarized microscope images [41]. Once the orientations are determined, the degree of alignment can be evaluated by calculating an alignment index (AI) [87]. An AI calculates the degree of alignment with reference to a fixed point and assigns a value between 0 (randomly oriented) and 1 (perfectly aligned). However, since cells can align independent of a fixed point of reference, we have proposed using the direction in which most cells are oriented as the point of reference [41].

Fusion

Myoblasts can fuse to form myotubes *in vitro* and the success of fusion varies can be assessed by evaluating morphological characteristics of myotubes, such as width and length, compared to a control [88]. Furthermore, a fusion index (FI) may be determined which calculates the percentage of nuclei in myotubes (with ≥3 nuclei) relative to the total number of nuclei in a field of view [89]. Myotube density has been shown to be directly proportional to the FI [90,91]. Therefore, automated image processing strategies have been developed to rapidly identify myotubes dyed with histological stains, such as LADD stain and Jenner-Giemsa stain, which stain protein-rich myotubes a darker colour than myoblasts; this allows myotubes to be easily distinguished from unfused cells [90,91].

Evaluating Cellular Signalling and Behavioural Mechanisms

Communication between myogenic and non-myogenic cells and the regulation of cellular behaviour often involves a myriad of proteins and several signal transduction pathways [34,47]. Myogenesis is regulated by the timely expression of Pax and the myogenic regulatory factors (MRFs) MyoD, Myf5, myogenin and MRF4. Quiescent satellite cells (Pax 7^+) become activated to undergo self-renewal *and* commit to differentiation as proliferating myoblasts ($Myf5^+$ and $MyoD^+$). Myoblasts later become terminally differentiated myocytes ($myogenin^+$ and MRF^+) which align and fuse into multinucleated myofibres (MHC^+ and MCK^+) [92]. Expression of these muscle cell specific genes is regulated by an array of signalling molecules (e.g. HGF and insulin-like growth factor-I (IGF-I)) and transduction pathways (e.g. Wnt, Notch and MAPK pathways) [93].

The *in vivo* mechanisms can be elucidated by generating transgenic mice which overexpress, or are deficient for, specific genes [94,95]. Alternatively, inhibitors or recombinant proteins can be administered *in vivo* [96]. The mechanism by which proteins regulate cellular behaviours during intercellular communication *in vitro* can be evaluated via the addition of monoclonal antibodies and/or inhibitors. Neutralizing antibodies bind to an antigen (e.g. cytokines) and prevent its function [44]. Blocking antibodies bind to an antigen (e.g. receptors and integrins) and prevent its interaction with any other factors (e.g. cytokines) [34]. Inhibitors can be used to specifically inhibit enzyme activity; these enzymes can be externally secreted (e.g. iNOS and its inhibitor L-NAME) [97] or internally involved in signalling transduction pathways (e.g. p38 MAPK and its inhibitor SB202190) [47].

Conclusions and Future Perspectives

Myogenesis represents a complex process involving multiple cell types and a sequence of regulated interactions. There are numerous models to study muscle regeneration *in vitro*, each with its own set of capabilities, limitations and challenges. The choice of model greatly depends on a researcher's aims and experimental requirements. In this article, we have highlighted some of the most popular and accessible methods for generating *in vitro* muscle models; we then describe some of the most commonly used methods to assess cell behaviour and mechanism of effect during myogenesis. Future studies may potentially utilize any number of these methods to further investigate the roles of non-myogenic cells on myogenesis.

Acknowledgments

The work was supported by the South African National Research Foundation, South African Medical Research Council and University of KwaZulu-Natal.

References

1. Bentzinger CF, Wang YX, Dumont NA, Rudnicki MA. Cellular dynamics in the muscle satellite cell niche. *EMBO Rep*, 14(12), 1062-1072 (2013).
2. Mann CJ, Perdiguero E, Kharraz Y *et al.* Aberrant repair and fibrosis development in skeletal muscle. *Skelet Muscle*, 1(1), 21 (2011).
3. Cornelison DD. Context matters: in vivo and in vitro influences on muscle satellite cell activity. *J Cell Biochem*, 105(3), 663-669 (2008).
4. Passey S, Martin N, Player D, Lewis MP. Stretching skeletal muscle in vitro: does it replicate in vivo physiology? *Biotechnol Lett*, 33(8), 1513-1521 (2011).
5. Collins CA, Morgan JE. Duchenne's muscular dystrophy: animal models used to investigate pathogenesis and develop therapeutic strategies. *Int J Exp Pathol*, 84(4), 165-172 (2003).
6. Ansell DM, Holden KA, Hardman MJ. Animal models of wound repair: Are they cutting it? *Exp Dermatol*, 21(8), 581-585 (2012).
7. Murphy MM, Lawson JA, Mathew SJ, Hutcheson DA, Kardon G. Satellite cells, connective tissue fibroblasts and their interactions are crucial for muscle regeneration. *Development*, 138(17), 3625-3637 (2011).
8. Summan M, Warren GL, Mercer RR *et al.* Macrophages and skeletal muscle regeneration: a clodronate-containing liposome depletion study. *Am J Physiol Regul Integr Comp Physiol*, 290(6), R1488-1495 (2006).
9. Liu X, Liu Y, Zhao L, Zeng Z, Xiao W, Chen P. Macrophage depletion impairs skeletal muscle regeneration: The roles of regulatory factors for muscle regeneration. *Cell Biol Int*, 41(3), 228-238 (2017).
10. Mathew SJ, Hansen JM, Merrell AJ *et al.* Connective tissue fibroblasts and Tcf4 regulate myogenesis. *Development*, 138(2), 371-384 (2011).

11. Collins CA, Olsen I, Zammit PS *et al.* Stem cell function, self-renewal, and behavioral heterogeneity of cells from the adult muscle satellite cell niche. *Cell*, 122(2), 289-301 (2005).
12. Fan Y, Maley M, Beilharz M, Grounds M. Rapid death of injected myoblasts in myoblast transfer therapy. *Muscle Nerve*, 19(7), 853-860 (1996).
13. Moens PDJ, Colson Van-Schoor M, Marchal G. Lack of myoblasts migration between transplanted and host muscles of mdx and normal mice. *J Muscle Res Cell Motil*, 17(1), 37-43 (1996).
14. Lesault PF, Theret M, Magnan M *et al.* Macrophages improve survival, proliferation and migration of engrafted myogenic precursor cells into MDX skeletal muscle. *PLoS One*, 7(10), e46698 (2012).
15. Bencze M, Negroni E, Vallese D *et al.* Proinflammatory macrophages enhance the regenerative capacity of human myoblasts by modifying their kinetics of proliferation and differentiation. *Mol Ther*, 20(11), 2168-2179 (2012).
16. Holt DJ, Chamberlain LM, Grainger DW. Cell-cell signaling in co-cultures of macrophages and fibroblasts. *Biomaterials*, 31(36), 9382-9394 (2010).
17. Gottrup F, Agren MS, Karlsmark T. Models for use in wound healing research: A survey focusing on in vitro and in vivo adult soft tissue. *Wound Repair Regen*, 8(2), 83-96 (2000).
18. Prisk V, Huard J. Muscle injuries and repair: the role of prostaglandins and inflammation. *Histol Histopathol*, 18(4), 1243-1256 (2003).
19. Filippin LI, Moreira AJ, Marroni NP, Xavier RM. Nitric oxide and repair of skeletal muscle injury. *Nitric Oxide*, 21(3-4), 157-163 (2009).
20. Saclier M, Cuvellier S, Magnan M, Mounier R, Chazaud B. Monocyte/macrophage interactions with myogenic precursor cells during skeletal muscle regeneration. *FEBS J*, 280(17), 4118-4130 (2013).
21. Tidball JG. Inflammatory processes in muscle injury and repair. *Am J Physiol Regul Integr Comp Physiol*, 288(2), R345-353 (2005).
22. Tidball JG, Villalta SA. Regulatory interactions between muscle and the immune system during muscle regeneration. *Am J Physiol Regul Integr Comp Physiol*, 298(5), R1173-1187 (2010).
23. Arnold L, Henry A, Poron F *et al.* Inflammatory monocytes recruited after skeletal muscle injury switch into antiinflammatory macrophages to support myogenesis. *J Exp Med*, 204(5), 1057-1069 (2007).
24. Brown BN, Londono R, Tottey S *et al.* Macrophage phenotype as a predictor of constructive remodeling following the implantation of biologically derived surgical mesh materials. *Acta Biomater*, 8(3), 978-987 (2012).
25. Vidal B, Serrano AL, Tjwa M *et al.* Fibrinogen drives dystrophic muscle fibrosis via a TGFbeta/alternative macrophage activation pathway. *Genes Dev*, 22(13), 1747-1752 (2008).
26. Webber J, Jenkins RH, Meran S, Phillips A, Steadman R. Modulation of TGFbeta1-dependent myofibroblast differentiation by hyaluronan. *Am J Pathol*, 175(1), 148-160 (2009).
27. Darby I, Skalli O, Gabbiani G. Alpha-smooth muscle actin is transiently expressed by myofibroblasts during experimental wound healing. *Lab Invest*, 63(1), 21-29 (1990).
28. Hinz B, Phan SH, Thannickal VJ, Galli A, Bochaton-Piallat ML, Gabbiani G. The myofibroblast: one function, multiple origins. *Am J Pathol*, 170(6), 1807-1816 (2007).
29. Forbes SJ, Rosenthal N. Preparing the ground for tissue regeneration: from mechanism to therapy. *Nat Med*, 20(8), 857-869 (2014).

30. Rigamonti E, Touvier T, Clementi E, Manfredi AA, Brunelli S, Rovere-Querini P. Requirement of inducible nitric oxide synthase for skeletal muscle regeneration after acute damage. *J Immunol*, 190(4), 1767-1777 (2013).
31. Huang WC, Sala-Newby GB, Susana A, Johnson JL, Newby AC. Classical macrophage activation up-regulates several matrix metalloproteinases through mitogen activated protein kinases and nuclear factor-kappaB. *PLoS One*, 7(8), e42507 (2012).
32. Ko MH, Li CY, Lee CF, Chang CK, Fang SH. Scratch wound closure of myoblasts and myotubes is reduced by inflammatory mediators. *Int Wound J*, 13(5), 680-685 (2016).
33. Saclier M, Yacoub-Youssef H, Mackey AL *et al.* Differentially activated macrophages orchestrate myogenic precursor cell fate during human skeletal muscle regeneration. *Stem Cells*, 31(2), 384-396 (2013).
34. Sonnet C, Lafuste P, Arnold L *et al.* Human macrophages rescue myoblasts and myotubes from apoptosis through a set of adhesion molecular systems. *J Cell Sci*, 119(Pt 12), 2497-2507 (2006).
35. Ploeger DT, Hosper NA, Schipper M, Koerts JA, de Rond S, Bank RA. Cell plasticity in wound healing: paracrine factors of M1/ M2 polarized macrophages influence the phenotypical state of dermal fibroblasts. *Cell Commun Signal*, 11(1), 29 (2013).
36. Steinhauser ML, Kunkel SL, Hogaboam CM, Evanoff H, Strieter RM, Lukacs NW. Macrophage/fibroblast coculture induces macrophage inflammatory protein-1a production mediated by intercellular adhesion molecule-1 and oxygen radicals. *J Leukoc Biol*, 64(5), 636-641 (1998).
37. Oshikawa K, Yamasawa H, Sugiyama Y. Human lung fibroblasts inhibit macrophage inflammatory protein-1alpha production by lipopolysaccharide-stimulated macrophages. *Biochem Biophys Res Commun*, 312(3), 650-655 (2003).
38. Vancheri C, Crimi N, Conte E *et al.* Human lung fibroblasts inhibit tumor necrosis factor-alpha production by LPS-activated monocytes. *Am J Respir Cell Mol Biol*, 15(4), 460-466 (1996).
39. Fadok VA, Bratton DL, Konowal A, Freed PW, Westcott JY, Henson PM. Macrophages that have ingested apoptotic cells in vitro inhibit proinflammatory cytokine production through autocrine/paracrine mechanisms involving TGF-beta, PGE2, and PAF. *J Clin Invest*, 101(4), 890-898 (1998).
40. Gordon S. Alternative activation of macrophages. *Nat Rev Immunol*, 3(1), 23-35 (2003).
41. Venter C, Niesler CU. Cellular alignment and fusion: Quantifying the effect of macrophages and fibroblasts on myoblast terminal differentiation. *Exp Cell Res*, 370(2), 542-550 (2018).
42. Kjaer M. Role of extracellular matrix in adaptation of tendon and skeletal muscle to mechanical loading. *Physiol Rev*, 84(2), 649-698 (2004).
43. Kaariainen M, Jarvinen T, Jarvinen M, Rantanen J, Kalimo H. Relation between myofibers and connective tissue during muscle injury repair. *Scand J Med Sci Sports*, 10(6), 332-337 (2000).
44. Rao N, Evans S, Stewart D *et al.* Fibroblasts influence muscle progenitor differentiation and alignment in contact independent and dependent manners in organized co-culture devices. *Biomed Microdevices*, 15(1), 161-169 (2013).
45. Venter C, Niesler C. A triple co-culture method to investigate the effect of macrophages and fibroblasts on myoblast proliferation and migration. *Biotechniques*, 64(2), 52-58 (2018).

46. Goetsch KP, Snyman C, Myburgh KH, Niesler CU. Simultaneous isolation of enriched myoblasts and fibroblasts for migration analysis within a novel co-culture assay. *Biotechniques*, 58(1), 25-32 (2015).
47. Zhang Y, Li H, Lian Z, Li N. Myofibroblasts protect myoblasts from intrinsic apoptosis associated with differentiation via beta1 integrin-PI3K/Akt pathway. *Dev Growth Differ*, 52(8), 725-733 (2010).
48. Cooper ST, Maxwell AL, Kizana E *et al.* C2C12 co-culture on a fibroblast substratum enables sustained survival of contractile, highly differentiated myotubes with peripheral nuclei and adult fast myosin expression. *Cell Motil Cytoskeleton*, 58(3), 200-211 (2004).
49. Abarzua-Illanes PN, Padilla C, Ramos A *et al.* Improving myoblast differentiation on electrospun poly(epsilon-caprolactone) scaffolds. *J Biomed Mater Res A*, 105(8), 2241-2251 (2017).
50. Goers L, Freemont P, Polizzi KM. Co-culture systems and technologies: taking synthetic biology to the next level. *J R Soc Interface*, 11(96), pii: 20140065 (2014).
51. Bogdanowicz DR, Lu HH. Studying cell-cell communication in co-culture. *Biotechnol J*, 8(4), 395-396 (2013).
52. Fitzpatrick LE, McDevitt TC. Cell-derived matrices for tissue engineering and regenerative medicine applications. *Biomater Sci*, 3(1), 12-24 (2015).
53. Stacey G. Primary Cell Cultures and Immortal Cell Lines. In: *Encyclopedia of Life Sciences.* (2006)
54. Antonios JK, Yao Z, Li C, Rao AJ, Goodman SB. Macrophage polarization in response to wear particles in vitro. *Cell Mol Immunol*, 10(6), 471-482 (2013).
55. Howard EW, Crider BJ, Updike DL *et al.* MMP-2 expression by fibroblasts is suppressed by the myofibroblast phenotype. *Exp Cell Res*, 318(13), 1542-1553 (2012).
56. Lawson MA, Purslow PP. Differentiation of myoblasts in serum-free media: effects of modified media are cell line-specific. *Cells Tissues Organs*, 167(2-3), 130-137 (2000).
57. Hayflick L, Moorhead PS. The serial cultivation of human diploid cell strains. *Exp Cell Res*, 25(3), 585-621 (1961).
58. Kaur G, Dufour JM. Cell lines: Valuable tools or useless artifacts. *Spermatogenesis*, 2(1), 1-5 (2012).
59. Hinds S, Tyhovych N, Sistrunk C, Terracio L. Improved tissue culture conditions for engineered skeletal muscle sheets. *Sci World J*, 2013, 370151 (2013).
60. Chamberlain LM, Godek ML, Gonzalez-Juarrero M, Grainger DW. Phenotypic non-equivalence of murine (monocyte-) macrophage cells in biomaterial and inflammatory models. *J Biomed Mater Res A*, 88(4), 858-871 (2009).
61. Tarique AA, Logan J, Thomas E, Holt PG, Sly PD, Fantino E. Phenotypic, functional, and plasticity features of classical and alternatively activated human macrophages. *Am J Respir Cell Mol Biol*, 53(5), 676-688 (2015).
62. Hecker L, Jagirdar R, Jin T, Thannickal VJ. Reversible differentiation of myofibroblasts by MyoD. *Exp Cell Res*, 317(13), 1914-1921 (2011).
63. Charge SB, Rudnicki MA. Cellular and molecular regulation of muscle regeneration. *Physiol Rev*, 84(1), 209-238 (2004).
64. Parakati R, DiMario JX. Repression of myoblast proliferation and fibroblast growth factor receptor 1 promoter activity by KLF10 protein. *J Biol Chem*, 288(19), 13876-13884 (2013).
65. Dowling P, Clynes M. Conditioned media from cell lines: a complementary model to clinical specimens for the discovery of disease-specific biomarkers. *Proteomics*, 11(4), 794-804 (2011).

66. Jeong D, Han C, Kang I *et al.* Effect of Concentrated Fibroblast-Conditioned Media on In Vitro Maintenance of Rat Primary Hepatocyte. *PLoS One*, 11(2), e0148846 (2016).
67. Ng CP, Hinz B, Swartz MA. Interstitial fluid flow induces myofibroblast differentiation and collagen alignment in vitro. *J Cell Sci*, 118(Pt 20), 4731-4739 (2005).
68. Kutys ML, Doyle AD, Yamada KM. Regulation of cell adhesion and migration by cell-derived matrices. *Exp Cell Res*, 319(16), 2434-2439 (2013).
69. Mewhort HE, Lipon BD, Svystonyuk DA *et al.* Monocytes increase human cardiac myofibroblast-mediated extracellular matrix remodeling through TGF-beta1. *Am J Physiol Heart Circ Physiol*, 310(6), H716-724 (2016).
70. Chazaud B, Sonnet C, Lafuste P *et al.* Satellite cells attract monocytes and use macrophages as a support to escape apoptosis and enhance muscle growth. *J Cell Biol*, 163(5), 1133-1143 (2003).
71. Domeij H, Modeer T, Quezada HC, Yucel-Lindberg T. Cell expression of MMP-1 and TIMP-1 in co-cultures of human gingival fibroblasts and monocytes: the involvement of ICAM-1. *Biochem Biophys Res Commun*, 338(4), 1825-1833 (2005).
72. Cho CH, Park J, Tilles AW, Berthiaume F, Toner M, Yarmush ML. Layered patterning of hepatocytes in co-culture systems using microfabricated stencils. *Biotechniques*, 48(1), 47-52 (2010).
73. Javaherian S, Li KJ, McGuigan AP. A simple and rapid method for generating patterned co-cultures with stable interfaces. *Biotechniques*, 55(1), 21-26 (2013).
74. Hui EE, Bhatia SN. Micromechanical control of cell-cell interactions. *Proc Natl Acad Sci U S A*, 104(14), 5722-5726 (2007).
75. Shimasaki T, Yamamoto S, Arisawa T. Exosome Research and Co-culture Study. *Biol Pharm Bull*, 41(9), 1311-1321 (2018).
76. Strober W. Trypan blue exclusion test of cell viability. *Curr Protoc Immunol*, Appendix 3, Appendix 3B (2001).
77. Venter C, Niesler CU. Rapid quantification of cellular proliferation and migration using ImageJ. *Biotechniques*, 66(2), 99-102 (2019).
78. Feoktistova M, Geserick P, Leverkus M. Crystal violet assay for determining viability of cultured cells. *Cold Spring Harb Protoc*, 2016(4), pdb prot087379 (2016).
79. van Meerloo J, Kaspers GJ, Cloos J. Cell sensitivity assays: the MTT assay. *Methods Mol Biol*, 731, 237-245 (2011).
80. Goetsch KP, Myburgh KH, Niesler CU. *In vitro* myoblast motility models: Investigating migration dynamics for the study of skeletal muscle repair. *J Muscle Res Cell Motil*, 34(5-6), 333-347 (2013).
81. Goetsch KP, Niesler CU. Optimization of the scratch assay for in vitro skeletal muscle wound healing analysis. *Analytal Biochemistry*, 411(1), 158-160 (2011).
82. Hartman CD, Isenberg BC, Chua SG, Wong JY. Vascular smooth muscle cell durotaxis depends on extracellular matrix composition. *Proc Natl Acad Sci U S A*, 113(40), 11190-11195 (2016).
83. Hadden WJ, Young JL, Holle AW *et al.* Stem cell migration and mechanotransduction on linear stiffness gradient hydrogels. *Proc Natl Acad Sci U S A*, 114(22), 5647-5652 (2017).
84. Tonar Z, Nemecek S, Holota R *et al.* Microscopic image analysis of elastin network in samples of normal, atherosclerotic and aneurysmatic abdominal aorta and its biomechanical implications. *J Appl Biomed*, 1, 149-159 (2003).

85. Chaudhuri BB, Kundu P, Sarkar N. Detection and gradation of oriented texture. *Pattern Recognition Letters*, 14(2), 147-153 (1993).
86. Xu F, Beyazoglu T, Hefner E, Gurkan UA, Demirci U. Automated and adaptable quantification of cellular alignment from microscopic images for tissue engineering applications. *Tissue Eng Part C Methods*, 17(6), 641-649 (2011).
87. Sun M, Bloom AB, Zaman MH. Rapid Quantification of 3D Collagen Fiber Alignment and Fiber Intersection Correlations with High Sensitivity. *PLoS One*, 10(7), e0131814 (2015).
88. Dumont N, Frenette J. Macrophages protect against muscle atrophy and promote muscle recovery in vivo and in vitro: a mechanism partly dependent on the insulin-like growth factor-1 signaling molecule. *Am J Pathol*, 176(5), 2228-2235 (2010).
89. Bajaj P, Reddy B, Jr., Millet L *et al.* Patterning the differentiation of C2C12 skeletal myoblasts. *Integr Biol (Camb)*, 3(9), 897-909 (2011).
90. Velica P, Bunce CM. A quick, simple and unbiased method to quantify C2C12 myogenic differentiation. *Muscle Nerve*, 44(3), 366-370 (2011).
91. McColl R, Nkosi M, Snyman C, Niesler C. Analysis and quantification of in vitro myoblast fusion using the LADD Multiple Stain. *Biotechniques*, 61(6), 323-326 (2016).
92. Bentzinger CF, Wang YX, Rudnicki MA. Building muscle: molecular regulation of myogenesis. *Cold Spring Harb Perspect Biol*, 4(2), pii: a008342 (2012).
93. Sakuma K, Yamaguchi A. Molecular and Cellular Mechanism of Muscle Regeneration. In: *Skeletal Muscle - From Myogenesis to Clinical Relations.* Cseri, J (Ed. (InTech, 2012) 380.
94. Lu B, Rutledge BJ, Gu L *et al.* Abnormalities in Monocyte Recruitment and Cytokine Expression in Monocyte Chemoattractant Protein 1–deficient Mice. *J Exp Med*, 187(4), 601-608 (1998).
95. Fuentes ME, Durham SK, Swerdel MR *et al.* Controlled recruitment of monocytes and macrophages to specific organs through transgenic expression of monocyte chemoattractant protein-1. *J Immunol*, 155(12), 5769-5776 (1995).
96. Labbe K, Danialou G, Gvozdic D *et al.* Inhibition of monocyte chemoattractant protein-1 prevents diaphragmatic inflammation and maintains contractile function during endotoxemia. *Crit Care*, 14(5), R187 (2010).
97. Villalta SA, Nguyen HX, Deng B, Gotoh T, Tidball JG. Shifts in macrophage phenotypes and macrophage competition for arginine metabolism affect the severity of muscle pathology in muscular dystrophy. *Hum Mol Genet*, 18(3), 482-496 (2009).

CHAPTER 3: RAPID QUANTIFICATION OF CELLULAR PROLIFERATION AND MIGRATION USING IMAGEJ

Venter C, Niesler CU*

Discipline of Biochemistry, School of Life Sciences, University of KwaZulu-Natal, Private Bag X01, Scottsville 3209, South Africa

**Corresponding author: Prof C.U. Niesler, Tel: (033) 260 5465, Fax: (033) 260 6127, email: niesler@ukzn.ac.za*

Published: Venter and Niesler (2019). Rapid quantification of cellular proliferation and migration using ImageJ. *BioTechniques* 66 (2), 99-102

Abstract
Cellular proliferation and migration are crucial during development, regeneration and disease. Methods to quantify these processes are available, however many are time consuming and require specialised equipment and costly reagents. Simple cell counts (proliferation analysis) and the scratch assay (migration analysis) are favourable methods as a result of their simplicity and cost-effectiveness, however they rely on subjective and labour intensive manual analysis, resulting in low throughput. We have developed optimized protocols to rapidly and accurately quantify adherent cell number and wound area using ImageJ, an open-source image processing program. Notably, these adaptable protocols facilitate quantification with significantly greater accuracy than manual identification.

Keywords: proliferation, adherent cell counts, myoblasts, migration, scratch assay, ImageJ

Method Summary: Optimized automated methods to rapidly quantify proliferation and migration of adherent cells using ImageJ. These methods support high throughput and deliver enhanced accuracy when compared to manual analysis.

Cellular proliferation and migration are important processes during tissue development, repair and disease. Following skeletal muscle injury, proliferation and migration of activated muscle stem cells (myoblasts) is crucial to ensure that sufficient progenitor cells reach the wound site and facilitate repair [1]. Myoblast proliferation and migration are regulated by signalling molecules released from the extracellular matrix (ECM) and resident/infiltrating cells such as macrophages and fibroblasts [2]. Proliferation can be quantified by measuring changes in DNA (via BrdU, ^{3}H-Thymidine), metabolism (via MTT), proliferation-specific proteins (e.g. Ki-67) or simple cell counts (e.g. haemocytometer, TC20™) [3-7]. Migration can be assessed by determining the number of cells that move across a microporous membrane (transwell migration assay) or by measuring the surface area that cells occupy over time after creating a "cell-free" area (scratch assay) [8-10]. Of these, cell counts and the scratch assay are favourable methods as a result of their cost-effective and simple nature, with fewer steps and a reduced need for specialized equipment.

ImageJ, a popular opensource image processing program, has previously been used to manually count cells (selecting and tallying individual cells) and assess wound closure (tracing the wound perimeter and calculating percentage closure) [11-13]. These manual approaches are laborious and time-consuming, whereas automated image analyses would facilitate a higher throughput and greater objectivity. In the current study, we utilised the image processing capabilities of ImageJ to develop an optimized batch processing macro for rapid and accurate identification and quantification of adherent cell number and wound area from images captured using a brightfield phase contrast microscope. We demonstrate that these protocols are easier, faster and more objective than alternative methods.

Murine C2C12 myoblasts (ATCC, cat. CRL-1772™, USA) were cultured at 37˚C and 5% CO_2 and maintained in growth medium (GM) containing Dulbecco's Modified Eagle's Medium (Sigma, cat. D5648, USA) supplemented with 10% (v/v) Fetal Bovine Serum (Gibco, cat. 10500, USA), 2% (v/v) Penicillin-Streptomycin (LONZA, cat. DE17-602E, Switzerland). Media was changed every 48 hours. Results were analysed using either a paired, two-tailed Student's T-test (for comparison *between* methods at a single cell number or timepoint; Figure 1B, 2C) or one way ANOVA (for cell number changes *within* a method; Figure 1C), and values of $p < 0.05$ considered statistically significant. All data was represented as mean ± SEM.

For proliferation analysis, myoblasts (5, 10, 20, 40, 60, 80 and 100 x 10^3 cells) were cultured in GM (500 µl) in a 24-well plate for three hours to promote adherence. Media was then removed, and cells stained with 0.2% (w/v) crystal violet (Sigma, cat. C-3886) in methanol (Sigma, cat. 24229) for 15 minutes; excess stain was subsequently removed by water submergence and the plate left to airdry. Cells were visualized using an Olympus CKX41 microscope (4x objective lens) and images captured (three fields of view per replicate; three replicates) with a Motic 3.0 megapixel camera. Cell number was assessed and compared using three methods: manual cell identification, automated cell identification and the spectrophotometric (crystal violet) assay.

For manual identification, captured images were converted to grayscale in ImageJ (*Image → Type → 8-bit*) (Figure 1Ai), the cells were manually marked out with a red pencil dot (size: 4 px) in Microsoft Paint (Figure Aii), the dots were then automatically identified (*Image → Adjust → Color Threshold (Hue 225 to 255; Dark Background: True)*) and counted (*Analyze → Analyze Particles*) using ImageJ. For automated identification, the images were converted to grayscale, image noise removed (*Process → Noise → Despeckle*), brightness and contrast adjusted (*Image → Adjust → Brightness/Contrast: min = 87; max = 167*), and a Phansalkar threshold (*Image → Adjust → Auto Local Threshold: Phansalkar*) and watershed (*Process → Binary → Watershed*) were finally applied (Figure Aiii). Adjusting the brightness and contrast, and applying the Phansalkar threshold, made the cells more distinguishable from the background, while the watershed step segmented any clustered cells from one another. The identified cells were finally counted using ImageJ. For spectrophotometric analysis, the crystal violet-stained cells were solubilized with 200 µl SDS (1% w/v; Merck, cat. SAAR5823610EM, USA) for 1 hour; 100 µl of the solution was then removed and added to a 96-well microplate [14]. The absorbance (595 nm) was read using the FLUOoptima micro 96-well plate reader.

For proliferation analysis, myoblasts were manually counted or identified and assessed using ImageJ. ImageJ could automatically identify cells at lower (5 x 10^3 cells) *and* higher (100 x 10^3 cells) numbers, despite the cells being clustered closely together; however, this is likely to become increasingly challenging as confluence is attained. No significant difference was found between automated (ImageJ) versus manual identification, confirming the accuracy of

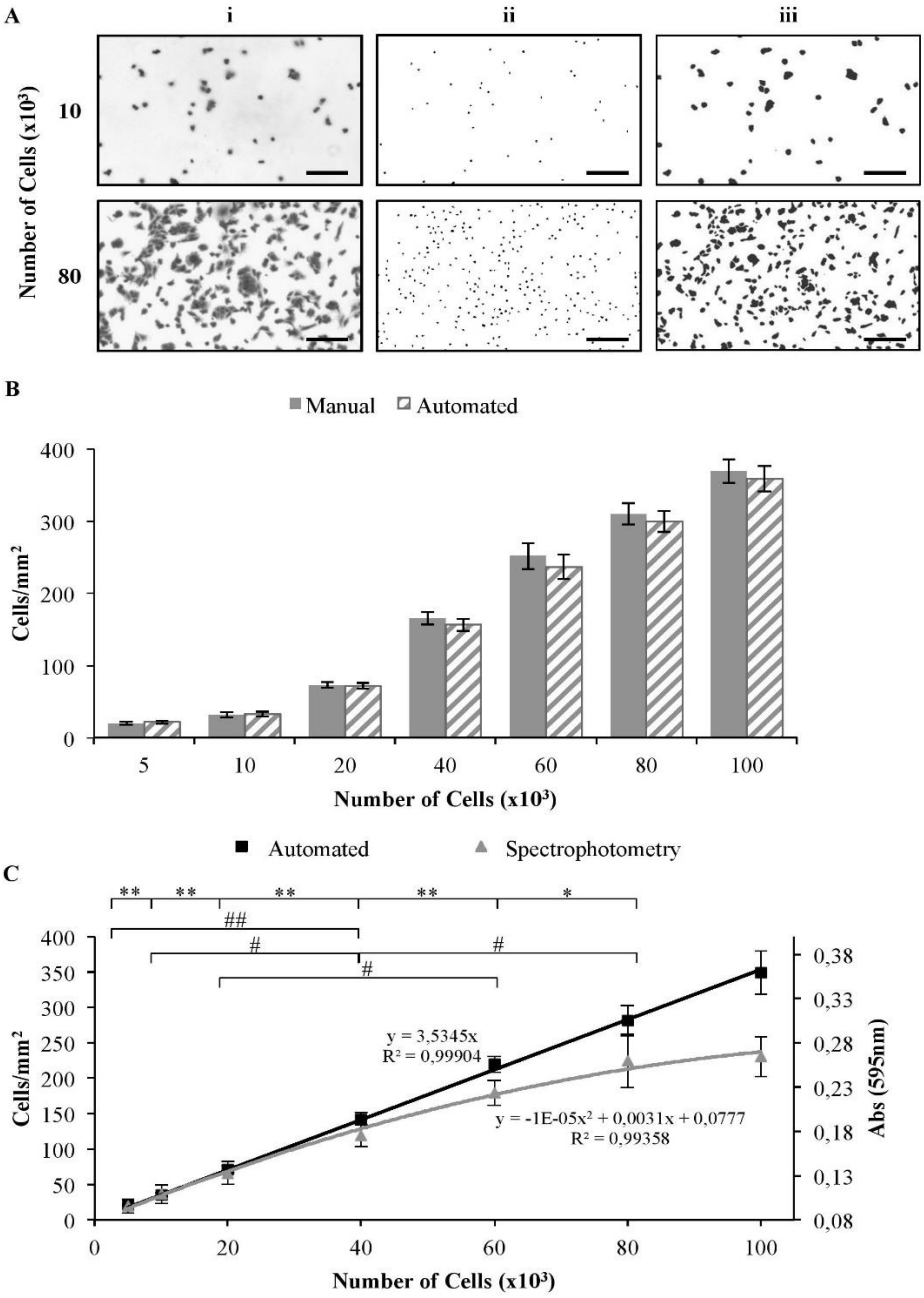

Figure 1. Quantification of cell number: a comparison of manual, automated (ImageJ) and spectrophotometric identification methods. (A) C2C12 myoblasts (10 x 10^3 and 80 x 10^3 are shown) were stained with crystal violet and captured with an Olympus CKX41 microscope coupled to a Motic 3.0 megapixel camera: (i) Brightfield images prior to processing, (ii) cells manually marked in Microsoft Paint and subsequently counted, (iii) cells automatically identified using the optimized ImageJ macro and subsequently counted. Scale bar = 200 µm (B) Standard curve of cell density (cells/mm^2) following application of the manual versus the automated ImageJ analysis. (C). Standard curve of cell density (cells/mm^2) following application of automated ImageJ analysis versus spectrophotometry. *p<0.05 and **p<0.005 for automated ImageJ analysis; #p<0.05 and ##p< 0.005 for spectrophotometric analysis; N=4-9.

the automated method (Figure 1B). Manual cell identification was also a slow and laborious task compared to automated assessment. We then compared our automated cell number analysis with spectrophotometric analysis of crystal violet-stained cells; the latter assay is a simple, inexpensive method commonly used to quantify cell number (Figure 1C). The standard curve generated using the spectrophotometric assay yielded a polynomial line ($y = -1E\text{-}05x^2 + 0.0031x + 0.0777$; $R^2 = 0.9936$); as the number of plated cells increased, the absorbance (at 595 nm) increased, but plateaued after 60 x 10^3 cells (~65% confluence), possibly as a result of crystal violet saturation (Figure 1C). In contrast, the standard curve generated using the automated ImageJ macro resulted in a straight line ($y = 3.5345x$; $R^2 = 0.999$), indicating a directly proportional relationship between the number of cells plated and the number calculated per mm^2. In addition, each *sequential* increase in plated cell number was reflected as a significant increase in cell density when utilising the automated counting method; this was not the case for the polynomial generated from crystal violet absorbance readings (Figure 1C). Therefore, ImageJ was sensitive enough to accurately detect both smaller changes in cell numbers and a wider range of cellular densities than spectrophotometric analysis of crystal violet-stained cells.

For migration analysis, myoblasts (120 x 10^3) were plated out in GM (1 ml) in a 12-well plate for 24 hours, before performing a scratch assay as described by Goetsch *et. al.* (2011). Briefly, the confluent monolayer of myoblasts was scratched with a sterile 200 µl loading tip to create a linear "wound" devoid of cells. The cells were then washed twice with sterile PBS and fresh GM (500 µl) was added. The cells were incubated for 7 hours and images captured at 0, 3, 5 and 7 hours using the camera-attached microscope (4x objective lens) (two fields of view per replicate, for two replicates). To measure wound area *manually*, the edges of the wound were traced using the Motic Images Plus 2.0 ML software [15]. To carry out *automated* wound area measurements, the captured image was converted to grayscale, the edges found (*Process → Find Edges*) and the image blurred (*Process → Smooth*) multiple times (x 37). The *Find Edges* step highlighted sharp changes in intensity with a white outline so that when the image was blurred numerous times, these outlines blurred together; as a result, the areas containing cells were white whereas the wound area (devoid of cells) remained black. A *MinError threshold* was then applied (*Image → Adjust → Auto Threshold: MinError*) to automatically detect the wound area. If the wound area was not accurately selected, it could be manually thresholded (*Image → Adjust → Threshold*). Once the wound

area was identified, it was then quantified (*Analyze → Analyze Particles (size: 10 000 – infinity)*).

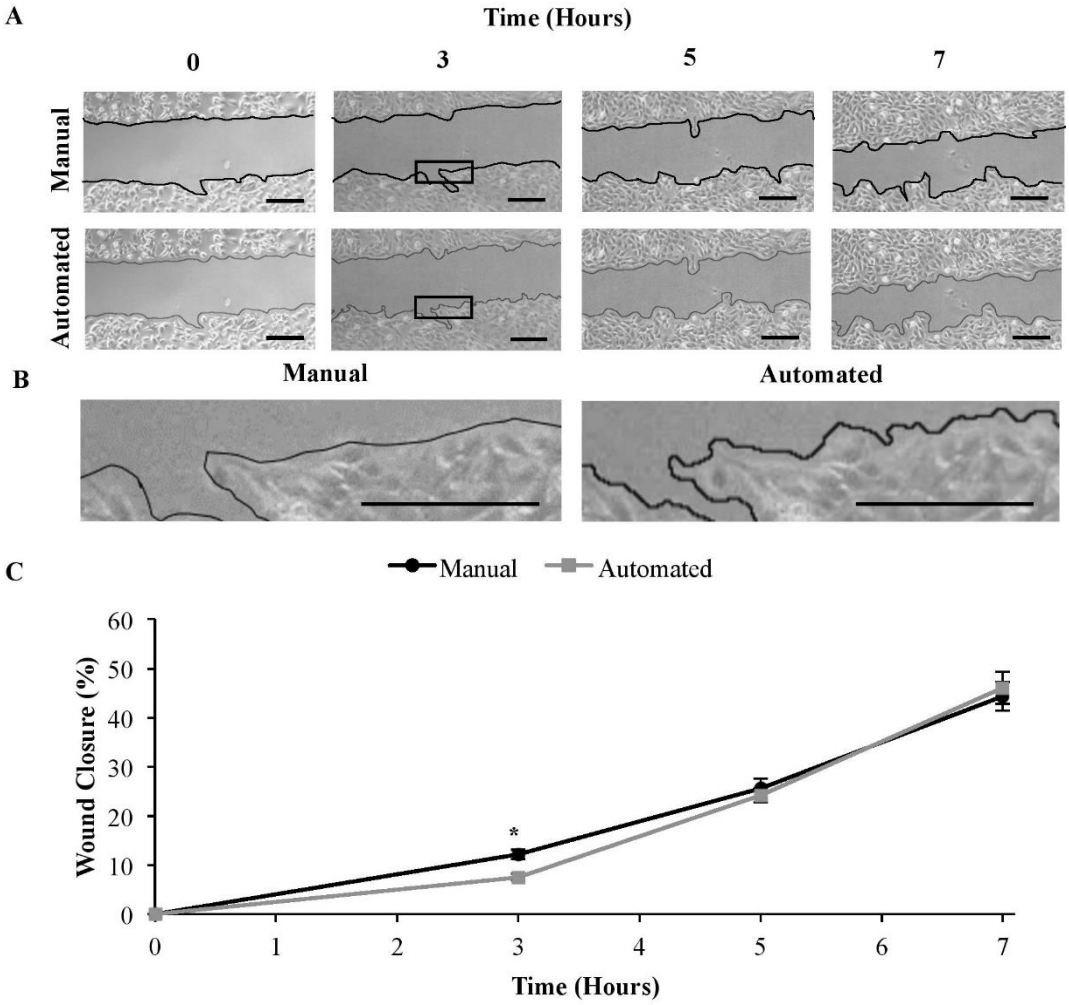

Figure 2: Quantification of wound area: a comparison of manual and automated (ImageJ) identification methods. (A) C2C12 myoblasts (120 x 10^3) were scratched and images captured with an Olympus CKX41 microscope coupled to a Motic 3.0 megapixel camera (0, 3, 5 and 7 hours): manual identification using Motic Images Plus 2.0 ML software to trace the wound edge and automated identification using ImageJ. (B) Zoomed-in images of wound edges following manual and automated identification at 3 hours. (C) Percentage wound closure (%) at 3,5 and 7 hours post-injury. *$p<0.05$; N=16. Scale bar = 200 µm

The percentage wound closure was calculated and the results generated using the manual versus automated methods were compared (Figure 2). The use of ImageJ to detected wound edges revealed that, when compared to manual assessment, automated analysis was able to accurately define these edges (Figure 2A); in fact, the automated analysis seemed to define the wound edges *more* accurately than the manual method (Figure 2B). As a result, when the percentage wound closure was assessed, a significant difference between the manual (12.13 ±

0.98%) and automated (7.54 ± 0.76%) method was detected at 3 h post-wounding ($p < 0.05$). This was attributed to the fact that ImageJ could trace the outline of the wound more accurately than the researcher's manual attempt; this was particularly evident during early wound repair when the wound borders were not well defined and therefore harder to accurately trace. The ability of ImageJ to sensitively and accurately measure wound area would be dependent on the image quality. We used a high-quality image (aspect ratio: 1280x1024) with many pixels to allow ImageJ to accurately identify the edges of the wound. In contrast, a lower quality images with fewer pixels would make it difficult for ImageJ to accurately identify the wound. In addition to increased sensitivity and accuracy, the application of the ImageJ macro was less laborious and faster than manual analysis (manual analysis can take up to 10 minutes per image whereas our automated approach can complete the analysis of an image within a few seconds).

In summary, we have developed an optimized ImageJ-based automated method for rapid quantification of cell number and migration *in vitro*. ImageJ could automatically identify and accurately quantify cell numbers and wound area; in some cases, the results were superior to those generated via traditional manual or spectrophotometric methods. In addition, our macros generated data faster than previous manual methods. Although programs have previously been developed to count cells (e.g. CellC and CellCounter) or measure wound closure (e.g. TScratch) [16-19], they did not match the flexibility of ImageJ which, as a single program, can be extended to quantify cell number in tissue sections and suspension cultures or adapted to monitor important cellular processes [19]. Finally, the opensource nature of this software permits further optimization depending on user requirements, yielding a superior and versatile method compared to previous protocols.

References

1. Mann CJ, Perdiguero E, Kharraz Y *et al.* Aberrant repair and fibrosis development in skeletal muscle. *Skelet Muscle*, 1(1), 21 (2011).
2. Bosurgi L, Manfredi AA, Rovere-Querini P. Macrophages in injured skeletal muscle: a perpetuum mobile causing and limiting fibrosis, prompting or restricting resolution and regeneration. *Frontiers in immunology*, 2, 62 (2011).
3. Hughes WL, Bond VP, Brecher G *et al.* Cellular proliferation in the mouse as revealed by the autoradiography with tritiated thymidine. *Proc. Natl. Acad. Sci. USA.*, 44(5), 476-483 (1958).
4. Gratzner HG. Monoclonal antibody to 5-bromo- and 5-iododeoxyuridine: A new reagent for detection of DNA replication. *Science*, 29(4571), 474-475 (1982).

5. Mosmann T. Rapid colorimetric assay for cellular growth and survival: Application to proliferation and cytotoxicity assays. *J. Immunol. Meth.*, 65(1-2), 55-63 (1983).
6. Scholzen T, Gerdes J. The Ki-67 protein: From the known to the unknown. *J. Cell. Physiol.*, 182(3), 311-322 (2000).
7. Boulton RA, Hodgson JF. Assessing cell proliferation: A methodological review. *Clin. Sci. (Lond.)*, 88(2), 119-130 (1995).
8. Boyden S. The chemotactic effect of mictures of antibody and antigen on polymorphonuclear leucocytes. *J. Exp. Med.*, 115(3), 453-466 (1962).
9. Lampugnani MG. Cell migration into a wounded area in vitro. *Methods. Mol. Biol.*, 96, 177-182 (1999).
10. Hulkower KI, Herber RL. Cell migration and invasion assays as tools for drug discovery. *Pharmaceutics*, 3(1), 107-124 (2011).
11. Schindelin J, Rueden CT, Hiner MC, Eliceiri KW. The ImageJ ecosystem: An open platform for biomedical image analysis. *Mol. Reprod. Dev.*, 82(7-8), 518-529 (2015).
12. De Vos K. Cell Counter. (2001). Available at: https://imagej.nih.gov/ij/plugins/cell-counter.html [Accessed 6 September 2018]
13. Goetsch KP, Myburgh KH, Niesler CU. *In vitro* myoblast motility models: Investigating migration dynamics for the study of skeletal muscle repair. *J. Muscle. Res. Cell. Motil.*, 34(5-6), 333-347 (2013).
14. Feoktistova M, Geserick P, Leverkus M. Crystal violet assay for determining viability of cultured cells. *Cold. Spring. Harb. Protoc.*, 2016(4), pdb prot087379 (2016).
15. Goetsch KP, Niesler CU. Optimization of the scratch assay for in vitro skeletal muscle wound healing analysis. *Anal. Biochem.*, 411(1), 158-160 (2011).
16. Selinummi J, Seppala J, Yli-Harja O, Puhakka JA. Software for quantification of labeled bacteria from digital microscope images by automated image analysis. *Biotechniques*, 39(6), 859-863 (2005).
17. Li X, Yang H, Huang H, Zhu T. CELLCOUNTER: Novel open-source software for counting cell migration and invasion in vitro. *Biomed. Res. Int.*, 2014(2014), 6 (2014).
18. Geback T, Schultz MM, Kousmoutsakos P, Detmar M. TScratch: A novel and simple software tool for automated analysis of monolayer wound healing assays. *Biotechniques*, 46(4), 265-274 (2009).
19. Abràmoff MD, Magalhães PJ, Ram SJ. Image processing with ImageJ. *J. Biophotonics*, 11(7), 36-42 (2004).

CHAPTER 4: A TRIPLE CO-CULTURE METHOD TO INVESTIGATE THE EFFECT OF MACROPHAGES AND FIBROBLASTS ON MYOBLAST PROLIFERATION AND MIGRATION

Venter C, Niesler CU*

Discipline of Biochemistry, School of Life Sciences, University of KwaZulu-Natal, Private Bag X01, Scottsville 3209, South Africa

**Corresponding author: Prof C.U. Niesler, Tel: (033) 260 5465, Fax: (033) 260 6127, email: niesler@ukzn.ac.za*

Published: Venter and Niesler (2018). A triple co-culture method to investigate the effect of macrophages and fibroblasts on myoblast proliferation and migration. *BioTechniques* 64, 52-58

Abstract

The communication between non-myogenic cells, such as macrophages and fibroblasts, and myoblasts is crucial for successful skeletal muscle repair. *In vitro* co-culture methods can be utilised to increase our understanding of these cellular interactions; however, current protocols are restricted to two, often physically separate, cell populations. Here, we demonstrate a novel, inexpensive *in vitro* triple co-culture method that facilitates the co-culture of at least three cell populations with some degree of cell-cell contact. Using this method, we determined the effect of macrophages and fibroblasts on myoblast proliferation and migration. A significant increase in myoblast proliferation and migration was observed following co-culture with either macrophages *or* fibroblasts. However, triple co-culture of macrophages, fibroblasts *and* myoblasts revealed that the presence of macrophages prevented fibroblasts from maintaining this positive effect on myoblast migration. Macrophages, on the other hand, continued to promote myoblast proliferation whether in the presence of fibroblasts or not. Our triple co-culture system highlights the significance of *multicellular* communication in regulating myoblast proliferation and migration and emphasizes the importance of more complex co-culture systems when investigating myogenesis *in vitro*.

Keywords: macrophages, fibroblasts, myoblasts, triple co-culture, myogenesis

Method Summary: A novel *triple* co-culture method has been established to facilitate the co-culture of macrophages, fibroblasts and myoblasts. This assay, which permits some cell-cell contact, can be extended to include more than three cell types, and represents a simple, cost-effective way to probe complex multicellular communication *in vitro*.

Introduction

Severe skeletal muscle injury causes damage to myofibres and surrounding extracellular matrix (ECM) [1]. As a result, the damaged muscle undergoes sequential and overlapping stages of wound repair, where several cell types are activated to proliferate and migrate into the wound [2,3]. Macrophages and fibroblasts are present during these stages and are critical to the successful completion of the wound healing program [4]. Soon after injury, tissue degeneration, characterised by ruptured and necrotizing myofibres, is evident [5,6]. This is followed by inflammation, where macrophages residing in the epimysium and perimysium enter the wound to clear cell debris and secrete cytokines to initiate regeneration [2,7]. During the regenerative phase, infiltrating tissue fibroblasts are induced to differentiate into contractile myofibroblasts, which display a greater synthetic phenotype than fibroblasts. Myofibroblasts secrete cytokines, growth and extracellular matrix factors as well as enzymes that assist in remodelling the wound matrix [8-11]. This provides a mechanical scaffold for activated satellite cells (myoblasts) to proliferate and move from their niche between the basal lamina and sarcolemma to the area of damage [12]. At the wound site, they differentiate into myotubes and fuse with existing skeletal muscle tissue to repair damaged myofibres. The interplay of non-myogenic cells with activated satellite cells is therefore crucial for myogenesis and successful repair; a cellular imbalance may lead to impaired wound healing and, in the long term, chronic disease due to conditions such as fibrosis [4].

In order to fully understand the complex mechanisms controlling myogenesis, it is important to take into account the relevant cells that regulate this process. There are a number of methods which can be used to achieve this; these include the use of *in vivo* approaches, *in vitro* 3D tissue engineered skeletal muscle or *in vitro* co-culture systems. *In vivo* models are more accurate in reflecting the process of muscle wound repair, but due to the array of interactions that take place, this environment is highly complex, making it difficult to identify individual mechanisms [13]. Muscle is a three-dimensional tissue consisting of contractive bundles of muscle fibres and blood vessels. The use of *in vitro* 3D tissue engineered skeletal muscle mimics these *in vivo* conditions more closely than *in vitro* monolayer studies to gain a comprehensive insight into muscle wound repair. However, 3D tissue culture is more time-consuming in its establishment and requires extensive optimization.[14]. *Co-culture systems* make use of two or more cell populations, within the same *in vitro* microenvironment, thereby allowing some degree of interaction to study intercommunication between different cell types

[13]. This creates an experimental model that more closely mimics the intercellular communication within the *in vivo* environment and is therefore superior to conventional mono-culture [13,15,16].

Co-culture systems fall into one of two categories. Firstly, those that *physically* separate the cell populations from one another, typically by using a multi-compartment approach (e.g. transwell plates or "overflow" culture chambers) that allows communication only via soluble factors (Figure 1Ai and ii) [17,18]. A disadvantage of this type of method is that cells are not permitted to come in direct contact with one another, as would occur under *in vivo* conditions. Diffusion rates of soluble factors in larger culture volumes (as required in the overflow chamber) is also a consideration; if the rate of diffusion is too low, signalling factors may not be able to reach their targets timeously [13,19]. Secondly, there are those that allow direct interactions between cells (i.e. micropatterning); this is usually achieved by spatially controlling the position of the adhering cell populations within a culture dish (such as that reported by Javaherian *et. al.* (2013) or the co-culture method presented in this paper) (Figure 1Aiii and iv) [20]. Co-culturing by way of micropatterning involves the creation of a distinct population of cells within a culture dish by selectively controlling the attachment of cells (Figure 1Aiii). This can be achieved by creating a non-adhesive area via a *physical* barrier (using stamps for example [21]) or a *chemical* barrier (e.g. BSA [20]). The first population of cells will adhere to the area surrounding the barrier; once the barrier is removed (either by physical removal or by coating the non-adhesive area with an adhesive matrix factor [20]), the second cell population binds in the remaining space [22]. This method has the advantage of allowing cells to interact via both secreted factors and cell-cell interactions, but is laborious, requiring additional steps and specialised equipment.

Here, we describe a novel triple co-culture method (Figure Aiv), where a standard circular well-containing plate can be employed to culture multiple distinct cell populations, allowing for both direct and indirect cellular communication. Using this method, we investigate the regulatory role of macrophages and fibroblasts on myoblast proliferation and migration, and demonstrate the importance of macrophage resolution to facilitate fibroblast-regulated wound repair *in vitro*.

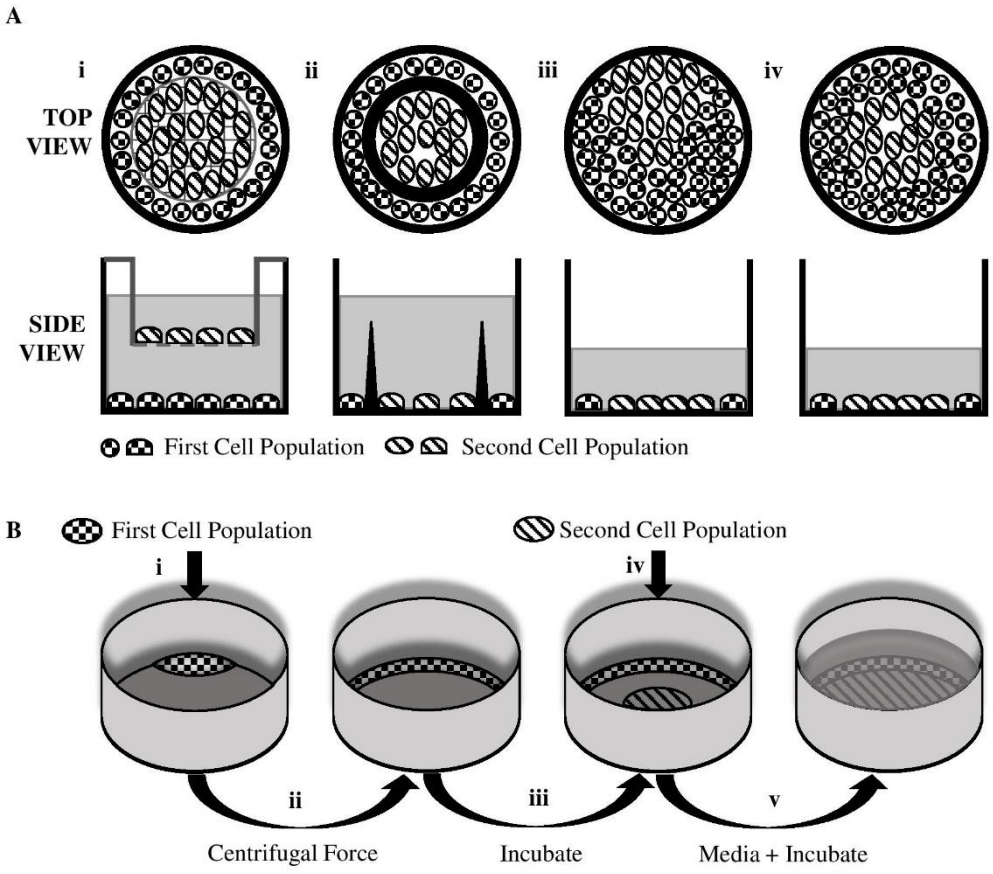

Figure 1: Schematic of co-culture methods and steps. A) Transwell inserts (i), "Overflow" co-culture chamber (ii), Micropatterning (iii) and our novel co-culture method (iv). **B)** Steps to establish novel triple co-culture method: first cell populations are plated at the outer edge of a well (i); culture plate is rotated to distribute the cells along the outer edge of the well (ii); cells are incubated for 1 hour to promote adherence (iii); subsequent cell population is then plated in the centre of the well (iv); media is added (v).

Materials and Methods

Cell Culture

Mouse C2C12 myoblasts (Cat. CRL-1772™, ATCC, Manassas, VA, USA), LMTK fibroblasts (Cat. CCL-1.3™, ATCC) and J774A.1 macrophages (Cat. TIB-67™, ATCC) were cultured at 37°C and 5% CO_2 and maintained in growth medium containing Dulbecco's Modified Eagle's Medium (DMEM, Cat. D5648, Sigma, St Louis, MO, USA) supplemented with 10% (v/v) Fetal Bovine Serum (FBS, Cat. 10500, Gibco, Thermo Fisher Scientific, Waltham, MA, USA) and 2% (v/v) Penicillin-Streptomycin (PenStrep, Cat. DE17-602E, Lonza, Basel, Switzerland). Media was changed every 48 hours.

Co-Culture Method

For co-culture of two cell types, either macrophages or fibroblasts (0, 5, 10, 20, 40, 80 x 10^3 cells) were plated along the outer edge of a dry 24-well plate in a volume of growth medium not exceeding 100 µl, but not less than 30 µl (Figure 1Bi). For co-culture of three cell types (i.e. "triple co-culture) 40 x 10^3 macrophages and 40 x 10^3 fibroblasts were combined in 100 µl growth medium and plated as above. A centrifugal force was then applied to the plate to ensure that the cells only attached to the outer edge of the well; this was achieved by simply rotating the plate in a circular motion (2 minutes) by hand, or using a rotational device (20 rpm) set at a 45^o angle (Figure 1Bii). Cohesion of the low medium volume ensures the cells do not spread towards the centre of the well. The cells were then incubated at 37°C and 5% CO_2 for 1 hour to promote adherence (Figure 1Biii). Following this, myoblasts were plated in the *centre* of the well and allowed to adhere to the unoccupied area (Figure 1Biv and v). Proliferation and migration of myoblasts in the centre of the well was then analysed as described below. The cells lines used with the co-culture method were cultured in the same culture medium and required no additional optimization. If cell types require different culture media, this method may not be suitable.

Proliferation Analysis

To analyse the effect of macrophages and fibroblasts on myoblast proliferation, 20 x 10^3 C2C12 cells were allowed to adhere for 2 hours, then washed twice with sterile PBS and cultured in serum-free DMEM (500 µl). Cells were co-cultured for 24 hours, washed with PBS and stained with basic Fuchsin (Cat. 47860, Sigma) for 10 minutes (1% w/v basic Fuchsin dissolved in 100% methanol). Cells were then submerged in water to remove excess stain and manually counted following visualization and image capture with an Olympus CKX41 microscope (Olympus Corporation, Tokyo, Japan) and a Motic 3.0 megapixel camera (4x objective; Motic, Kowloon, Hong Kong). Three randomly selected fields of view per replicate (taken from the centre of the well), with three replicates per experiment, were utilised. C2C12 cells, plated in the absence of macrophages or fibroblasts, served as a control. Changes in myoblast number were calculated relative to the number of myoblasts *initially* plated out and expressed as a percentage increase (%).

Migration Analysis

For migration analysis, 50 x 10^3 C2C12 myoblasts were allowed to adhere for 24 hours before undergoing a scratch assay as described by Goetsch *et. al.* (2011) in serum-free DMEM (500 µl). Briefly, while being careful not to disturb the cells on the outer edge, the confluent monolayer of myoblasts at the centre of the well was scratched with a sterile 200 µl loading tip to physically remove myoblasts and create a linear "wound". The remaining cells were washed twice with sterile PBS and serum-free DMEM added (500 µl). They were then incubated for 7 hours and images taken at 0 and 7 hours using an Olympus CKX41 microscope and a Motic 3.0 megapixel camera (4x objective). Percentage wound closure was calculated after tracing the wound edges using the Motic Images Plus 2.0 ML software (Goetsch *et. al.* (2011)).

Immunocytochemistry and Confocal Microscopy

To immunocytochemically identify cells in co-culture, cells were cultured on glass coverslips as described above. Briefly, macrophages (40 x 10^3) or fibroblasts (40 x 10^3) were plated in growth medium at the edge of the well, followed by myoblasts (20 x 10^3) in the centre of the well. The cells were then washed twice with PBS and switched to serum-free DMEM for 24 hours to mimic the proliferation time-frame. To analyse the effect of macrophages on fibroblast *phenotype*, macrophages (40 x 10^3) were plated in growth medium at the edge of the well after which fibroblasts (40 x 10^3) were allowed to adhere in the centre of the well. The cells were then washed twice with PBS and switched to serum-free DMEM for 7 h to mimic the migration time-frame.

Cells were then fixed with 4% paraformaldehyde, washed with PBS, blocked at 4ºC with 5% donkey serum (Cat. D9663, Sigma) and incubated at room temperature for 2 hours with the following primary antibodies as appropriate: polyclonal rabbit anti-desmin antibody (1:500; Cat. ab15200, Abcam, Cambridge, UK), monoclonal mouse anti-TCF-4 antibody (1:20; Cat. 05-511, Merck Millipore, Billerica, MA, USA), polyclonal rabbit anti-E-cadherin (1:40; Cat. sc-7870, Santa Cruz Biotechnology, Dallas,TX, USA) or monoclonal mouse anti-α-smooth muscle actin (SMA) (1:500; Cat. A2547, Sigma). The cells were then washed with PBS and incubated at room temperature for 1 hour in the dark with one of the following appropriate secondary antibodies: Dylight488-conjugated donkey anti-rabbit antibody (1:1000; Cat. 711-485-152, Jackson ImmunoResearch, Newmarket, Suffolk, UK), Dylight594-conjugated

donkey anti-mouse antibody (1:1000; Cat. 715-515-151, Jackson ImmunoResearch) or Dylight488-conjugated donkey anti-mouse antibody (1:2000; Cat. 715-485-151, Jackson ImmunoResearch). Hoescht (1:100; stock 10 mg/ml; Cat. B2261, Sigma) was subsequently added for 10 minutes and coverslips washed with PBS prior to being fixed again with 4% paraformaldehyde (10 mins), washed with PBS and mounted on glass slides with Mowiol (Cat. 81381, Sigma). The cells were viewed with a Zeiss 710 confocal microscope (Carl Zeiss GmbH, Oberkochen, Germany).

Statistical Analysis

Data was determined to be normally distributed; results were analysed using a parametric paired, two-tailed Student's T-test and values of $p < 0.05$ were considered to be statistically significant compared to the control. All data was represented as mean ± SEM.

Results

To initially co-culture two cell populations, macrophages were plated at the outer edge of the well, while myoblasts were cultured in the centre of the well (Figure 2A, B). J774A.1 macrophages are relatively small, circular cells, easily distinguishable from larger, spindle-shaped myoblasts that overlap to an extent with macrophages, allowing for a degree of cell-cell interaction (Figure 2B). This method of co-culture was then successfully repeated using fibroblasts instead of macrophages (Figure 2C). LMTK fibroblasts are larger than J774A.1 macrophages, but smaller than C2C12 myoblasts and have an elongated shape. To establish the "*triple co-culture*", macrophages and fibroblasts were both cultured at the outer edge of the well, while myoblasts were cultured at the centre of the well (Figure 2D). Fibroblasts and macrophages were clearly identified at the *outer edge of the well* via their expression of TCF-4 and E-cadherin respectively (Figure 2E); significant numbers of macrophages and fibroblasts were not observed in amongst the myoblasts at the *centre of the well* (Figure 2E). Our method was established using a 24-well plate, but can be adapted to any culture vessel with circular wells. The advantage of this method over others lies in its simplicity and the fact that it can be established quickly without the need for additional, specialized equipment. A further benefit of our system is that it can be expanded to include more than three cell types; this is crucial when one is trying to mimic the *in vivo* environment.

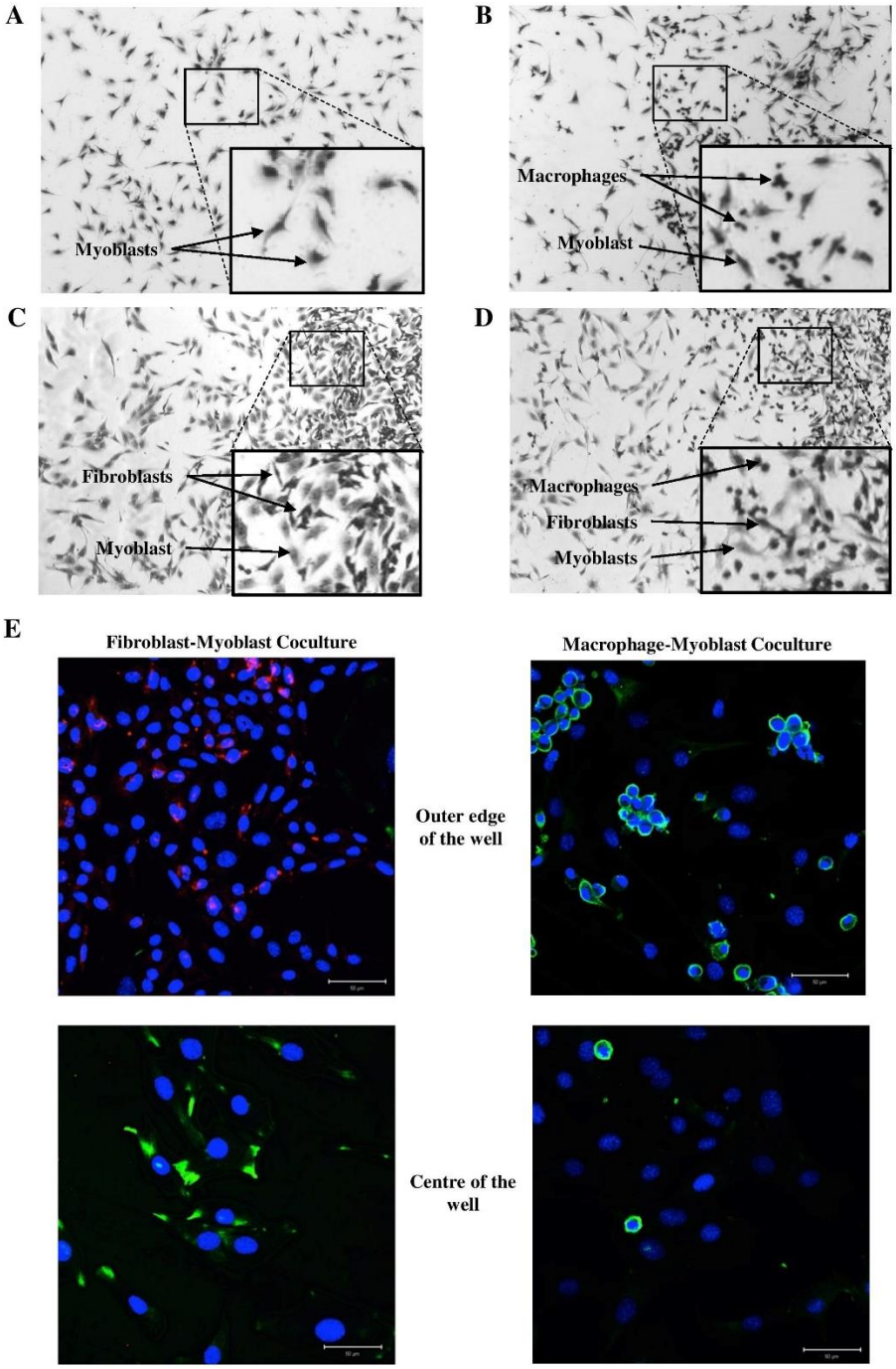

Figure 2: Cell populations in distinct regions of the co-culture plate. A) Myoblasts are at the centre of the well, while **B)** macrophages, **C)** fibroblasts or **D)** macrophages *and* fibroblasts are present predominantly at the outer edge of the culture well (right side of the image) with some overlap with myoblasts. **E)** Fibroblast-myoblast co-cultures (left panel) immunostained with both mouse monoclonal anti-TCF-4 (red; fibroblasts) and rabbit polyclonal anti-desmin (green; myoblasts), while macrophage-myoblast co-cultures (right panel) were immunostained with rabbit polyclonal anti-E-cadherin (green; macrophages). Hoeschst (blue) was used as a nuclear stain. Images were captured using a Zeiss 710 confocal microscope with a 25x objective lens. Scale bar = 50µm. Representative images from the outer edge and centre of the well are shown.

Using our co-culture method, we sought to determine the effect of macrophages and fibroblasts on myoblast proliferation and migration. Co-culture experiments revealed that macrophages and fibroblasts promote the proliferation of myoblasts (Figure 3A). Relative myoblast numbers already showed a small significant increase from 130 ± 4.38% to 146 ± 4.12% (16% increase; $p < 0.05$) when co-cultured for 24 hours with 5 x 10^3 macrophages compared to control (Figure 3B). A maximal effect was reached following co-culture with 80 x 10^3 macrophages (188 ± 1.75%; $p < 0.05$; Figure 3B). Fibroblasts also increased the proliferation of myoblasts, however a significant, maximal effect was only achieved in response to 20 x 10^3 fibroblasts; when fibroblast numbers were increased further, this pro-proliferative effect was lost (Figure 3C). In response to 20 x 10^3 fibroblasts, relative myoblast numbers increased significantly from 189 ± 8.31% to 232 ± 16.76% ($p < 0.05$); whereas in response to co-culture with 80 x 10^3 fibroblasts, relative myoblast numbers returned to control levels of 187 ± 7.72% (Figure 3C).

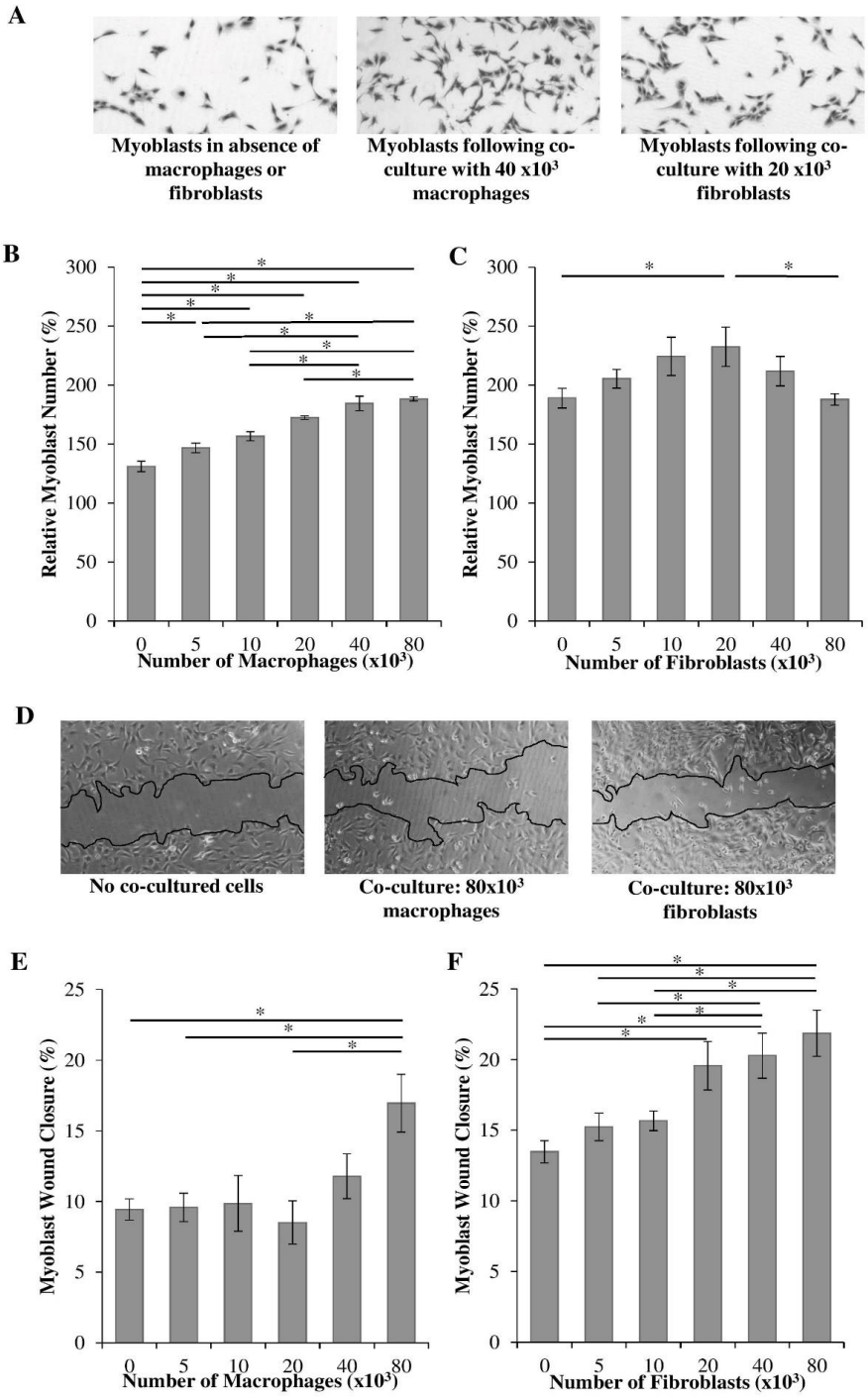

Figure 3: The effect of macrophages or fibroblasts on myoblast proliferation and migration. **A)** Cells were stained with 1% Fuchsin in methanol and viewed using an Olympus CKX41 microscope and images captured with a Motic 3.0 megapixel camera (4x objective lens). **B) and C)** Relative cell number for myoblasts cultured in the presence of increasing numbers of macrophages or fibroblasts, respectively. **D)** The wound area of myoblasts was visualized using an Olympus CKX41 microscope and images captured with a Motic 3.0 megapixel camera (4x objective lens). **E and F)** Percentage wound closure at 7 hours for myoblasts cultured in the presence of increasing numbers of macrophages or fibroblasts, respectively. * = $p < 0.05$; B, C and E: N=6; F: N=5).

Analysis of myoblast migration revealed that co-culture with 80 x 10^3 macrophages resulted in a significant increase in the percentage wound closure (17.0 ± 2.04%) compared to the control (9.42 ± 0.75%), 5 x 10^3 (9.58 ± 1.00%) and 20 x 10^3 (8.51 ± 1.52%) macrophages (Figure 3D and E; $p < 0.05$). The presence of lower numbers of macrophages had no significant effect on myoblast migration (Figure 3E). When co-cultured with fibroblasts, myoblasts responded by increasing their migration in a cell-density dependent manner (Figure 3D and F). Significant effects were already observed in response to 20 x 10^3 fibroblasts (Figure 3F), rather than at only 80 x 10^3 as seen with macrophages (Figure 3E). Following co-culture with 20 x 10^3 cells, myoblast wound closure had increased significantly to 19.57 ± 1.71% with a maximal significant effect observed in response to 80 x 10^3 cells (21.9 ± 1.62%) compared to the control (13.5 ± 0.79%) ($p < 0.05$; Figure 3F). This data suggests that rising fibroblast numbers promote myoblast motility, while macrophages lose their pro-migratory effect as their numbers decrease.

To determine the *combined* effect of macrophages and fibroblasts on myoblast proliferation and migration, a triple co-culture experiment was carried out where myoblasts were co-cultured with 40 x 10^3 macrophages and 40 x 10^3 fibroblasts. Total cell numbers exceeding 80 x 10^3 cells caused the fibroblasts and macrophages to move to the centre of the well, hence 40 x 10^3 of each cell type was used. Analysis of myoblast *proliferation* revealed that triple co-culture of myoblasts with both macrophages *and* fibroblasts did not significantly change myoblast numbers when compared to conditions using macrophages *or* fibroblasts alone (Figure 4A). The pro-proliferative effect of macrophages on myoblasts was therefore observed, both in the absence and presence of fibroblasts. However, when myoblast *migration* was analysed, triple co-culture of myoblasts with both macrophages *and* fibroblasts abrogated the previous significant positive effect of fibroblasts on myoblast migration (Figure 4B). The pro-migratory effect of fibroblasts on myoblasts was therefore lost in the presence of macrophages. Further immunocytochemistry and confocal microscopy revealed that, whether in the absence or presence of macrophages, fibroblasts expressed alpha smooth muscle actin (α-SMA; Figure 4C). It is well known that the presence of serum promotes the myofibroblast phenotype [23]; it was therefore not unexpected to observe α-SMA expression in these cells. Our results suggest that macrophages do not initiate de-differentiation of myofibroblasts over

the 7h migration period. Interestingly, a decrease in cell number was observed, suggesting perhaps a pro-apoptotic effect of macrophages. This requires further investigation.

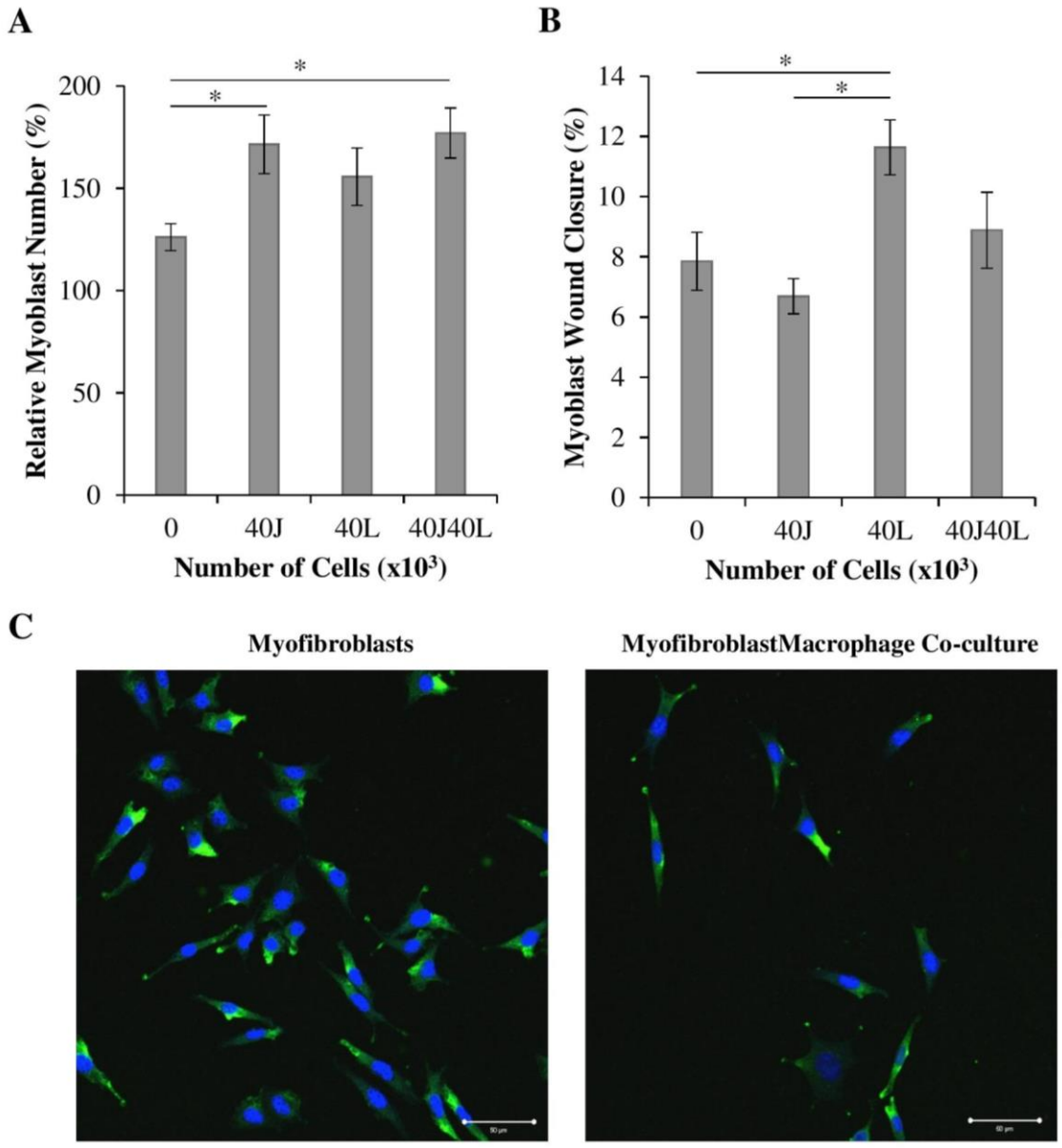

Figure 4: The effect of both macrophages and fibroblasts on myoblast proliferation and migration. A) Relative cell number or **B)** percentage wound closure for myoblasts cultured in the presence of both 40 x 10^3 macrophages and 40 x 10^3 fibroblasts (40J40L). Controls include: no macrophages or fibroblasts (0), 40 x 10^3 fibroblasts alone (40L) or 40 x 10^3 macrophages alone (40J). **C)** Myofibroblasts were cultured alone (left image) or co-cultured with macrophages (right image), immunostained with mouse monoclonal anti-α-SMA antibody (green) and stained with Hoescht (blue). Images were captured using a Zeiss 710 confocal microscope (25x objective). Scale bar = 50μm. * = $p < 0.05$; N=5).

Following muscle injury, the inflammatory response is accompanied by an increasing population of macrophages, followed by the migration of resident fibroblasts that are promoted to proliferate and differentiate to myofibroblasts [24-29]. Triple co-culture studies, utilising macrophages, fibroblasts and myoblasts, revealed that the presence of macrophages negates the pro-migratory effects of fibroblasts on myoblasts. This supports the premise that although an inflammatory response is crucial for repair, under certain conditions, it can negatively affect repair. The pro-proliferative effect of macrophages on myoblasts was however maintained, even in the presence of fibroblasts, suggesting less of an influence of fibroblasts on macrophage-myoblast communication. Previous studies using more than two cell types in culture, the so-called "triple" co-culture, are very limited [30]; in fact, no previous studies have been performed to determine the combined effect of *macrophages* and *fibroblasts* on *myoblast* proliferation and migration. A crucial advantage of the current protocol is that it can be expanded to include additional relevant cell types, such as endothelial cells. In addition, the format allows the user to a) determine the phenotype of the participating cells (e.g. M1 versus M2 macrophages or fibroblasts versus myofibroblasts) using immunocytochemistry and b) polarise the co-cultured cells in order to determine whether distinct populations have differential effects on myoblast proliferation and migration. Our results underscore the importance of including cellular complexity in *in vitro* co-culture systems in order to gain a better understanding of how cellular communication regulates regenerative outcomes in skeletal muscle.

In previous *in vitro* studies, the conditioned media of pro-inflammatory M1 macrophages was found to increase the proliferation of myoblasts, while inhibiting migration [31-34]. In our study, we used unmanipulated macrophages. This may account for some of the differences seen in our results compared to these published studies. It would be valuable to determine whether any change in macrophage phenotype is observed in response to myoblast injury. *In vivo* studies suggest that ablation of fibroblasts leads to depletion of satellite cells, premature satellite cell differentiation and results in smaller regenerated myofibres [35]. *In vitro* studies have shown that increasing fibroblasts in co-culture also promotes the migration of myoblasts [18] and that fibroblasts protect myoblasts from apoptosis during differentiation, promoting myotube formation [36]. This agrees with our current studies showing that the presence of fibroblasts promotes myoblast cell number and migration.

In summary, our optimised triple co-culture assay has numerous advantages: it is easier, simpler and cheaper to establish than conventional techniques, it allows for both direct and indirect cellular communication and it can be expanded in its complexity to include additional cell types such as endothelial cells. Using this model, we confirm that macrophages and fibroblasts are important regulators of myoblast proliferation and migration. We also show, for the first time, that macrophages can negatively influence the ability of fibroblasts to promote myoblast migration, in an *in vitro* wound healing setting. Knowledge generated from this method will further our understanding of the role of cellular interplay in regenerative processes.

Acknowledgements

The work was supported by the South African National Research Foundation (Grant CPRR13091035184; 90502) and the University of KwaZulu-Natal.

References

1. Kaariainen M, Jarvinen T, Jarvinen M, Rantanen J, Kalimo H. Relation between myofibers and connective tissue during muscle injury repair. *Scand J Med Sci Sports*, 10(6), 332-337 (2000).
2. Baoge L, Van Den Steen E, Rimbaut S *et al.* Treatment of skeletal muscle injury: a review. *ISRN Orthop*, 2012, 689012 (2012).
3. Prisk V, Huard J. Muscle injuries and repair: the role of prostaglandins and inflammation. *Histol Histopathol*, 18(4), 1243-1256 (2003).
4. Mann CJ, Perdiguero E, Kharraz Y *et al.* Aberrant repair and fibrosis development in skeletal muscle. *Skelet Muscle*, 1(1), 21 (2011).
5. Ebisui C, Tsujinaka T, Morimoto T *et al.* Interleukin-6 induces proteolysis by activating intracellular proteases (cathepsins B and L, proteasome) in C2C12 myotubes. *Clin Sci (Lond)*, 89(4), 431-439 (1995).
6. Mbebi C, Hantai D, Jandrot-Perrus M, Doyennette MA, Verdiere-Sahuque M. Protease nexin I expression is up-regulated in human skeletal muscle by injury-related factors. *J Cell Physiol*, 179(3), 305-314 (1999).
7. Brigitte M, Schilte C, Plonquet A *et al.* Muscle resident macrophages control the immune cell reaction in a mouse model of notexin-induced myoinjury. *Arthritis Rheum*, 62(1), 268-279 (2010).
8. Chazaud B, Brigitte M, Yacoub-Youssef H *et al.* Dual and beneficial roles of macrophages during skeletal muscle regeneration. *Exerc Sport Sci Rev*, 37(1), 18-22 (2009).
9. Sanderson RD, Fitch JM, Linsernmayer TR, Mayne R. Fibroblasts promote the formation of a continuous basal lamina during myogenesis *in vitro*. *J Cell Biol*, 102(3), 740-747 (1986).
10. Hinz B. Formation and function of the myofibroblast during tissue repair. *J Invest Dermatol*, 127(3), 526-537 (2007).

11. Turner NA, Porter KE. Function and fate of myofibroblasts after myocardial infarction. *Fibrogenesis Tissue Repair*, 6(1), 5 (2013).
12. Thomas K, Engler AJ, Meyer GA. Extracellular matrix regulation in the muscle satellite cell niche. *Connect Tissue Res*, 56(1), 1-8 (2015).
13. Goers L, Freemont P, Polizzi KM. Co-culture systems and technologies: taking synthetic biology to the next level. *J R Soc Interface*, 11(96), pii: 20140065 (2014).
14. Snyman C, Goetsch KP, Myburgh KH, Niesler CU. Simple silicone chamber system for *in vitro* three-dimensional skeletal muscle tissue formation. *Front Physiol*, 4, 349 (2013).
15. Bacchus W, Fussenegger M. Engineering of synthetic intercellular communication systems. *Metab Eng*, 16, 33-41 (2013).
16. Miki Y, Ono K, Hata S, Suzuki T, Kumamoto H, Sasano H. The advantages of co-culture over mono cell culture in simulating *in vivo* environment. *J Steroid Biochem Mol Biol*, 131(3-5), 68-75 (2012).
17. Zhang C, Barrios MP, Alani RM, Cabodi M, Wong JY. A microfluidic Transwell to study chemotaxis. *Exp Cell Res*, 342(2), 159-165 (2016).
18. Goetsch KP, Snyman C, Myburgh KH, Niesler CU. Simultaneous isolation of enriched myoblasts and fibroblasts for migration analysis within a novel co-culture assay. *Biotechniques*, 58(1), 25-32 (2015).
19. Goetsch KP, Myburgh KH, Niesler CU. *In vitro* myoblast motility models: Investigating migration dynamics for the study of skeletal muscle repair. *J Muscle Res Cell Motil*, 34(5-6), 333-347 (2013).
20. Javaherian S, Li KJ, McGuigan AP. A simple and rapid method for generating patterned co-cultures with stable interfaces. *Biotechniques*, 55(1), 21-26 (2013).
21. Cho CH, Park J, Tilles AW, Berthiaume F, Toner M, Yarmush ML. Layered patterning of hepatocytes in co-culture systems using microfabricated stencils. *Biotechniques*, 48(1), 47-52 (2010).
22. D'Arcangelo E, McGuigan AP. Micropatterning strategies to engineer controlled cell and tissue architecture *in vitro*. *Biotechniques*, 58(1), 13-23 (2015).
23. Vaughan MB, Howard EW, Tomasek JJ. Transforming growth factor-beta1 promotes the morphological and functional differentiation of the myofibroblast. *Exp Cell Res*, 257(1), 180-189 (2000).
24. Iyer SS, Pulskens WP, Sadler JJ *et al.* Necrotic cells trigger a sterile inflammatory response through the Nlrp3 inflammasome. *Proc Natl Acad Sci U S A*, 106(48), 20388-20393 (2009).
25. Kharraz Y, Guerra J, Mann CJ, Serrano AL, Munoz-Canoves P. Macrophage plasticity and the role of inflammation in skeletal muscle repair. *Mediators of Inflammation*, 2013(2013), 491497 (2013).
26. Otis JS, Niccoli S, Hawdon N *et al.* Pro-inflammatory mediation of myoblast proliferation. *PLoS One*, 9(3), e92363 (2014).
27. Maxson S, Lopez EA, Yoo D, Danilkovitch-Miagkova A, LeRoux MA. Concise review: Role of mesenchymal stem cells in wound repair. *Stem Cells Transl Med*, 1(2), 142-149 (2012).
28. Bentzinger CF, Wang YX, Dumont NA, Rudnicki MA. Cellular dynamics in the muscle satellite cell niche. *EMBO Rep*, 14(12), 1062-1072 (2013).
29. Landen NX, Li D, Stahle M. Transition from inflammation to proliferation: A critical step during wound healing. *Cell Mol Life Sci*, 73(20), 3861-3885 (2016).
30. Hatherell K, Couraud PO, Romero IA, Weksler B, Pilkington GJ. Development of a three-dimensional, all-human *in vitro* model of the blood-brain barrier using mono-,

co-, and tri-cultivation Transwell models. *J Neurosci Methods*, 199(2), 223-229 (2011).
31. Wynn TA. Cellular and molecular mechanisms of fibrosis. *J Pathol*, 214(2), 199-210 (2008).
32. Cornelison DDW. Context matters: *In vivo* and *in vitro* influences on muscle satellite cell activity. *J Cell Biochem*, 105(3), 663-669 (2008).
33. Martinez FO, Gordon S. The M1 and M2 paradigm of macrophage activation: Time for reassessment. *Reports*, 6, 13 (2014).
34. Ko MH, Li CY, Lee CF, Chang CK, Fang SH. Scratch wound closure of myoblasts and myotubes is reduced by inflammatory mediators. *Int Wound J*, 13(5), 680-685 (2016).
35. Murphy MM, Lawson JA, Mathew SJ, Hutcheson DA, Kardon G. Satellite cells, connective tissue fibroblasts and their interactions are crucial for muscle regeneration. *Development*, 138(17), 3625-3637 (2011).
36. Zhang Y, Li H, Lian Z, Li N. Myofibroblasts protect myoblasts from intrinsic apoptosis associated with differentiation via beta1 integrin-PI3K/Akt pathway. *Dev Growth Differ*, 52(8), 725-733 (2010).

CHAPTER 5: CELLULAR ALIGNMENT AND FUSION: QUANTIFYING THE EFFECT OF MACROPHAGES AND FIBROBLASTS ON MYOBLAST TERMINAL DIFFERENTIATION

Venter C, Niesler CU*

Discipline of Biochemistry, School of Life Sciences, University of KwaZulu-Natal, Private Bag X01, Scottsville 3209, South Africa

**Corresponding author: Prof C.U. Niesler, Tel: (033) 260 5465, Fax: (033) 260 6127, email: niesler@ukzn.ac.za*

Published: Venter and Niesler* (2018). Cellular alignment and fusion: Quantifying the effect of macrophages and fibroblasts on myoblast terminal differentiation. *Experimental Cell Research* 370 (2), 542-550

Abstract

Successful skeletal muscle wound repair requires the alignment and fusion of myoblasts to generate multinucleated myofibers. *In vitro*, the accurate quantification of cellular *alignment* remains a challenge. Here we present the application of ImageJ and ct-FIRE to quantify muscle cell orientation by means of an alignment index (AI). Our optimised method, which does not require programming skills, allows the alignment of myoblasts *in vitro* to be determined independently of a predefined reference point. Using this method, we demonstrate that co-culture of myoblasts with macrophages, but not fibroblasts, promotes myoblast alignment in a cell density-dependent manner. Interestingly, myoblast fusion was significantly *decreased* in response to co-culture with macrophages, while the effect of fibroblasts on fusion was density-dependent. At lower numbers, fibroblasts significantly *increased* myoblast fusion, whereas at higher numbers a significant *decrease* was observed. Finally, triple co-culture revealed that the effect of macrophages on myoblast alignment and fusion is unaltered by the additional presence of fibroblasts. Application of our optimized method has therefore revealed quantitative differences in the roles of macrophages versus fibroblasts during alignment and fusion: while successful myoblast alignment is promoted by increasing macrophage numbers, regenerative fusion coincides with a decreasing macrophage population and initial rise in fibroblast numbers.

Keywords: cellular alignment; co-culture; differentiation; myoblast; macrophage; fibroblast

Introduction

Skeletal muscle represents a heterogenous tissue with multiple cell types that each play distinct and important roles in wound repair [1]. Damage to skeletal muscle results in the disruption of myofibres and the extracellular matrix (ECM) that surrounds them [2]. Myogenesis, the differentiation and fusion of mono-nucleated myoblasts into multi-nucleated myofibers, is a critically important stage of muscle regeneration and serves to restore muscle structure and function [3]. Non-myogenic cell types, such as macrophages and fibroblasts, mediate the behaviour of muscle cells during wound repair by secreting an array of signalling molecules and matrix factors [4,5]. We have previously investigated the effect of these non-myogenic cells on myoblast proliferation and migration. We demonstrated that macrophages promote the proliferation of myoblasts in co-culture, while fibroblasts promote migration, during *in vitro* wound repair; the latter pro-migratory effect was reduced when myoblasts were co-cultured in the presence of both fibroblasts and macrophages under triple co-culture conditions [6,7].

During the terminal phase of myogenesis, myoblasts align to organize themselves relative to each other and to existing myofibres [8]. This process brings the lipid bilayers in close contact with one another in order for the cells to fuse together to form functional muscle with myotubes orientated in the same direction [8]. Several strategies can be used to promote myotube *alignment*, including topographical patterning (e.g. grooved culture plates [9]), mechanical stimulation (e.g. stretch [10]) or application of magnetic/electrical fields [11,12]. In order to *quantify* the exact effect of these strategies on alignment, one has to identify the cell/nuclear outline or actin cytoskeleton, then determine the orientation of these elements and finally calculate a value that represents the extent of alignment [13]. To achieve this, cells are visually identified in images, their outlines manually selected, and their orientation ascertained by determining the angle of deviation of the longitudinal axis of the cell (in degrees) from the x-axis (set to 0°). In the study performed by Xu et. al. (2011), manual analysis (using several individuals to limit human bias) was compared to automated image processing techniques, such as the Fast Fourier Transform and local intensity gradient [14,15]. Manual analysis was accurate, but arduous and time-consuming with low throughput. [13]. Furthermore, the automated image processing techniques have previously been used to determine cellular orientation; however, these approaches were designed for determining the

orientation of a type of pattern rather than determining the orientation of cells and therefore yield low alignment scores [13].

Xu *et. al.* (2011) addressed the challenges of these techniques by developing the Binarization-based Extraction of Alignment Score (BEAS) method to rapidly and accurately quantify the alignment of cells [13]. However, a major challenge with BEAS (and other previous methods) is that the information required to determine cellular orientation is presented as a complex image-processing algorithm, which needs to be computed in MATLAB (a costly computer programming language and computing environment). This implementation is problematic for researchers who have neither programming experience nor access to MATLAB. An easily accessible, automated method to quantify *cellular* orientation was therefore required.

ct-FIRE is a freely available, standalone and fully developed framework designed to determine the orientation of *collagen fibres;* it has not been tested for its ability to determine *cellular* orientation [16]. In order to adapt ct-FIRE to measure cellular orientation, a number of approaches can be used. Data can be organized into 10° bins and either represented as a histogram of frequency distribution (however, this gives no indication of the extent of alignment and makes significance testing problematic) or used to calculate the degree of alignment. In the latter method, cells within less than 10° of the preferred orientation are considered aligned and the percentage of cells in that particular frequency is then calculated [17,18]. Alternatively, an alignment index (AI), which determines how well cells align in a specified direction can be calculated [18-20]. An AI is generally easier to calculate if there is a set direction to which orientation can be compared (e.g. directional angle of the grooves on a plate or the average direction of the cells in a culture dish). However, under standard myoblast culture conditions, there is often no set direction to which alignment can be compared as the cells align independently of physical properties of culture plate and subsequently self-organize in response to elongating myoblasts during fusion [21].

In the current study, we present a method for determining cellular alignment; this method does not require a pre-defined reference direction. ct-FIRE is first tested for its ability to determine the alignment of elliptical shapes (representing hypothetical cells) compared to linear collagen shapes (for which the programme was developed); the orientation determined by ct-FIRE is compared to actual orientation using the AI (Figure 1A). We then generate an

alignment model, creating data sets with defined standard deviations, which represent hypothetical images of cells aligned to different extents (Figure 1B). These hypothetical images are then rotated, and an AI calculated using either the *average* (i.e. the mean direction of cell alignment) or *preferred* (i.e. direction in which most cells are aligned) orientation (Figure 1B). Lastly, we test our method using images of cultured myoblasts, where the image processing capability of ImageJ is first applied to automatically mark the boundaries of cells and ct-FIRE is subsequently used to analyse cellular orientation and calculate an AI (Figure 1C) [13,16]. Once established, we then apply this protocol to assess the effect of macrophages and fibroblasts on the alignment of myoblasts during fusion. This accessible, optimised method for the analysis of cellular orientation presents a tool for analysis of alignment *in vitro*. Our results highlight the distinct regulatory role of non-myogenic cells on alignment and fusion during terminal skeletal muscle differentiation.

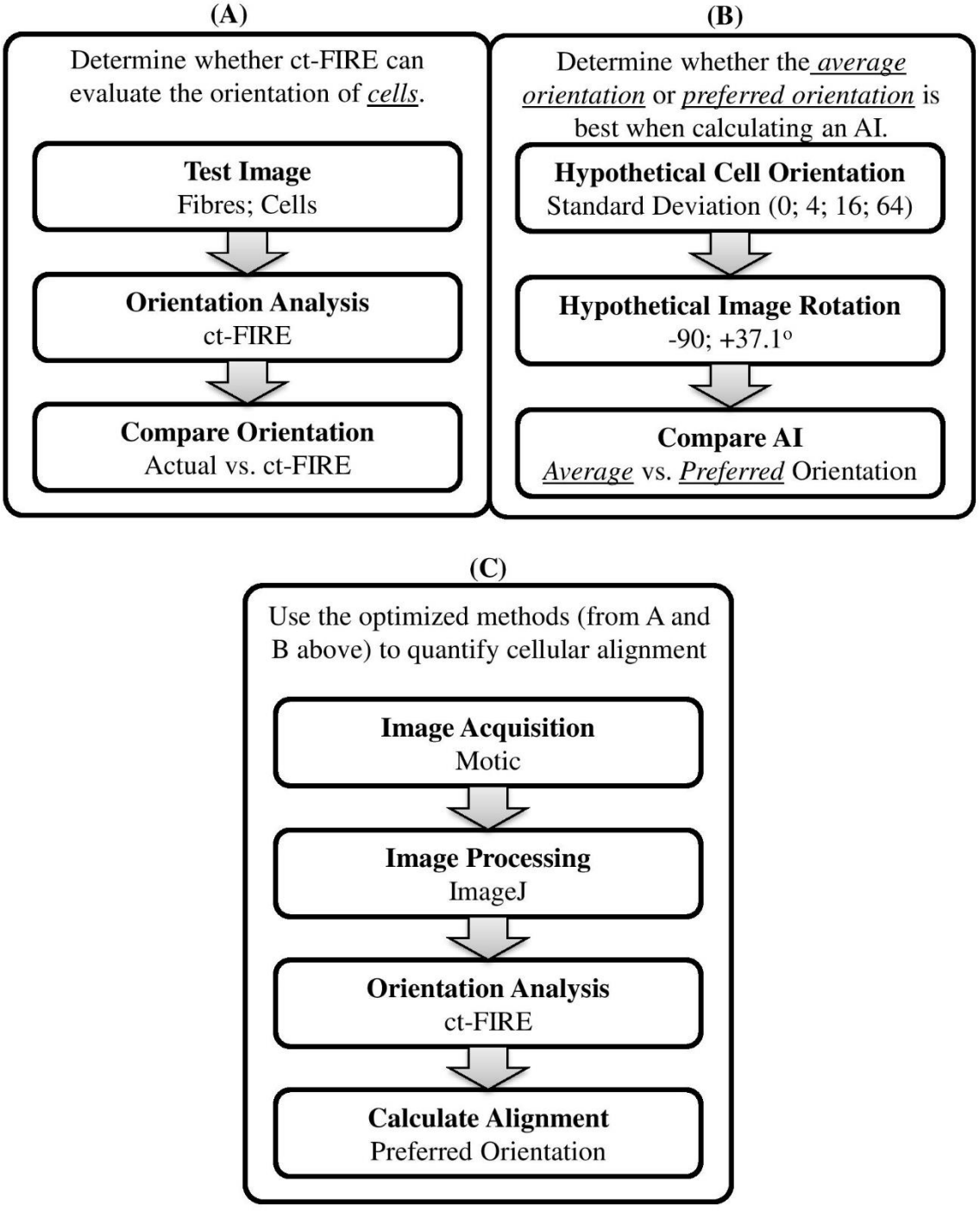

Figure 1: Overview of methodology development. A) ct-FIRE was tested for its ability to determine the orientation of linear versus elliptical shapes, representing either collagen or cells, respectively. **B)** A model for alignment was created using Microsoft Excel to represent hypothetical cells that were then rotated at -90 and +37.1˚ ; their alignment was calculated and compared using the *average* orientation versus *preferred orientation*. **C)** Images of differentiating myoblasts were then acquired, and the AI calculated using the preferred orientation.

Materials and Methods

Testing ct-FIRE on Images of Hypothetical Cells

The programme ct-FIRE was initially developed to determine the alignment of collagen fibres; these fibres have linear shapes as opposed to elliptical shapes that are classically associated with elongated spindle-shaped cells. Linear and elliptical shapes were therefore created using Microsoft PowerPoint (2016) and orientated at 0˚, 30˚, 60˚, 90˚, 120˚ and 150˚ (Figure 2); these orientations represent *x* in the equation below, where N is the total number of orientations [20,22]:

$$\textit{Alignment Index (AI)} = \frac{1}{N}\sum_{i=1}^{N}(2\,[cos(x-y)]^2 - 1)$$

ct-FIRE was then tested to determine whether it would be able to measure the orientation of both shapes, generating the value *y* in the above equation. An AI value of 0 represents no agreement between *x* and *y*, while a value of 1 represents a perfect agreement (i.e. *x* equals *y*). This evaluated how well the orientation determined by ct-FIRE agrees with the actual orientation.

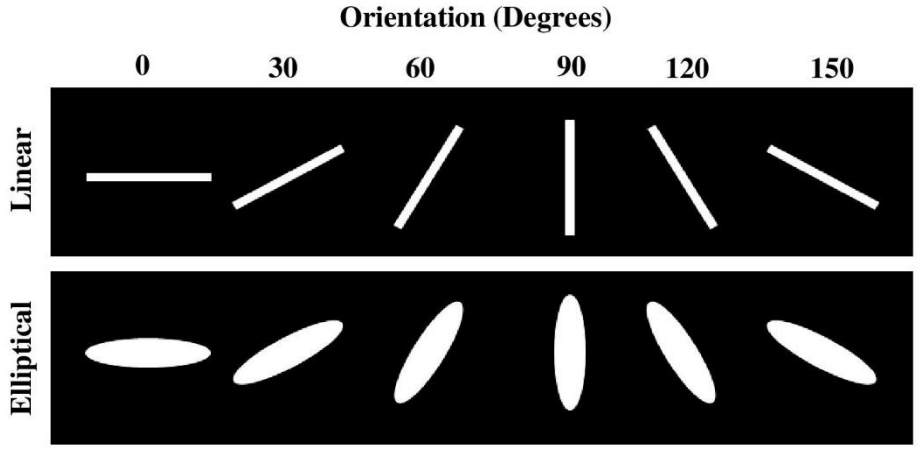

Figure 2: Representative images of collagen fibres (linear) and cells (elliptical). Hypothetical shapes representing collagen fibres and cells were created using Microsoft PowerPoint orientated at 0˚, 30˚, 60˚, 90˚, 120˚ and 150˚.

Alignment Modelling

A set of normally distributed random data (N=98) around a mean (set to 90) with a specified standard deviation (0, 4, 16, 64) (Supplementary Table 1) was created using the Microsoft Excel (2016) *=NORM.INV (probability; mean; standard deviation)* function with *=RAND()* as the probability (which creates a random factional value: $0 \leq \alpha \leq 1$). The values in this data set represent theoretical directions in which an "image" containing 98 cells are likely to be orientated (the smaller the standard deviation, the greater the extent of alignment, and *vice versa*). Using this model, a cell orientated at 180˚ has the same alignment as a cell orientated at 0˚. Similarly, 225˚ equals 45°, 270˚ equals 90˚ and so on. Therefore, 180˚ was subtracted from values ≥ 180˚ and added to values < 0˚ in order to represent cell direction exclusively between 0˚ and 180˚. In order to rotate hypothetical images of these cells, every theoretical cell in a data set was shifted by -90˚ or +37.1˚ and values ≥ 180˚ or < 0˚ adjusted accordingly. For every data set, the *average orientation* (an average of all orientations) and *preferred orientation* (an average of cell orientations in the frequency bin with the largest value) was calculated and used in the same alignment index equation stated earlier, where N is now the total number of cells, *x* is the *average* OR *preferred orientation* used as a reference point of the data set and *y* is the orientation of an individual cell within that data set. This equation determines how well a cell aligns along a particular direction (e.g. a fixed point of reference) or along the average/preferred direction of cells within each individual cell in a data set. The alignment index of every cell in a data set was used to calculate an average alignment index (of all the cells in that data set) between 0 and 1, where 0 represents a group of cells that are randomly orientated and 1 represents a population that is perfectly aligned [22]. The AI was first calculated using the *average orientation* (often associated with a defined reference point [17,18,20]) and this was repeated using the *preferred orientation* of the data set, in order to compare the two.

Cell Culture

Mouse C2C12 myoblasts (ATCC, USA, cat. CRL-1772™), LMTK fibroblasts (ATCC, USA, cat. CCL-1.3™) and J774A.1 macrophages (ATCC, USA, cat. TIB-67™) were cultured at 37˚C and 5% CO_2 and maintained in growth medium (GM) containing Dulbecco's Modified Eagle's Medium (DMEM, Capital Lab Supplies, South Africa, cat. D5648) supplemented with 10% (v/v) Fetal Bovine Serum (FBS, Gibco, USA, cat. 10500) and 2% (v/v) Penicillin-

Streptomycin (PenStrep, LONZA, Switzerland, cat. DE17-602E). Media was changed every 48 hours.

Co-culture of macrophages and/or fibroblasts with myoblasts was established as described in Venter and Niesler (2018) [6]. Briefly, for double co-culture, macrophages or fibroblasts (0, 5, 10, 20, 40 and 80 x 10^3) were plated on the outer edge of the well of a 24-well culture plate in GM for an hour to promote adherence; C2C12 myoblasts (50 x 10^3 cells) were then plated and left to adhere in the centre of the same well for 24 hours in GM. For triple co-culture, both macrophages (40 x 10^3) and fibroblasts (40 x 10^3) were plated on the outer edge and myoblasts plate in the centre as described above. Myoblasts were differentiated for 5 days in differentiation medium (DM; 2% FBS in DMEM) with media changed every 2-3 days. After differentiation, the cells were stained with 1% Fuchsin (Capital Lab Supplies, South Africa, cat. 47860) in methanol (15 minutes), washed three times with distilled water, left to air dry overnight, and evaluated for alignment and fusion.

Evaluating Alignment

Images (5 randomly selected fields of view; 2 replicates per experiment; 10 images in total) of differentiated myoblasts were taken with an Olympus CKX41 microscope and a Motic 3.0 megapixel camera (10x objective lens) (Supplementary Figure 1A) and processed with ImageJ, using an adaptation of the binarization method described by Xu *et. al.* [13] (Supplementary Figure 1B). The image was converted to grayscale (*Image → Type → 8-bit*), image noise removed (*Process → Noise → Despeckle*) and a mean threshold applied (*Image → Adjust → Auto Local Threshold: Mean; Uncheck "White objects on black background"*) and further processed with ct-FIRE (Supplementary Figure 1C). The AI was then calculated using the *preferred* orientation of cells (as described earlier).

Fusion Index

Images (5 randomly selected fields of view; 2 replicates per experiment) of differentiated C2C12 myoblasts (day 5) were taken with an Olympus CKX41 microscope and a Motic 3.0 megapixel camera (20x objective lens) and the fusion index calculated as follows:

$$\text{Fusion Index (\%)} = (\text{No. of myotube nuclei } (\geq 3 \text{ nuclei})/\text{Total no. nuclei}) \times 100$$

Statistical Analysis

Data was determined to be normally distributed; all results were analysed using a parametric paired, two-tailed Student's T-test and values of $p < 0.05$ were considered to be statistically significant compared to the control. All data was represented as mean ± SEM. Experiments were repeated 3 to 5 times.

Results

ct-FIRE can determine the orientation of cell-like shapes

ct-FIRE was originally developed to determine the orientation of linear collagen fibres, but its ability to determine the orientation of elliptical cell-like shapes had not been evaluated. The AI's of linear versus elliptical shapes were determined to be 0.9992 versus 0.9999 respectively (Table 1), demonstrating that ct-FIRE is able to determine the orientation of both shapes with a very high degree of accuracy (maximum AI = 1). No significant differences in AI calculation between linear and elliptical shapes were observed. This demonstrates that ct-FIRE can be used to accurately determine the orientation of elliptical shaped objects, such as cells.

Table 3: Comparison of the alignment index for hypothetical linear and elliptical shapes.

Shape	Linear	Elliptical
Mean	0,9992	0,9999
SD	0,0005	0,0002

An alignment index (AI) was calculated to determine how well the orientation of the linear and elliptical shapes, as determined by ct-FIRE, agrees with the actual known orientation.

Calculation of cellular alignment should use preferred rather than average orientation

The rotation of a hypothetical image of aligned cells (orientated at 90˚) by -90˚ or +37.1˚ (Figure 3) does not change *how* they are aligned, but merely shifts the *direction* in which they are aligned (0˚ or 127.1˚, respectively). The data set in Supplementary Table 1 represents either a population of hypothetical cells that are perfectly aligned (SD = 0), somewhat aligned (SD = 4 or 16) or unaligned and randomly orientated (SD = 64).

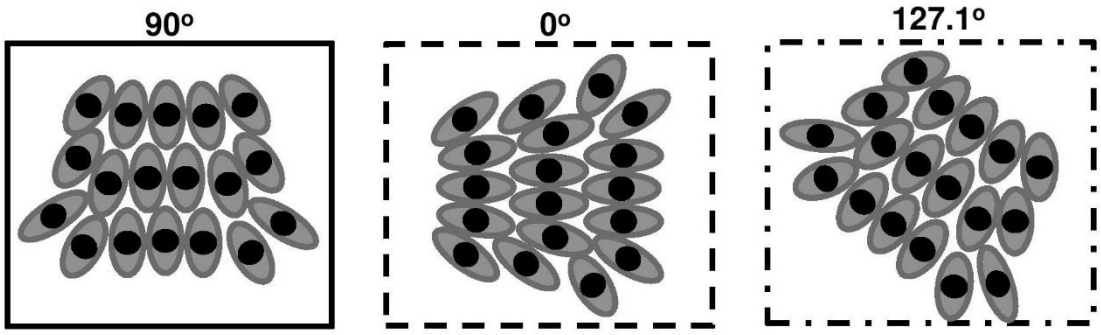

Figure 3: Model of Alignment. Schematic to show that a group of cells can be orientated in any direction (90˚, 0˚ or 127.1˚) and still have the same degree of alignment.

The alignment index (AI), for each data set representing a hypothetical image of cells (Table 2) with different degrees of alignment (SD = 0, 4, 16 and 64) was then compared, following calculation, using the *average orientation* and *preferred orientation;* the significance within SD's was subsequently tested between 90˚ and either 0˚ or 127.71˚ orientations. When comparing the AI generated for cells orientated at 90˚ and 127.71˚ using the *average orientation*, there was no significant difference irrespective of the SD (Table 2). When comparing cells orientated at 90˚ with those oriented 0˚, there was significant difference for SD's 4, 16 and 64. For instance, for SD = 4, the AI was 0.98 at 90˚ when using the *average orientation* which was significantly different when compared with -0.94 at 0˚ (Table 2). There was no significant difference between 90˚ versus 0˚ and 90˚ versus 127.1˚ for any of the standard deviations when using the *preferred orientation*. This suggests that using the *average orientation* as a point of reference to calculate the AI of cells will yield inaccurate results when an image is orthogonally rotated; using the preferred orientation yields the same AI regardless of which direction an image may be rotated.

Table 4: Comparison of the alignment index of data sets with different standard deviations, calculated using the *average* vs. the *preferred orientation*.

Alignment Index (AI)						
	Average Orientation			Preferred Orientation		
SD	90°	0°	127.1°	90°	0°	127.1°
0	1	1	1	1	1	1
4	0,98	-0,94*	0,98	0,98	0,98	0,98
16	0,87	-0,85*	0,88	0,85	0,85	0,86
64	0,16	-0,15*	0,02	0,14	0,14	0,15

Data sets with increasing standard deviations (and orientated about 90˚) were created using Microsoft Excel. These data sets represent hypothetical cells aligned to different extents. Hypothetical cells were shifted to 0° and 127.1˚ and the alignment index calculated compared to the *average* and the *preferred orientation*. * = $p < 0.05$ compared to the alignment index (AI) at 90˚.

Macrophages inhibit fusion, but promote alignment of myoblasts in a density-dependent manner

Once we had determined that the *preferred orientation* was more appropriate in determining cellular AI's, we went on to evaluate the effect of macrophages on myoblast alignment. Visual analysis of co-culture of macrophages with myoblasts (Figure 4) suggested that macrophages had differing effects of alignment versus fusion (Figure 4A). Following calculation, it was evident that the myoblast AI was significantly increased in response to 5 x 10^3 macrophages (0.21 ± 0.02; $p < 0.05$) and continued to increase in a cell density-dependent manner reaching a maximum effect at 80 x 10^3 cells (0.46 ± 0.03; $p < 0.05$), compared to the control (0.14 ± 0.02) (Figure 4B). Co-culture with macrophages, however, was observed to negatively impact fusion (Figure 4C), with 20 x 10^3 macrophages causing a significant decrease in the fusion at day 5 (14.88 ± 0.75 %; $p < 0.05$) compared to the control (19.55 ± 0.15 %). Macrophages continued to negatively affect myoblast fusion in a density-dependent manner with 80 x 10^3 macrophages having the greatest significant effect (6.08 ± 0.49 %; $p < 0.05$) compared to the control.

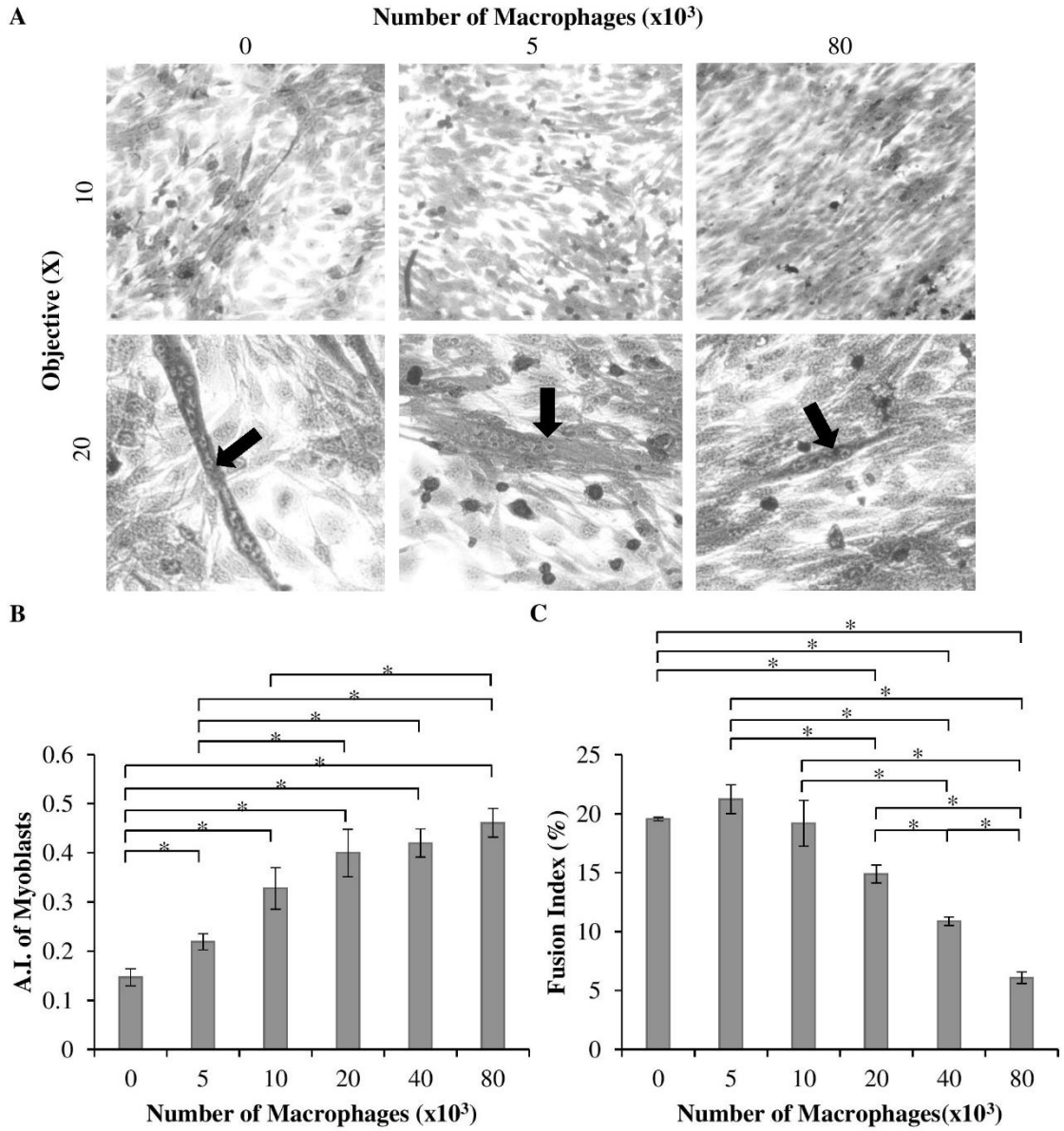

Figure 4: The effect of macrophages on the alignment and fusion of myoblasts. Macrophages (0 (control), 5, 10, 20, 40 and 80 x 10^3) were co-cultured with differentiating myoblasts for 5 days, stained with Fuchsin and viewed using an Olympus CKX41 microscope **A)** Images of myoblasts co-cultured with increasing numbers of macrophages (0, 5 and 80 x 10^3) captured with a Motic 3.0 megapixel camera; arrows indicate differentiated myotubes. **B)** Cell orientation and alignment index (AI) evaluated using ct-FIRE and the alignment index (AI) calculated. **C:** Fusion index (%). * = $p < 0.05$; Alignment: N=4; Fusion: N=3

Fibroblasts do not significantly alter myoblast alignment, but have differential effects on fusion

Co-culturing fibroblasts with myoblasts resulted in no observable difference in alignment; it appears though that lower fibroblast numbers were associated with larger myotubes, while co-cultures with higher fibroblast numbers displayed smaller myotubes (Figure 5A). Quantification of AI revealed no significant increase in myoblast alignment in response to these non-myogenic cells; indeed, AI values did not exceed 0.27 under any conditions (Figure 5B). However, a significant increase in the fusion index was observed in response to 5×10^3 fibroblasts (42.28 ± 3.47 %; $p<0.05$) in comparison with the control (24.23 ± 1.93 %) (Figure 5C). When further increasing the number of fibroblasts, this positive effect was slowly lost until in fact, at 80×10^3 fibroblasts, a significant decrease in fusion is observed (12.62 ± 0.75 %; $p < 0.05$) compared to control (Figure 5C).

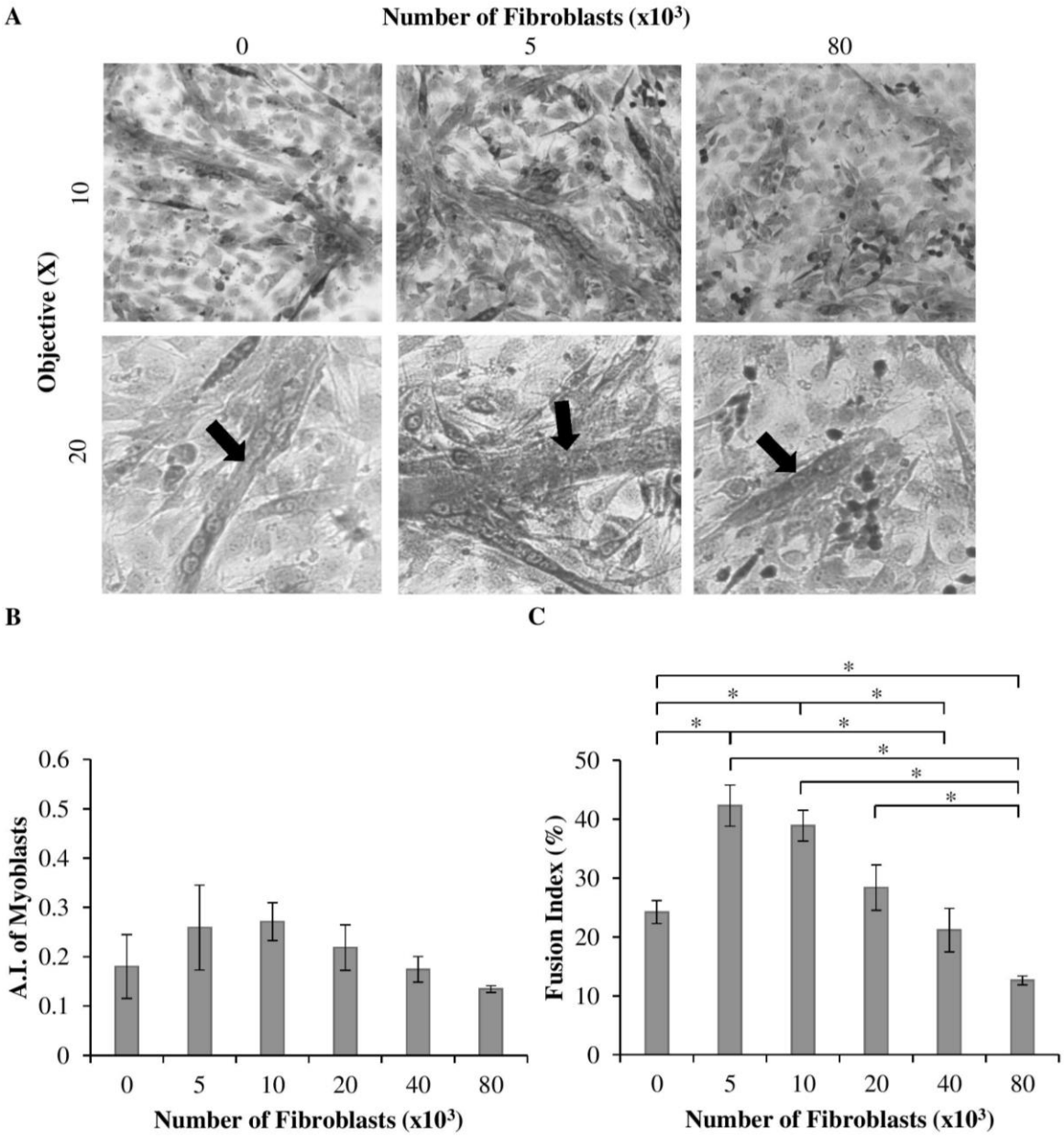

Figure 5: The effect of fibroblasts on the alignment and fusion of myoblasts. Fibroblasts (0, 5, 10, 20, 40 and 80 x 10^3) were co-cultured with differentiating myoblasts for 5 days, stained with Fuchsin and viewed using an Olympus CKX41 microscope. **A)** Images of myoblasts co-cultured with increasing numbers of fibroblasts (0, 5 and 80 x 10^3) captured with a Motic 3.0 megapixel camera; arrows indicate differentiated myotubes. **B)** Cell orientation and alignment index (AI) evaluated using ct-FIRE. **C)** Fusion index (%). * = $p < 0.05$; Alignment: N=3; Fusion: N=3

Macrophages continue to promote myoblast alignment and inhibit fusion in the presence of fibroblasts

In order to determine the effect of an inflammatory *and* fibrotic environment on myoblast differentiation, triple co-cultures of macrophages and fibroblasts with myoblasts were carried out (Figure 6). Analysis of myoblast alignment showed that macrophages (40 x 10^3) on their own continued to significantly promote the alignment of myoblasts (0.45 ± 0.03) compared to the control (0.05 ± 0.01; $p < 0.05$), while fibroblasts (40 x 10^3) had no significant effect (Figure 6A). Co-culture of macrophages (40 x 10^3) with myoblasts continued to have a negative effect on myoblast fusion (6.37 ± 0.87%; $p < 0.5$) compared to the control (12.90 ± 1.00%), while fibroblasts (40 x 10^3) continued to have no significant effect on myoblast fusion (Figure 6B). When macrophages and fibroblasts were co-cultured with myoblasts, macrophages maintained both their positive effect on myoblast alignment (0.38 ± 0.03; $p < 0.05$; Figure 6A) and their negative effect on myoblast fusion (7.51 ± 0.51; $p < 0.05$; Figure 6B) compared to the control.

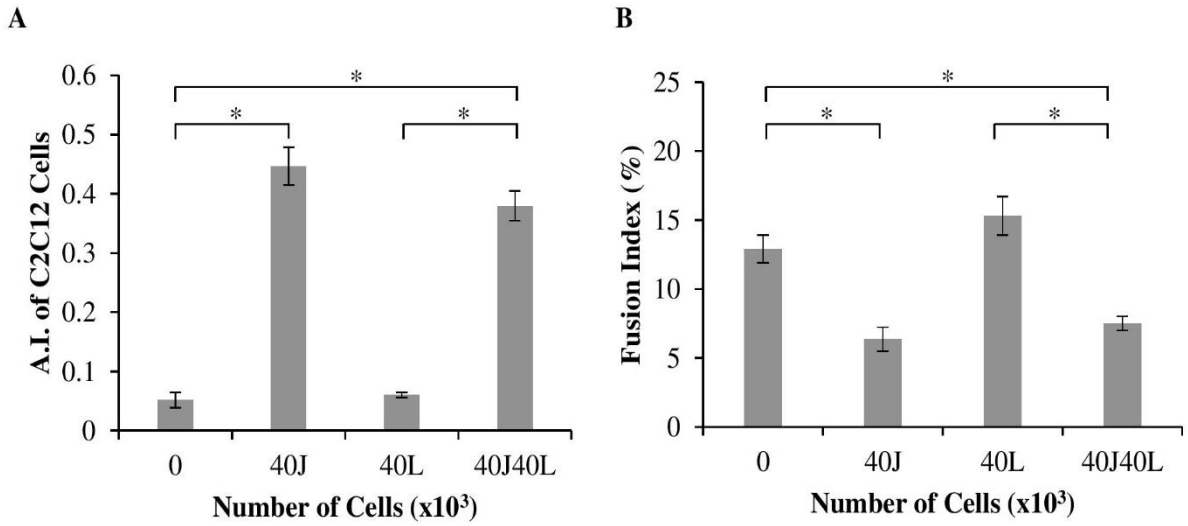

Figure 6: The effect of macrophages and fibroblasts on the alignment and fusion of myoblasts. Macrophages (40J; 40 x 10^3 cells), fibroblasts (40L; 40 x 10^3 cells) or both macrophages and fibroblasts (40J40L; 40 x 10^3 cells, each) were co-cultured with differentiating myoblasts for 5 days. **A)** Alignment index (AI). **B)** Fusion index (%). * = $p < 0.05$; Alignment: N=5; Fusion: N=5

Discussion

Skeletal muscle has the remarkable ability to repair itself post-injury. In order for this process to occur, satellite cells become activated, migrate into the wound, align with one another as well as existing muscle, and differentiate to form multi-nucleated myotubes [23]. Alignment is an important step during myogenesis, because it orientates the muscle cells in a similar direction and brings lipid membranes together; this allows the cells to fuse and form multinucleated myofibres with parallel longitudinal axes [8,24]. Muscle cells that are cultured *in vitro* maintain their ability to align and can do so without a predefined template [21].

A number of previous studies have used physical templates, such as grooves in a culture well, to improve myoblast alignment *in vitro* [19,21,25,26]. The alignment of these cells was quantified by determining their orientation relative to these grooves, which were set as the reference. Cells orientated in the direction of these grooves were classified as perfectly aligned (AI = 1), whereas those that were randomly orientated around the reference point were deemed unaligned (AI = 0) [13,22]. A problem however arises when cells are able to align in the absence of a template; under these circumstances there is no point of reference for assessment of AI. We therefore sought to develop a method to address this shortcoming.

Random data sets with a range of standard deviations were created in order to represent cells aligned to different degrees. The smaller the standard deviation within this set, the better the alignment; conversely, the higher the standard deviation, the greater the random orientation. The overall alignment of all the "cells" in the image can be determined by either calculating the mean (referred to as the "*average orientation*") or the mode (referred to as the "*preferred orientation*") of the data set. Rotating this image (irrespective of the standard deviation) should not change the AI, because it merely shifts the direction in which all the "cells" are all distributed. When the AI was calculated using the *average orientation*, it did not however remain the same when the data set was shifted; on the other hand, when the *preferred orientation* was used, the AI remained the same no matter what direction the data set was shifted. For this reason, we subsequently used the *preferred orientation* in all subsequent calculations.

The orientation of each individual cell can be manually determined by measuring the angle at which it lies relative to another cell [13]. However, this becomes unfeasible when dealing

with high numbers of cells. There are few available programs that can perform automated alignment assessment without the need for programming skills. ct-FIRE, software originally designed to determine the orientation of collagen fibres (in essence, straight lines) is one such program [16]. In order to test and compare its ability to determine the orientation of elliptical cell-like shapes, images of straight lines (akin to "collagen") and ellipsis (akin to "cells") were created, orientated in known directions. ct-FIRE was then employed to determine the orientation of these shapes; the measured orientation was then evaluated to determine how well it matched the actual alignment. It was determined that ct-FIRE could not only precisely determine the orientation of *straight* lines as it was intended, but could also be used to measure alignment of *elliptical* cell-like shapes. ct-FIRE is therefore an appropriate tool for the calculation of cellular AI *in vitro*.

Next, we sought to use our established method to determine the effect of macrophages and fibroblasts on myoblast alignment and fusion. Pro-inflammatory macrophages are prevalent in the early stages of wound repair and are important for clearing necrotic debris and apoptotic cells [27,28]. These macrophages are also known to secrete a host of pro-inflammatory signalling molecules that regulate muscle regeneration, however the mechanisms regulating this are unclear [29,30]. Moreover, these soluble factors secreted by M1 macrophages have previously been shown to inhibit myoblast fusion without direct contact [31]. Co-cultures of macrophages with myoblasts demonstrated, for the first time, that macrophages significantly improve the *alignment* of myoblasts during differentiation. Co-culture with as few as 5×10^3 macrophages and up to 80×10^3 macrophages resulted in significantly increased myoblast alignment. Subsequent analysis of fusion suggests that, while the lower macrophage number has no effect on fusion, higher numbers significantly decrease it. Additional triple co-culture studies showed that this effect of macrophages on myoblasts differentiation was not altered by the presence of fibroblasts. This suggests that, whether in the presence or absence of fibroblasts, macrophages are important in the early stages of myogenesis in order to correctly orientate and align the cells. while their resolution may be crucial during terminal differentiation.

Fibroblasts are important in muscle regeneration because they are known secretors of ECM scaffold components, such as collagen I and III [32,33]. Fibroblasts, upon *in vivo* muscle injury, differentiate to form the ECM-secreting "myofibroblasts" [32,34]; *in vitro*, the

myofibroblast phenotype is commonly generated in response to serum [35]. As with macrophages, an extended presence of myofibroblasts may lead to aberrant muscle regeneration [5]. When fibroblasts were co-cultured with myoblasts, no significant effect was observed on alignment. Evaluating the effect of myofibroblasts on myoblast fusion, revealed that low numbers of myofibroblasts (5×10^3) significantly promoted fusion. However, as the number of myofibroblasts increased, fusion decreased in a cell density-dependent manner to the point where at the highest numbers, fibroblasts significantly lowered myoblast fusion in comparison to control. The data suggests that while fibroblasts may not be central regulators of myoblast alignment, their effect on fusion is significant, but highly dependent on their density.

In summary, we have optimised a protocol for the quantification of cellular alignment, which can calculate the alignment index of a population of cells in the absence of a predefined reference template. Evaluating the effect of macrophages and fibroblasts on myoblast alignment during differentiation, we showed that macrophages had opposing effects on myoblast alignment versus fusion, promoting and inhibiting these processes, respectively. Furthermore, while fibroblasts had no significant effect on myoblast alignment, they could either promote or inhibit fusion depending on their density. Finally, the presence of fibroblasts did not alter the effect of macrophages on myoblast differentiation. This accessible alignment analysis tool can now be used to provide further insight into the regulation of cellular orientation during myogenesis and other processes.

Acknowledgements
The work was supported by the South African National Research Foundation (Grant CPRR13091035184; 90502) and the University of KwaZulu-Natal.

References

1. Ceafalan LC, Popescu BO, Hinescu ME. Cellular players in skeletal muscle regeneration. *Biomed Res Int*, 2014(2014), 957014 (2014).
2. Kaariainen M, Jarvinen T, Jarvinen M, Rantanen J, Kalimo H. Relation between myofibers and connective tissue during muscle injury repair. *Scand J Med Sci Sports*, 10(6), 332-337 (2000).
3. Villalta SA, Nguyen HX, Deng B, Gotoh T, Tidball JG. Shifts in macrophage phenotypes and macrophage competition for arginine metabolism affect the severity of muscle pathology in muscular dystrophy. *Hum Mol Genet*, 18(3), 482-496 (2009).
4. Bosurgi L, Manfredi AA, Rovere-Querini P. Macrophages in injured skeletal muscle: a perpetuum mobile causing and limiting fibrosis, prompting or restricting resolution and regeneration. *Front Immunol*, 2, 62 (2011).
5. Mann CJ, Perdiguero E, Kharraz Y *et al.* Aberrant repair and fibrosis development in skeletal muscle. *Skelet Muscle*, 1(1), 21 (2011).
6. Venter C, Niesler C. A triple co-culture method to investigate the effect of macrophages and fibroblasts on myoblast proliferation and migration. *Biotechniques*, 64(2), 52-58 (2018).
7. Goetsch KP, Snyman C, Myburgh KH, Niesler CU. Simultaneous isolation of enriched myoblasts and fibroblasts for migration analysis within a novel co-culture assay. *Biotechniques*, 58(1), 25-32 (2015).
8. Rochlin K, Yu S, Roy S, Baylies MK. Myoblast fusion: When it takes more to make one. *Dev Biol*, 341(1), 66-83 (2010).
9. Wang PY, Yu HT, Tsai WB. Modulation of alignment and differentiation of skeletal myoblasts by submicron ridges/grooves surface structure. *Biotechnol Bioeng*, 106(2), 285-294 (2010).
10. Ahmed WW, Wolfram T, Goldyn AM *et al.* Myoblast morphology and organization on biochemically micro-patterned hydrogel coatings under cyclic mechanical strain. *Biomaterials*, 31(2), 250-258 (2010).
11. Coletti D, Teodori L, Albertini MC *et al.* Static magnetic fields enhance skeletal muscle differentiation in vitro by improving myoblast alignment. *Cytometry A*, 71(10), 846-856 (2007).
12. Tanaka T, Hattori-Aramaki N, Sunohara A *et al.* Alignment of skeletal muscle cells cultured in collagen gel by mechanical and electrical stimulation. *International Journal of Tissue Engineering*, 2014, 1-5 (2014).
13. Xu F, Beyazoglu T, Hefner E, Gurkan UA, Demirci U. Automated and adaptable quantification of cellular alignment from microscopic images for tissue engineering applications. *Tissue Eng Part C Methods*, 17(6), 641-649 (2011).
14. Tonar Z, Nemecek S, Holota R *et al.* Microscopic image analysis of elastin network in samples of normal, atherosclerotic and aneurysmatic abdominal aorta and its biomechanical implications. *J Appl Biomed*, 1, 149-159 (2003).
15. Chaudhuri BB, Kundu P, Sarkar N. Detection and gradation of oriented texture. *Pattern Recognition Letters*, 14(2), 147-153 (1993).
16. Bredfeldt JS, Liu Y, Pehlke CA *et al.* Computational segmentation of collagen fibers from second-harmonic generation images of breast cancer. *J Biomed Opt*, 19(1), 16007 (2014).
17. Aubin H, Nichol JW, Hutson CB *et al.* Directed 3D cell alignment and elongation in microengineered hydrogels. *Biomaterials*, 31(27), 6941-6951 (2010).

18. Hosseini V, Ahadian S, Ostrovidov S *et al.* Engineered contractile skeletal muscle tissue on a microgrooved methacrylated gelatin substrate. *Tissue Eng Part A*, 18(23-24), 2453-2465 (2012).
19. Peterbauer T, Yakunin S, Siegel J *et al.* Dynamics of spreading and alignment of cells cultured in vitro on a grooved polymer surface. *Journal of Nanomaterials*, 2011, 1-10 (2011).
20. Sun M, Bloom AB, Zaman MH. Rapid Quantification of 3D Collagen Fiber Alignment and Fiber Intersection Correlations with High Sensitivity. *PLoS One*, 10(7), e0131814 (2015).
21. Junkin M, Leung SL, Whitman S, Gregorio CC, Wong PK. Cellular self-organization by autocatalytic alignment feedback. *J Cell Sci*, 124(Pt 24), 4213-4220 (2011).
22. Pang Y, Wang X, Lee D, Greisler HP. Dynamic quantitative visualization of single cell alignment and migration and matrix remodeling in 3-D collagen hydrogels under mechanical force. *Biomaterials*, 32(15), 3776-3783 (2011).
23. Musaro A. The basis of muscle regeneration. *Advances in Biology*, 2014, 16 (2014).
24. Cossu G, Biressi S. Satellite cells, myoblasts and other occasional myogenic progenitors: Possible origin, phenotypic features and role in muscle regeneration. *Semin Cell Dev Biol*, 16(4-5), 623-631 (2005).
25. Bajaj P, Reddy B, Jr., Millet L *et al.* Patterning the differentiation of C2C12 skeletal myoblasts. *Integr Biol (Camb)*, 3(9), 897-909 (2011).
26. Ostrovidov S, Hosseini V, Ahadian S *et al.* Skeletal muscle tissue engineering: methods to form skeletal myotubes and their applications. *Tissue Eng Part B Rev*, 20(5), 403-436 (2014).
27. Kharraz Y, Guerra J, Mann CJ, Serrano AL, Munoz-Canoves P. Macrophage plasticity and the role of inflammation in skeletal muscle repair. *Mediators of Inflammation*, 2013(2013), 491497 (2013).
28. Rigamonti E, Zordan P, Sciorati C, Rovere-Querini P, Bruneli S. Macrophage plasticity in skeletal muscle repair. *Biomed Res Int*, 2014, 660629 (2014).
29. Otis JS, Niccoli S, Hawdon N *et al.* Pro-inflammatory mediation of myoblast proliferation. *PLoS One*, 9(3), e92363 (2014).
30. Cantini M, Giurisato E, Radu C *et al.* Macrophage-secreted myogenic factors: a promising tool for greatly enhancing the proliferative capacity of myoblasts in vitro and in vivo. *Neurol Sci*, 23(4), 189-194 (2002).
31. Saclier M, Yacoub-Youssef H, Mackey AL *et al.* Differentially activated macrophages orchestrate myogenic precursor cell fate during human skeletal muscle regeneration. *Stem Cells*, 31(2), 384-396 (2013).
32. Baum J, Duffy HS. Fibroblasts and myofibroblasts: What are we talking about? *J Cardiovasc Pharmacol*, 57(4), 376-379 (2011).
33. Darby IA, Laverdet B, Bonte F, Desmouliere A. Fibroblasts and myofibroblasts in wound healing. *Clin Cosmet Investig Dermatol*, 7, 301-311 (2014).
34. Lemons JM, Feng XJ, Bennett BD *et al.* Quiescent fibroblasts exhibit high metabolic activity. *PLoS Biol*, 8(10), e1000514 (2010).
35. Howard EW, Crider BJ, Updike DL *et al.* MMP-2 expression by fibroblasts is suppressed by the myofibroblast phenotype. *Exp Cell Res*, 318(13), 1542-1553 (2012).

Supplementary Information

Table S5: A data set representative of a cell population with different extents of alignment.

Cell No.	Standard Deviation				Cell No.	Standard Deviation				Cell No.	Standard Deviation			
	0	4	16	64		0	4	16	64		0	4	16	64
1	90,00	81,21	54,00	15,44	34	90,00	88,74	86,95	75,98	67	90,00	92,96	100,15	115,31
2	90,00	81,76	58,03	18,10	35	90,00	88,91	87,10	76,49	68	90,00	93,37	100,45	117,22
3	90,00	81,80	62,03	23,29	36	90,00	89,01	87,13	79,35	69	90,00	93,39	100,88	121,14
4	90,00	82,48	62,57	24,51	37	90,00	89,05	88,33	81,08	70	90,00	93,45	101,87	122,19
5	90,00	84,79	64,94	25,71	38	90,00	89,09	88,63	81,70	71	90,00	93,47	101,93	123,21
6	90,00	84,82	67,30	26,75	39	90,00	89,11	89,14	83,98	72	90,00	93,70	102,31	123,66
7	90,00	84,92	68,30	31,43	40	90,00	89,14	89,18	85,54	73	90,00	93,92	102,64	124,07
8	90,00	85,26	69,90	32,43	41	90,00	89,17	89,91	85,80	74	90,00	93,93	102,69	124,32
9	90,00	85,57	70,63	32,85	42	90,00	89,20	89,91	85,84	75	90,00	94,10	102,70	127,57
10	90,00	85,64	70,72	33,05	43	90,00	89,63	89,97	86,08	76	90,00	94,13	102,75	130,39
11	90,00	85,64	73,39	34,52	44	90,00	89,94	90,01	87,25	77	90,00	94,22	104,03	130,95
12	90,00	86,05	73,90	38,61	45	90,00	89,98	90,42	88,58	78	90,00	94,28	104,06	135,09
13	90,00	86,17	75,33	39,26	46	90,00	90,14	90,48	88,70	79	90,00	94,57	105,67	135,50
14	90,00	86,30	76,51	43,01	47	90,00	90,29	90,90	90,48	80	90,00	95,15	106,50	139,93
15	90,00	86,35	77,83	45,63	48	90,00	90,43	91,15	92,15	81	90,00	95,64	106,71	140,06
16	90,00	86,37	78,86	46,95	49	90,00	90,56	91,41	93,07	82	90,00	95,70	107,98	143,10
17	90,00	86,44	79,50	48,93	50	90,00	90,79	91,59	93,62	83	90,00	96,04	108,54	143,88
18	90,00	86,89	79,75	50,53	51	90,00	90,99	92,92	95,97	84	90,00	96,11	109,02	144,67
19	90,00	86,91	80,12	51,85	52	90,00	91,05	93,01	99,77	85	90,00	96,26	109,04	151,48
20	90,00	87,10	81,17	54,28	53	90,00	91,11	93,52	100,59	86	90,00	96,49	109,32	152,58
21	90,00	87,45	81,40	54,59	54	90,00	91,18	93,97	102,40	87	90,00	96,64	110,52	153,21
22	90,00	87,50	81,75	54,82	55	90,00	91,32	94,31	104,02	88	90,00	96,74	110,77	153,47
23	90,00	87,58	81,99	60,51	56	90,00	91,39	94,80	105,56	89	90,00	97,56	111,14	156,65
24	90,00	87,62	82,40	60,71	57	90,00	91,60	96,04	105,84	90	90,00	97,61	111,87	158,64
25	90,00	87,73	82,42	64,23	58	90,00	91,61	96,15	106,14	91	90,00	97,71	113,36	161,50
26	90,00	87,81	82,54	68,42	59	90,00	91,73	96,37	107,51	92	90,00	98,05	114,66	161,51
27	90,00	88,18	83,05	69,37	60	90,00	91,96	96,40	108,70	93	90,00	98,49	115,07	164,74
28	90,00	88,24	83,13	70,76	61	90,00	92,29	96,52	109,23	94	90,00	98,75	117,51	164,83
29	90,00	88,33	83,25	72,62	62	90,00	92,59	97,20	109,74	95	90,00	98,83	119,63	165,52
30	90,00	88,39	83,70	72,66	63	90,00	92,65	98,44	111,80	96	90,00	99,10	122,83	177,85
31	90,00	88,59	84,49	72,92	64	90,00	92,69	98,84	113,64	97	90,00	100,57	123,54	179,40
32	90,00	88,70	86,32	74,07	65	90,00	92,92	99,54	114,33	98	90,00	101,36	126,04	179,73
33	90,00	88,70	86,71	74,48	66	90,00	92,93	99,58	114,74					

A set of random data that represents the orientations of 98 hypothetical cells in an image with different extents of alignment was created using the Microsoft Excel (2016) *=NORM.INV (probability; mean; standard deviation)* function with *=RAND()* as the probability, 90 as the mean and standard deviations (SD) equal to 0, 4, 16 or 64.

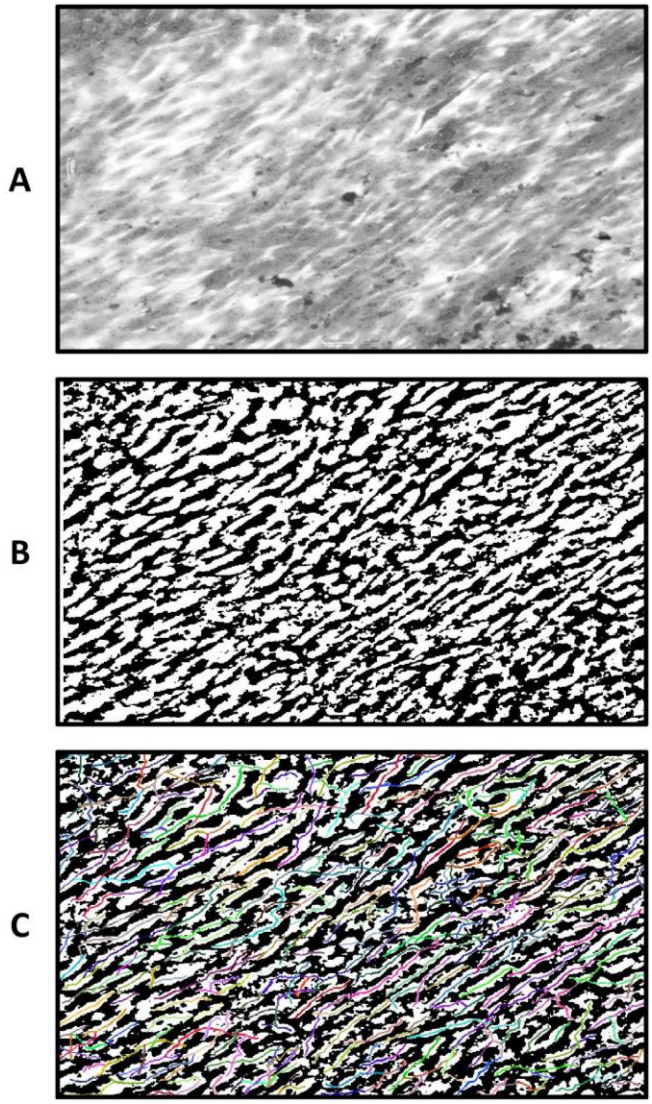

Figure S1: Stages of Image Processing. A) Image Acquisition: myoblasts stained with Fuchsin were captured using an Olympus CKX41 microscope and a Motic 3.0 megapixel camera (10x objective lens**). B)** ImageJ Pre-processing: images were processed using ImageJ, representing the cells as white and the spaces between them as black. **C)** ct-FIRE Analysis: cell orientation was evaluated using ct-FIRE that inserts coloured lines through the longitudinal axis of a cell, signifying the orientation of the cells.

CHAPTER 6: MYOFIBROBLAST CELL DEATH MEDIATED BY PRO-INFLAMMATORY MACROPHAGES IN A PI3-KINASE-DEPENDENT MANNER

Venter C, Niesler CU*

Discipline of Biochemistry, School of Life Sciences, University of KwaZulu-Natal, Private Bag X01, Scottsville 3209, South Africa

**Corresponding author: Prof C.U. Niesler, Tel: (033) 260 5465, Fax: (033) 260 6127, email: niesler@ukzn.ac.za*

In preparation for submission to: *Experimental Cell Research*

Abstract

Skeletal muscle regeneration is a complex process mediated by both myogenic and non-myogenic cell populations, including satellite cells, macrophages and fibroblasts. Dysregulated communication between these cell types can result in conditions such as impaired wound repair or fibrosis. In our previous studies, we evaluated the direct roles of macrophages and fibroblasts on myogenesis; in the current study, we sought to better understand the intercellular communication between macrophage and fibroblast populations. Macrophages and fibroblasts can acquire different phenotypes in response to changing experimental conditions; serum stimulates the differentiation of fibroblasts into myofibroblasts, while lipopolysaccharide stimulates the polarisation of M0 macrophages to acquire a M1 pro-inflammatory phenotype. We characterized these phenotypes using morphology (with circularity as a shape descriptor) as well as the expression of either α-smooth muscle actin (SMA) or CD86. Myofibroblasts were characterised by high circularity (corresponding to a round morphology) and high levels of α-SMA expression; de-differentiation to fibroblasts resulted in a lower circularity and decreased levels of α-SMA. When unstimulated (M0) macrophages were activated with LPS, there was a decrease in circularity and increased CD86 expression, indicative of a M1 macrophage population. Utilising these established conditions, we then co-cultured M1 macrophages with myofibroblasts and myoblasts; we found that M1 macrophages decreased myofibroblast, but not myoblast number. We subsequently evaluated the mechanism whereby M1 macrophages mediated this decrease in myofibroblast numbers and found that LY294002 and dexamethasone rescued myofibroblasts. LY294002 was also observed to decrease macrophage cell number, suggesting a mechanism whereby myofibroblasts were rescued. Dexamethasone, on the other hand, increased the circularity of the myofibroblast population, suggesting a decrease in the number of remaining fibroblasts within the population. In conclusion, macrophages and fibroblasts regulate myogenesis, but the phenotypes these cells acquire are also important. M1 macrophages have a detrimental effect on the population of fibroblasts; since fibroblasts have previously been shown to regulate muscle cell behaviour and promote myoblast migration and fusion, detrimental effects on fibroblasts would negatively impact myogenesis.

Keywords: skeletal muscle, macrophages, fibroblasts, phenotypes, LY294002, dexamethasone

Introduction

Skeletal muscle repair involves the differentiation and fusion of muscle stem cells (myoblasts) into regenerated muscle fibres. This process, known as myogenesis, is regulated by non-myogenic cells, such as macrophages and fibroblasts [1]. Macrophages are present during the early stages of wound repair and acquire a pro-inflammatory (M1) phenotype to produce factors (such as tumour necrosis factor (TNF)-α and nitric oxide (NO)) which activate myogenic satellite cells to myoblasts. M1 macrophages then stimulate the expansion of myoblasts by promoting their proliferation and inhibiting apoptosis [2-4]. As wound repair progresses, macrophages acquire an anti-inflammatory (M2) phenotype to secrete factors (such as interleukin (IL)-10) which attenuate the initial pro-inflammatory response and stimulate myoblast differentiation and fusion [4-6]. Anti-inflammatory macrophages additionally secrete pro-fibrotic factors (such as transforming growth factor (TGF)-β) to activate fibroblasts to differentiate into an intermediate proto-myofibroblast phenotype (absent of any contractile apparatus) before fully differentiating into contractile myofibroblasts [6-8]. Myofibroblasts are primarily responsible for depositing matrix factors (e.g. collagen I) to re-establish the extracellular matrix (ECM) surrounding healing muscle fibres, but also secrete soluble factors (e.g. fibroblast growth factor (FGF)-2) which regulate muscle regeneration [9,10]. Despite these distinct fibroblast populations, *in vitro* studies often do not actively distinguish between them.

Muscle regeneration during wound repair is a highly regulated process and effective reparation hinges on the proper communication within the myogenic and non-myogenic cell populations [11,12]. Aberrant wound repair can occur when certain non-myogenic cell populations and accompanied secreted factors persist without resolution [12]. Pathophysiological fibrosis occurs in response to a persistent M2 macrophage population, creating a sustained anti-inflammatory and pro-fibrotic environment; this leads to a persistent population of myofibroblasts and an excessive accumulation of matrix factors that ultimately impair muscle healing [11,12]. Other muscle diseases, such as muscular dystrophy and myositis, are characterized by muscle weakness and recurring muscle regeneration and often accompanied by an upregulated pro-inflammatory microenvironment mediated by inflammatory cells (e.g. T cells and macrophages) and certain cytokines (e.g. TNF-α and interferon (IFN)-γ) [12-14]. However, the effect of this pathological microenvironment on myofibroblast populations, and the implication on skeletal muscle wound repair, is unclear.

Intercellular communication between non-myogenic cells regulates myogenic cellular behaviours, such as proliferation, migration and apoptosis [15]. Signalling typically starts with an external stimulus (biomechanical or biochemical) which acts on cells to activate intracellular signalling pathways (e.g. phosphatidylinositol 3-kinase (PI3K), nuclear factor (NF)-κB and mitogen-activated protein kinase (MAPK) pathways) and ultimately control gene expression and regulate cell behaviour [16]. It is important to elucidate these signalling pathways involved in intercellular communication to understand which pathways can be targeted to effectively mitigate muscle diseases associated with aberrant non-myogenic cell communication [17,18]. Macrophages initially become activated by a pro-inflammatory stimulus (e.g. T-helper (Th) 1 cell-secreted IFN-γ), which leads to the production of inflammatory proteins (e.g. TNF-α, IL-6, cyclooxygenase (COX)-2 and inducible nitric oxide synthase (iNOS)) [19,20]. Pro-inflammatory macrophages have been shown to regulate fibroblast population behaviour in a paracrine manner to favour inflammation by upregulating expression of pro-inflammatory genes (e.g. IL-6 and chemokine (C-C motif) ligand 2 (CCL2)) [21]. Furthermore, M1 macrophages favour matrix degradation by increasing fibroblast production of matrix metalloproteinases (MMPs) and decreasing the production of collagen I and III; this negatively affects tissue architecture and is characteristic of non-healing wounds [21]. It is apparent that M1 macrophages regulate the behaviour of fibroblasts via the action of signalling pathways; pharmacological inhibitors are important tools to evaluate these signalling systems (Table 1).

Table 6: Summary of the effects of inhibitors on M1 macrophages.

Inhibitor	Pathway	Effect	Reference
L-NAME	iNOS/NO	↓ NO levels	[33]
Indomethacin	COX-2/PGE2	↓ PGE2 levels	[34]
LY294002	PI3K	↓ iNOS expression ↓ TNF-α levels ↓ TNF-α & IL-6 levels	[35] [36] [37]
SB203580	p38 MAPK	↓ COX-2 & iNOS expression ↓ IL-1β ↑ & ↓ TNF-α & IL-6 expression	[35] [38] [38, 39]
SP600125	JNK	↓ iNOS expression ↓ COX-2	[35] [40]
Dexamethasone	Unknown	↓ iNOS expression ↓ TNF-α expression	[41] [42]

Pathway and effect of L-NAME, indomethacin, LY294002, SB203580, SP600125 and dexamethasone on macrophages.

Fibroblasts and macrophages are therefore essential for muscle regeneration [22,23]. We have previously investigated the roles of these cell populations on myoblast behaviour [24,25]. We found that fibroblasts promote myoblast migration and fusion, but the addition of macrophages abrogated the pro-migratory effects of fibroblasts on myoblasts; we hypothesized that this may be as a result of a decrease in fibroblast numbers [24]. However, the macrophages were unstimulated and the phenotype of the fibroblast population was uncertain. Given that these non-myogenic cells can exists in various states, we first sought to establish and characterize the population of macrophages (in response to LPS) and fibroblasts (in response to serum) and then to expand on our initial studies and investigate the mechanism by which these cells regulate the *in vitro* muscle regenerative environment.

Methods

Reagents

Lipopolysaccharide (LPS; 1 mg/ml; Capital Lab Supplies, cat. L4391) and L-NAME (200 mM; BioVision, cat. 2356) were prepared in distilled water. Dexamethasone (100 mM; Sigma, cat. D1756), indomethacin (100 mM; Sigma, cat. I7378), SB203580 (10 mM; Santa Cruz, cat. SC-3533), LY294002 (10 mM; Santa Cruz, cat. SC-201426) and SP600125 (100

mM; Santa Cruz, cat. SC-200635) were prepared in DMSO (Sigma, cat. D2650). Fuchsine (1% w/v; Capital Lab Supplies, cat. 47860) was dissolved in 100% methanol. Serum-free medium (SFM) was prepared by supplementing Dulbecco's Modified Eagle's Medium (DMEM, Capital Lab Supplies, cat. D5648) with 2% (v/v) Penicillin-Streptomycin (PenStrep, LONZA, cat. DE17-602E). Serum-containing medium (SCM) was prepared by supplementing SFM with 2% (v/v) or 10% (v/v) Fetal Bovine Serum (FBS, Gibco, cat. 10500).

Cell Culture

Mouse C2C12 myoblasts (ATCC, USA, cat. CRL-1772™; passage 10-20), LMTK fibroblasts (ATCC, USA, cat. CCL-1.3™; passage 6-25) and J774A.1 macrophages (ATCC, USA, cat. TIB-67™; passage 60-90) were cultured at 37°C and 5% CO_2 and maintained in 10% SCM. Media was changed every 48 hours.

Mono-culture proliferation/morphology studies were performed by seeding macrophages (40 x 10^3) or fibroblasts (30 x 10^3) into 24-well culture plates in 10% SCM (500 µl) and incubated for 2 hours to promote adherence. Co-cultures were performed as previously described [24]: macrophages (0 or 40 x 10^3) were first plated on the outer edge of a 24-well plate in 10% SCM and incubated for 1 hour; fibroblasts (30 x 10^3) or myoblasts (5 or 20 x 10^3) were then plated in the centre of the well and incubated for 2 hours. Adherent mono- and co-cultures were washed twice with sterile PBS (500 µl) and treated as described below.

Cell Treatments

For proliferation/morphology studies, mono-cultures of macrophages and fibroblasts were either treated with different concentrations of SCM (0, 2 and 10%; 500 µl) or LPS (0 and 0.1 µg/ml; 500 µl) in 2% SCM for 24 hours. To evaluate the effect of M1 macrophages on fibroblasts and myoblasts, mono-cultures of myofibroblasts/myoblasts (negative controls) and co-cultures of these cells with macrophages were treated with LPS (0.1 µg/ml) in 2% SCM for 24 hours where indicated. To evaluate DMSO cytotoxicity, mono-cultures and co-cultures (pre-treated with LPS) of macrophages with myofibroblasts were cultured with different dilutions of DMSO (0, 1:1000 and 1:10000) in 2% SCM. To evaluate the effect of various drugs and inhibitors on macrophage-mediated myofibroblast death, mono-cultures of macrophages or co-cultures of macrophages with myofibroblasts were treated with an

inhibitor in 2% SCM before (30 mins), with (1 hour) and after (24 hours) LPS pre-treatment where indicated. Cells were washed twice with sterile PBS after LPS pre-treatment.

Morphology Analysis

Cells were briefly washed with PBS and stained with 1% Fuchsine (10 mins), submerged in water to remove the stain and left to dry. Cells were visualized and captured with an Olympus CKX41 microscope and a Motic 3.0 megapixel camera (10x objective lens; 5 fields of view per replicate for two replicates per experiment). Morphology was quantitively analysed by assessing cell circularity (circularity = 4π x ([Area]/ [Perimeter]^2) in ImageJ. ImageJ was first set to include circularity analysis (*Analyze → Set Measurements;* check *Shape descriptors*). Images were first converted to 8-bit (*Image →Type → 8-bit*), converted to a binary image (*Process → Binary → Make Binary*) and analysed (*Analyze → Analyze Particles*). The size was set between 100-800 pixels to limit background and excluded touching cells that prevented accurate analysis. The result was a value between 0 and 1 which indicated cells that are irregularly shaped or perfectly circular, respectively.

Proliferation Analysis

Proliferation studies were analysed as previously described [26]. Images of stained cells (4x objective lens; 5 randomly selected fields of view per replicate for two replicates per experiment) were automatically identified using ImageJ by converting the captured image to grayscale (*Image → Type → 8-bit*), removing the image noise (*Process → Noise → Despeckle*), adjusting the brightness and contrast (*Image → Adjust → Brightness/Contrast: min = 87; max = 167*) and finally applying first a Phansalkar threshold (*Image → Adjust → Auto Local Threshold: Phansalkar*), and then a watershed (*Process → Binary → Watershed*). The identified cells were then automatically quantified (*Analyze → Analyze Particles*).

Confocal Microscopy

Myofibroblasts (30 x 10^3) were plated in 24-well plates on top of glass coverslips in 10% SCM for 3 hours, washed twice with PBS and switched to 0, 2 and 10% SCM for 24 and 72 hours. Macrophages (40 x 10^3) were similarly plated in 2% SCM with or without 0.1 μg/ml LPS for 24 hours. The media was then removed, the cells fixed with 4% paraformaldehyde (10 mins), permeabilized with 0.3% Triton-X100 (Sigma, cat. X100) (10 mins), blocked with 5% donkey serum (Sigma, cat. D9663) for 30 mins at room temperature. The (myo)fibroblasts

were then incubated overnight at 4°C with mouse anti-α-smooth muscle actin (SMA; 1:1000; Sigma, cat. A2547), washed with PBS (3 x 5 mins) and incubated at room temperature (1 hour) in the dark with Dylight594-conjugated donkey anti-mouse antibody (1:1000; Jackson ImmunoResearch, cat. 715-515-151). Macrophages were incubated with PE-conjugated rat anti-CD86 (1:200; BioLegend, cat. 105008) overnight at 4°C. Hoescht (1:100; 10 mg/ml; Sigma, cat. B2261) was subsequently added for 10 mins and the coverslips washed with PBS (6 x 5 mins) and mounted on glass slides with Mowiol (Sigma, cat. 81381). The cells were viewed with a Zeiss 710 confocal microscope (Carl Zeiss GmbH, Oberkocken, Germany).

Statistical Analysis

Data was determined to be normally distributed; all results were analysed using a one-way ANOVA with post-hoc tests in GraphPad Prism 8 and values of $p < 0.05$ were considered to be statistically significant compared to the control. All data was represented as mean ± SEM.

Results

Phenotypic characterization of macrophages and fibroblast populations

Fibroblasts have been shown to differentiate into myofibroblasts in the presence of serum and/or TGF-β; differentiation is thought to be reversible [27-29]. LMTK cells were subsequently cultured in 0, 2 and 10% SCM for 24 hours and phenotypes characterised based on morphology and α-SMA (Figure 1). Cells cultured in media containing 0% serum acquired an elongated, thin morphology compared to those maintained in 10% SCM, which were clustered with thick, rounded shapes (Figure 1Ai); cells switched to 2% SCM had an intermediate morphology. Circularity was assessed to quantify these changes in morphology (Figure 1Aii). Cells maintained in 10% SCM had a peak frequency of circularity at 0.60-0.69. In response to 2% SCM, the peak frequency shifted cells to a circularity of 0.30-0.39, while 0% serum shifted the population further where the peak frequency of circularity was observed at 0.20-0.29. The average cell circularity for each serum concentration was determined to be 0.60 ± 0.03 (10% SCM), which decreased significantly ($p < 0.05$) to 0.47 ± 0.01 in response to 2% SCM and further decreased to 0.35 ± 0.02 when cultured in 0% SCM (Figure 1Aiii). Macrophages were also cultured in the presence of different concentrations of SCM to determine any changes in morphology (Figure 1Aiv): only a small but significant decrease ($p < 0.05$) was observed from 0.72 ± 0.02 to 0.63 ± 0.01 when the medium was changed from

10% to 0% SCM; cells cultured in 2% SCM had an average circularity of 0.69 ± 0.03, but this change was not significant when compared with circularity under low or high serum levels. Circularity data also shows that macrophages are, in general, rounder cells than both fibroblasts and myofibroblasts. Confocal microscopy was used to evaluate changes in α-SMA expression of the fibroblast population following incubation in SCM (0, 2 and 10%) (Figure 1B). Although myofibroblasts cultured in media containing either 0% or 2% serum still expressed α-SMA, the level of expression appeared lower at 72 h, when compared to those cells culture in the presence of 10% serum. In addition, cells cultured under low serum conditions morphologically displayed longer, thinner shapes, whereas those culture in the presence of 10% serum were much rounder. We therefore concluded that under 0% serum, fibroblasts are present with low α-SMA expression and a low circularity; in response to 2% and 10% serum, these cells differentiate into myofibroblasts with increased α-SMA expression and a high circularity.

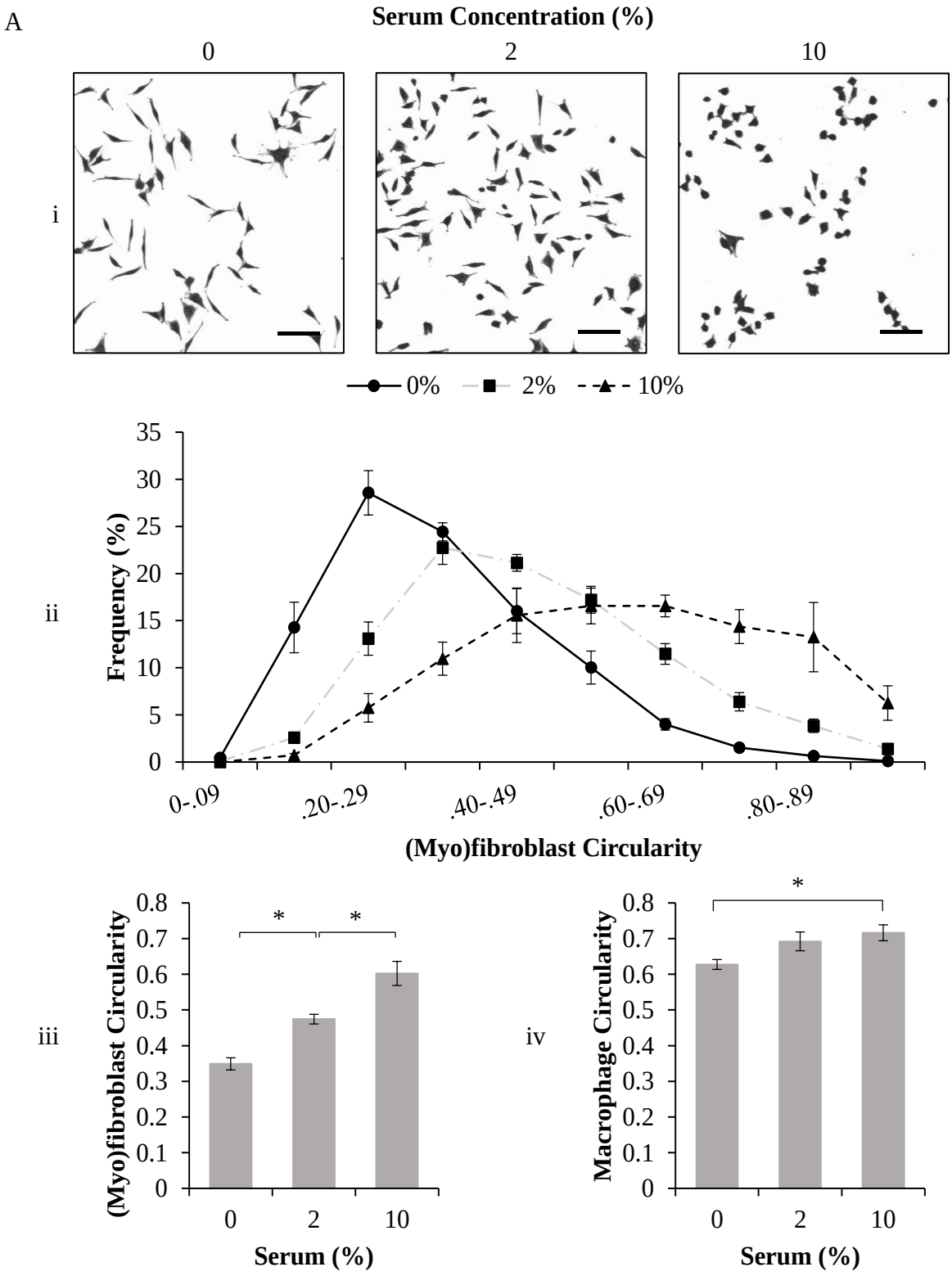
A
Serum Concentration (%)
0
2
10
i
0%
2%
10%
ii
Frequency (%)
0-.09
.20-.29
.40-.49
.60-.69
.80-.89
(Myo)fibroblast Circularity
iii
(Myo)fibroblast Circularity
Serum (%)
iv
Macrophage Circularity
Serum (%)

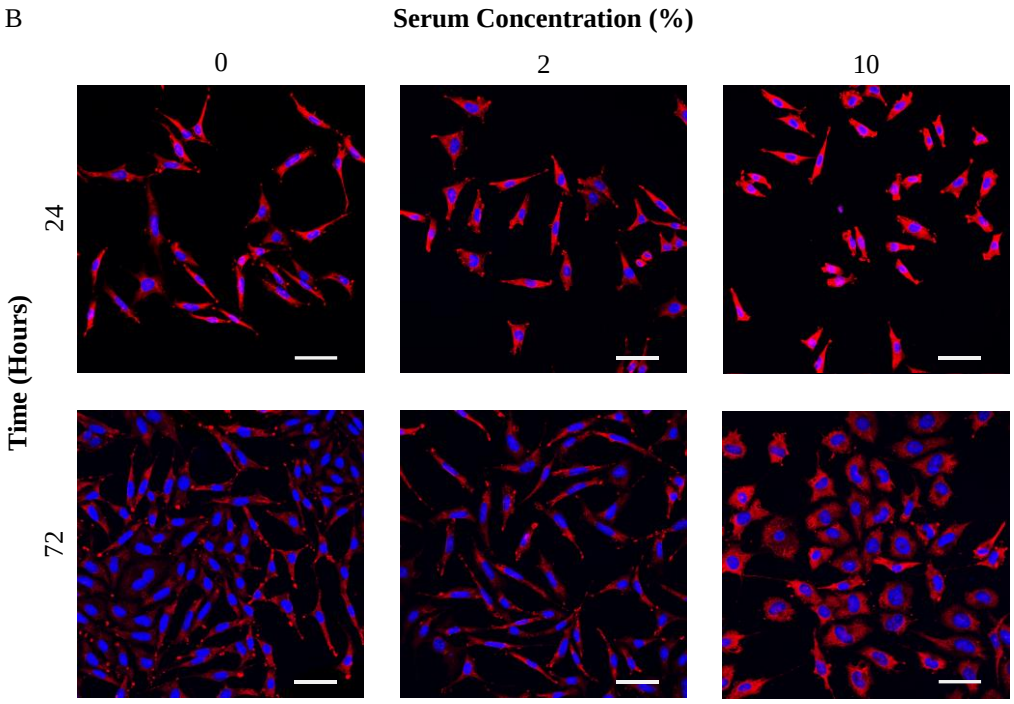

Figure 1: Characterization of fibroblast and macrophage population phenotypes in different concentrations of serum-containing medium (SCM). (A) Morphological analysis of cells maintained in 0, 2 and 10% SCM showing (i) Fuchsine-stained (myo)fibroblasts, (ii) frequency distribution of (myo)fibroblasts, and the average circularity of (iii) (myo)fibroblasts and (iv) macrophages. (B) Confocal microscopy of (myo)fibroblasts immunostained with mouse anti-α-SMA (red) maintained in different concentrations of SCM for 24 and 72 hours. Hoeschst was used as a nuclear stain (blue). Images were captured using an Olympus CKX41 microscope coupled to a Motic 3.0 megapixel camera (4x objective lens; scale bar = 200 μm) and a Zeiss 710 confocal microscope (25x objective lens; scale bar = 50 μm). * = $p < 0.05$; N = 7 ((myo)fibroblasts) and 4 (macrophages).

Macrophages were cultured with LPS to establish a M1 phenotype which was then characterized based on morphology and CD86 expression (Figure 2). Macrophages cultured in the absence of LPS were small with a very round morphology, while the cells cultured in the presence of LPS also had a round shape, but several cells acquired long bipolar protrusions (Figure 2i). The average circularity of macrophages was calculated (Figure 2ii): macrophage circularity in the absence of LPS was 0.72 ± 0.02 and this significantly decreased ($p < 0.05$) to 0.61 ± 0.02 when treated with LPS. The circularity of the fibroblast population in response to LPS in 2% SCM was also assessed (Figure 2iii). These cells displayed an average circularity of 0.37 ± 0.01 which very slightly, but significantly ($p < 0.05$), decreased to 0.34 ± 0.01 in response to LPS. Furthermore, macrophages stimulated with LPS in 2% SCM displayed a notable increase in CD86 expression compared to unstimulated cells (Figure 2iv).

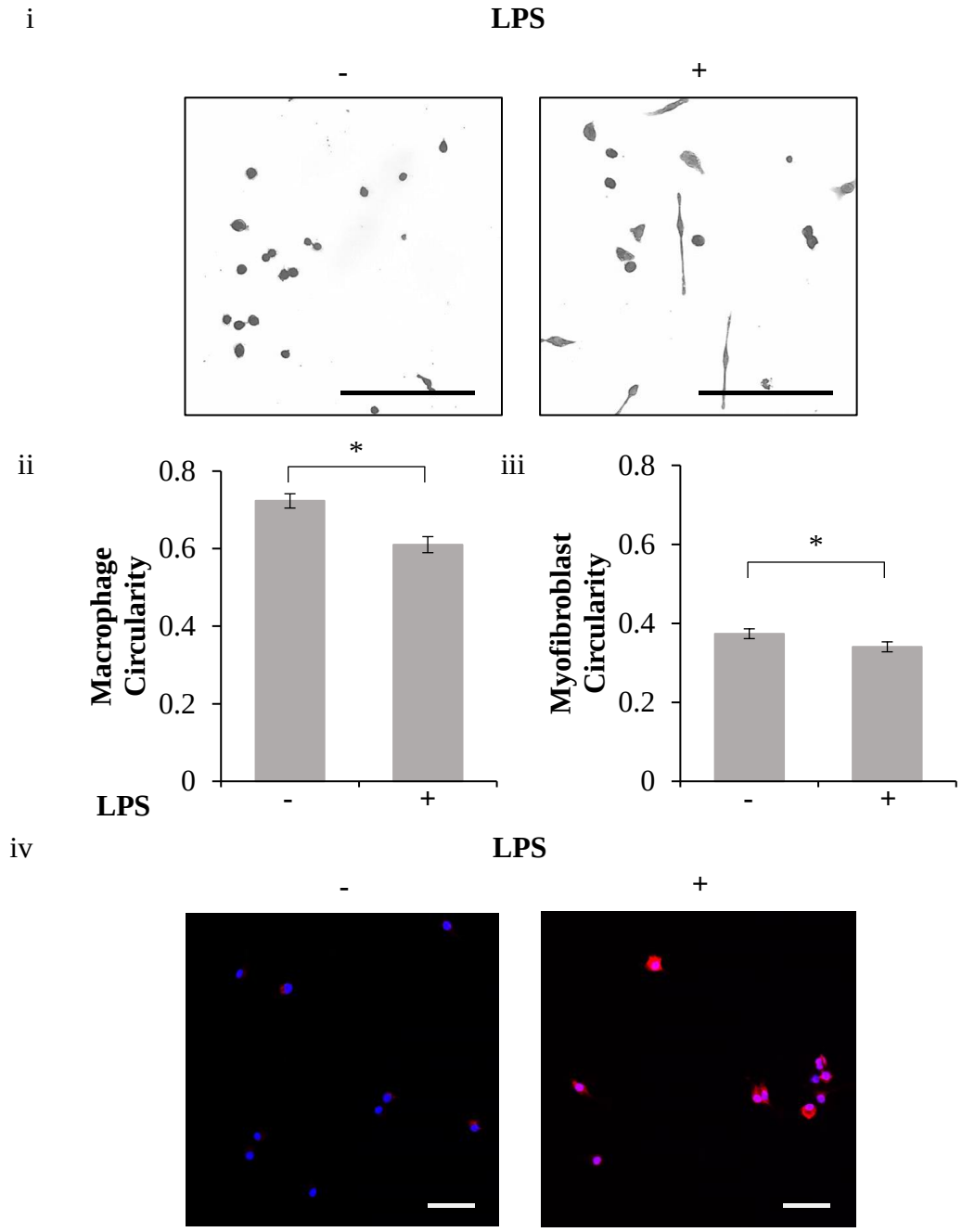

Figure 2: Characterization of macrophages and myofibroblasts in the presence of lipopolysaccharide (LPS). Morphological analysis of cells maintained in 2% SCM with and without LPS (0.1 µg/ml) showing (i) Fuchsine-stained macrophages and the average circularity of (ii) macrophages and (iii) myofibroblasts. (iv) Confocal microscopy of macrophages immunostained with rat anti-CD86 (red) treated with LPS for 24 hours. Hoeschst was used as a nuclear stain (blue). Images were captured using an Olympus CKX41 microscope coupled to a Motic 3.0 megapixel camera (10x objective lens; scale bar = 200 µm) and a Zeiss 710 confocal microscope (25x objective lens; scale bar = 50 µm). * = $p < 0.05$; N = 6 (macrophages and myofibroblasts).

Pro-inflammatory macrophages result in myofibroblast, but not myoblast, cell death

Macrophages were then co-cultured with myofibroblasts or myoblasts in the presence of LPS to determine the effect of a pro-inflammatory environment on myofibroblast and myoblast proliferation (Figure 3). Myofibroblasts alone ($M\phi^{-}LPS^{-}$) (Figure 3i, ii) were present with a relative cell number of 230 ± 23% which was not significantly different from 232 ± 27% and 223 ± 22% when the cells were cultured in the presence of M0 macrophages ($M\phi^{+}LPS^{-}$) or LPS ($M\phi^{-}LPS^{+}$) respectively. However, co-culture with M1 macrophages ($M\phi^{+}LPS^{+}$) caused a significant decrease ($p < 0.05$) in myofibroblast numbers to 64 ± 7% which was below the number of cells originally plated (i.e. 100%). Myoblasts alone ($M\phi^{-}LPS^{-}$) (Figure 3iii) were present with a relative cell number of 306 ± 63% and displayed no significant change compared to 325 ± 78% and 323 ± 95% when the cells were cultured in the presence of M0 macrophages ($M\phi^{+}LPS^{-}$) or LPS ($M\phi^{-}LPS^{+}$), respectively. Furthermore, myoblasts cultured in the presence of M1 macrophages ($M\phi^{+}LPS^{+}$) were present with a relative cell number of 297 ± 68% which was also not significantly different compared to myoblasts cultured with LPS alone. M0 macrophages ($M\phi^{+}LPS^{-}$) (Figure S1) continued to significantly increase ($p < 0.05$) relative myoblasts numbers in SFM from 141 ± 4% to 220 ± 15% in the presence of M0 macrophages ($M\phi^{+}LPS^{-}$) as previously shown [24]. Myoblasts maintained in the presence of LPS ($M\phi^{-}LPS^{+}$) and were present with relative cell numbers of 145 ± 6% which was not significantly different compared to the control. Co-culture with M1 macrophages ($M\phi^{+}LPS^{+}$) also significantly increased relative myoblast numbers to 191 ± 12%, but this was not significantly different compared to co-culture with M0 macrophages.

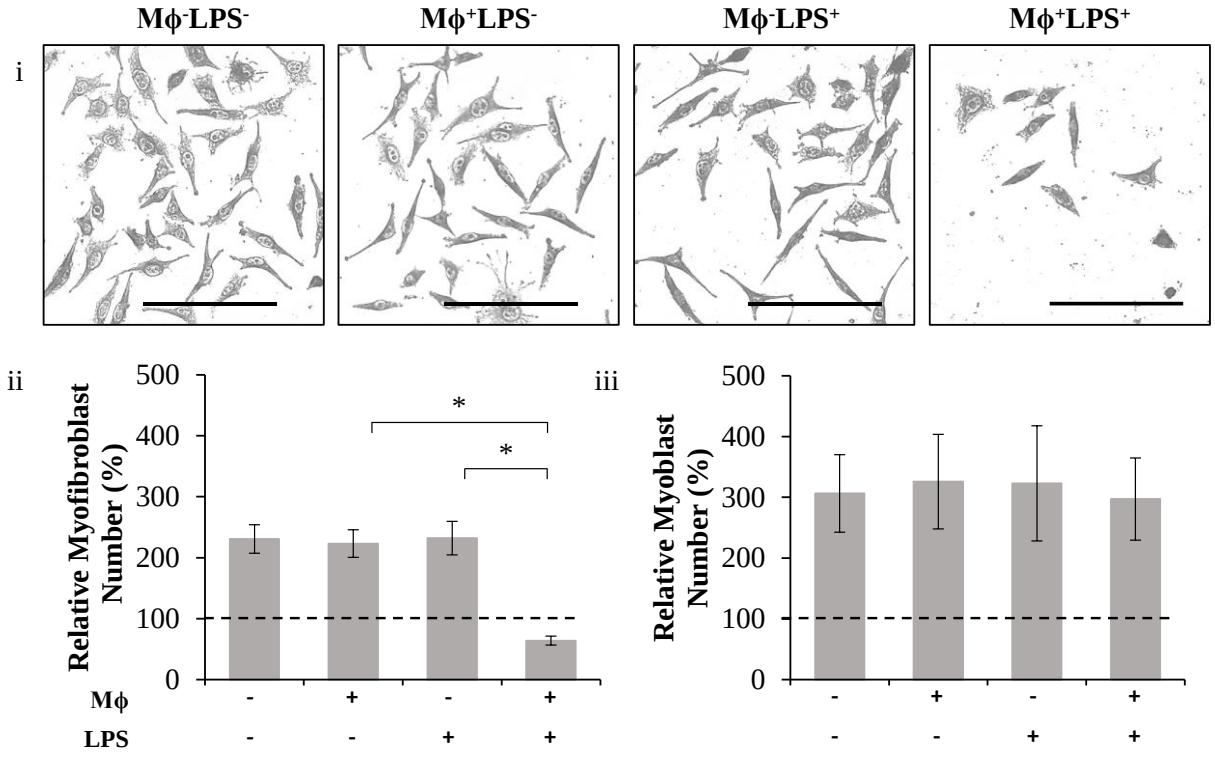

Figure 3: The effect of macrophages on myofibroblasts and myoblasts. Cells were cultured with or without macrophages (Mϕ; 40 x 10^3) in 2% SCM with or without LPS (0.1 μg/ml) pre-treatment. (i, ii) Fibroblasts and (iii) myoblasts were stained with Fuchsine and the relative cell numbers determined. Images were captured using an Olympus CKX41 microscope coupled to a Motic 3.0 megapixel camera (10x objective lens; scale bar = 200 μm). * = $p < 0.05$; N = 6 (myofibroblasts and myoblasts).

Mechanism of pro-inflammatory macrophage-mediated myofibroblast death

The mechanism by which M1 macrophages decrease myofibroblast numbers was assessed by co-culturing macrophages and myofibroblasts in the presence of LPS and 2% serum in the presence or absence of soluble inhibitors (Figure 4). DMSO (at any dilution) showed no significant effect on macrophages or myofibroblast numbers and had no significant effect on the ability of LPS pre-treated macrophages to decrease myofibroblast cell numbers (Figure S2). Myofibroblasts treated with L-NAME, an iNOS inhibitor (Figure 4i) or indomethacin (INDO), a COX-2 inhibitor, (Figure 4ii), p38 MAPK inhibitor SB203580 (SB) (Figure 4iii) or JNK inhibitor SP600125 (SP) (Figure 4iv) showed no significant ability in rescuing myofibroblast cell loss in response to M1 macrophages. However, addition of LY294002 (LY) to myofibroblasts co-cultured with M1 macrophages significantly ($p < 0.05$) rescued myofibroblast numbers from 156 ± 12% (LY^-LPS^+) to 219 ± 14% (LY^+LPS^+) (Figure 4v); incubation of myofibroblasts with LY294002 (LY^+LPS^-) were at relative cell numbers of 236 ± 16% which was not significantly different from 250 ± 16% when the cells were cultured in

the absence of LY294002 (LY^-LPS^-). Finally, myofibroblasts treated with dexamethasone alone (Figure 4vi) displayed a small decrease ($p = 0.05$) from 230 ± 22% (DEX^-LPS^-) to 188 ± 20% (DEX^+LPS^-); treating myofibroblasts co-cultured with M1 macrophages in the presence of dexamethasone rescued myofibroblast numbers from 136 ± 26% (DEX^-LPS^+) to 191 ± 21% (DEX^+LPS^+). However, this effect was not significant.

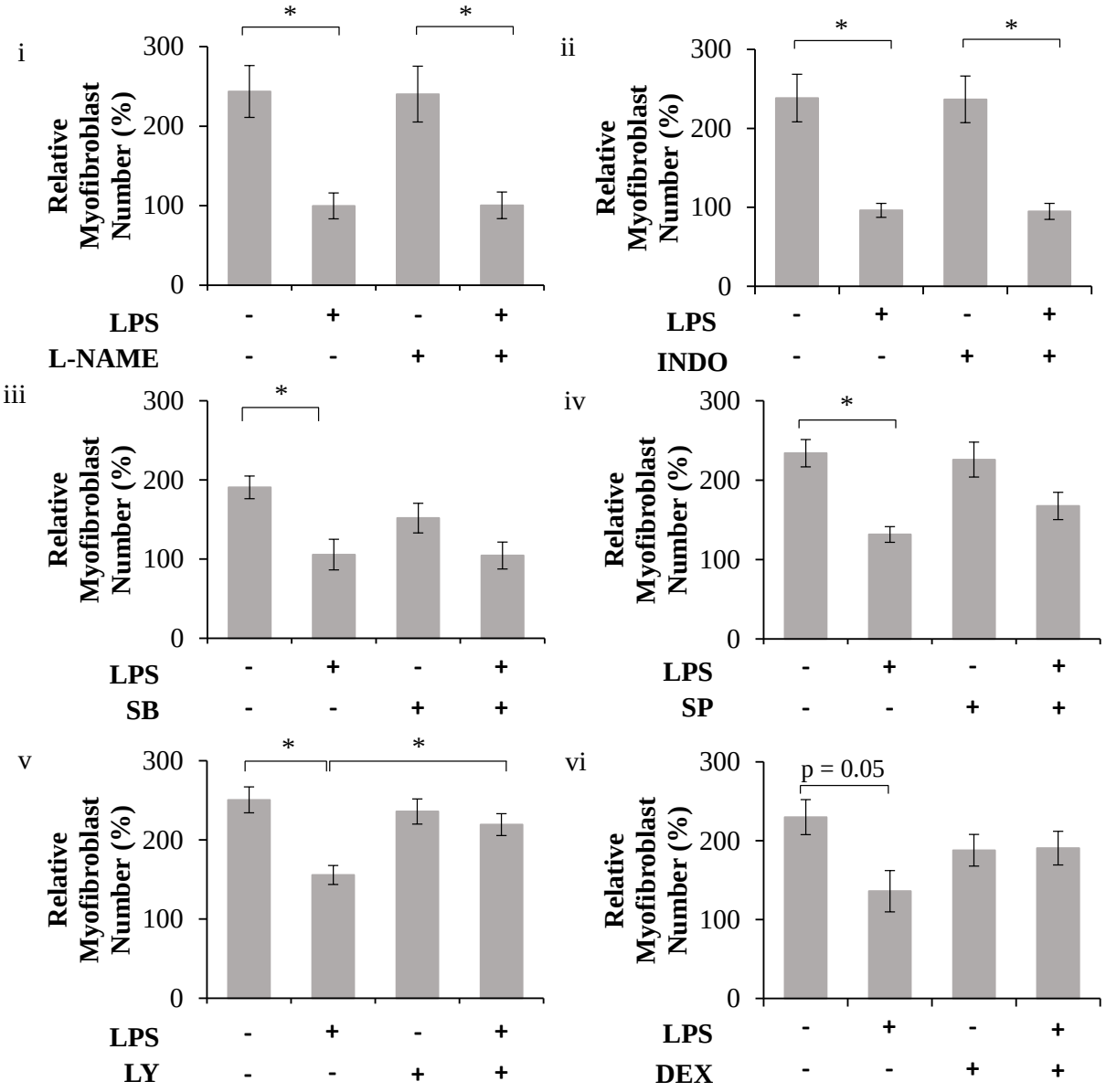

Figure 4: Evaluating the mechanism of pro-inflammatory macrophage-mediated myofibroblast death. Myofibroblasts were co-cultured with macrophages (Mϕ; 40 x 10^3) with or without LPS (0.1 µg/ml) with or without the inhibitors (i) L-NAME (200 µM), (ii) indomethacin (INDO; 10 µM), (iii) SB203580 (SB; 10 µM), (iv) SP600125 (SP; 10 µM), (v) LY294002 (LY; 10 µM), (vi) dexamethasone (DEX; 10 µM) and the relative cell numbers determined. * = $p < 0.05$; N = 4-7.

The effect of the inhibitor LY294002 and glucocorticosteroid dexamethasone on myofibroblast morphology in the presence of macrophages and LPS was evaluated (Figure 5). LY294002 had no observable (Figure 5i) or quantifiable (Figure 5ii) effects on myofibroblast morphology. Dexamethasone, however, caused myofibroblasts to acquire a more rounded morphology (Figure 5i); when an average circularity was calculated (Figure 5iii), dexamethasone significantly increased ($p < 0.05$) the average circularity from 0.38 ± 0.01 ($DEX^{-}LPS^{+}$) to 0.49 ± 0.003 ($DEX^{+}LPS^{-}$). Dexamethasone continued to significantly increase the average circularity of myofibroblasts from 0.36 ± 0.01 ($DEX^{-}LPS^{+}$) to 0.50 ± 0.01 ($DEX^{+}LPS^{+}$) in the presence of LPS. The effect of LY294002 and dexamethasone on macrophage numbers was also evaluated (Figure 5iv, v). M0 and M1 macrophages had relative cell numbers of 54 ± 9.6% ($LY^{-}LPS^{-}$) and 56 ± 6.9% ($LY^{-}LPS^{+}$), respectively, which were not significantly different. However, macrophages cultured in the presence of LY294002 displayed significant decreases in cell numbers of 16 ± 4.9% ($LY^{+}LPS^{-}$) and 16 ± 4% ($LY^{+}LPS^{+}$). Dexamethasone, however, had no significant effect on relative macrophage numbers (Figure 5v).

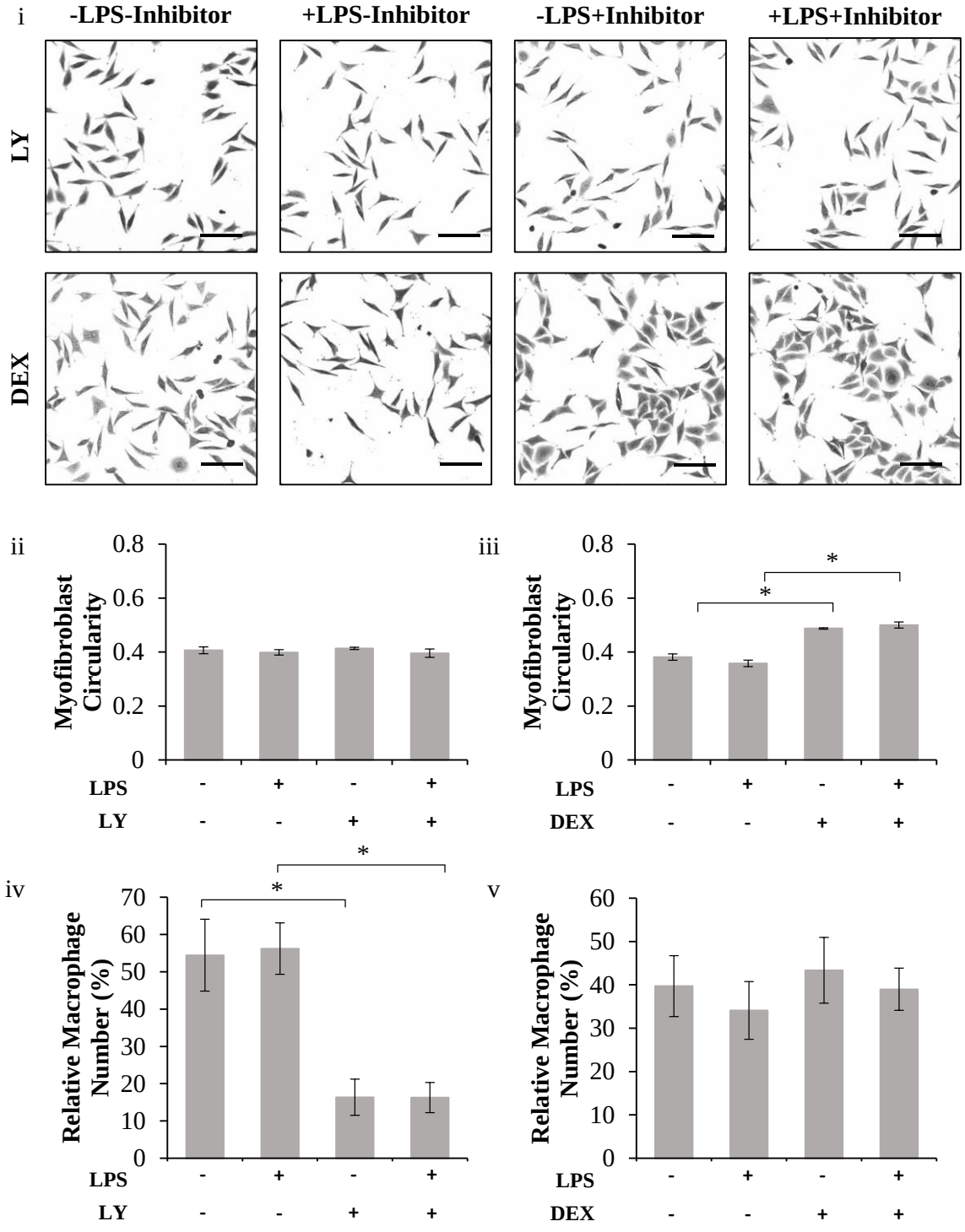

Figure 5: The effect of LY294002 and dexamethasone on myofibroblasts and macrophages. (i-iii) Myofibroblasts were co-cultured with macrophages (40 x 10^3) with or without LPS (0.1 µg/ml) pre-treatment and with or without the inhibitors (10 µM) LY294002 and dexamethasone and the average circularity determined. (iv, v) Macrophages were pre-treated with LPS and treated with or without LY294002 and dexamethasone and the relative cell numbers determined. Images were captured using an Olympus CKX41 microscope coupled to a Motic 3.0 megapixel camera (4x objective lens; scale bar = 200 µm). * = $p < 0.05$; N = 4.

Discussion

Diseases such as muscular dystrophy and myositis are often characterized by a pro-inflammatory microenvironment, but it is unclear what the effect is on the population of fibroblasts [12]. Pro-inflammatory macrophages have been shown to inhibit myoblast fusion; at low numbers, fibroblasts promote myoblast fusion, while at higher numbers they decrease this stage of terminal differentiation [6,25,30,31]. However, it is unclear what effect M1 macrophages have on the population of fibroblasts and what the subsequent implication on muscle wound repair would be [25]. We therefore sought to investigate the effect of M1 macrophages on the population of fibroblasts in experimental conditions that would promote myoblast differentiation and fusion *in vitro* (i.e. low serum).

Fibroblasts and macrophages can acquire different phenotypes and morphologies depending on the *in vivo* microenvironment or *in vitro* experimental conditions [21,32]. Studies often distinguish between M1 and M2 macrophages, but often make no such distinction between fibroblasts and myofibroblasts. Rapid assessment and quantification of cell shapes may be a useful tool to evaluate the effect of experimental conditions on the cells. Previous studies have shown that fibroblasts cultured in SFM *in vitro* can differentiate into myofibroblasts with the addition of TGF-β and/or serum [27,28]. Furthermore, fibroblasts first acquire a proto-myofibroblast phenotype before fully differentiating into myofibroblasts, and differentiation is reversible [8,29,32]. We therefore first sought to establish and characterize the different populations in our experimental model. We observed that myofibroblasts maintained in 10% SCM had a short and wide morphology and were consistently positive for high levels of α-SMA expression; these cells dedifferentiated to fibroblasts when the media was switched to 0% SCM (i.e. SFM) as evidenced by a decrease in α-SMA expression with a long and narrow morphology. Furthermore, we observed an intermediate morphology that also expressed low levels of α-SMA in response to 2% SCM; this is characteristic of the proto-myofibroblasts phenotype of myofibroblasts [8]. We then sought to rapidly and quantitatively assess morphology using circularity as a cell shape descriptor and found that myofibroblasts were the most circular and elongate as they acquire a fibroblast phenotype. Therefore, assessing circularity using image processing software, such as ImageJ, could be used to quantifiably describe cell shape and distinguish between these morphologies.

The plasticity of macrophages was further investigated in an *in vitro* muscle regenerative microenvironment by establishing a population of M1 macrophages in 2% SCM. We observed that macrophages displayed a high circularity, but when M0 macrophages (expressing low levels of CD86) were stimulated with LPS to yield M1 macrophages (expressing high levels of CD86), the cells acquired elongated protrusions with slightly decreased circularity.

We have previously shown that M0 macrophages abrogated the pro-migratory effects of fibroblasts on myoblasts, but it was unclear how macrophages mediated this effect [24]. We sought to determine whether these effects were mediated via a decrease in myofibroblast numbers. We observed that the co-culture of M1 macrophages resulted in a significant decrease in myofibroblast numbers. This suggests that LPS interacts with macrophages to stimulate a pro-inflammatory phenotype which in turn caused myofibroblast death. This M1 macrophage-induced cell death was specific to myofibroblasts, as the same effect was not observed with myoblasts.

We next sought to investigate the mechanism by which M1 macrophages cause a decrease in myofibroblast number. Macrophages typically respond to an inflammatory stimulus, such as LPS, by upregulating the secretion of an array of pro-inflammatory mediators, such as TNF-α, IL-1β, IL-6, iNOS/NO and COX-2/PGE-2; inhibitor studies have shown that these factors stimulate pathways such as PI3K, p38 MAPK and JNK (Table 1) [33-42]. Furthermore, some of the M1 macrophage-produced soluble factors (e.g. NO, TNF-α and PGE_2) have previously been shown to induce fibroblast death [43-45]. We therefore sought to screen several inhibitors to determine the pathways they targeted were responsible for the rescue of myofibroblast numbers when co-cultured with M1 macrophages. We showed that myofibroblast death was not mediated by iNOS/NO, COX-2/PGE, p38 MAPK or JNK, but that PI3K was involved. Furthermore, we showed that dexamethasone was also able to rescue myofibroblast numbers despite causing a decrease in numbers on its own; this glucocorticoid is known to inhibit fibroblast proliferation [46]. We further found that LY294002 potentially does not directly act on myofibroblasts since there was no observable effect on myofibroblast numbers or morphology. However, LY294002 decreased macrophage cell number; this suggests that LY294002 rescues myofibroblast numbers by decreasing M0 and/or M1 macrophage numbers. The PI3K/Akt pathway is an important cell survival pathway in

macrophages and inhibition via LY294002 has previously resulted in macrophage death [47]. In contrast to LY294002, dexamethasone had no effect on macrophages, but caused the myofibroblasts to acquire a more rounded morphology. Previous studies have shown that dexamethasone confers protection to fibroblasts against TNF-α-induced cytotoxicity by activating NF-κB to promote cell survival [48]. Furthermore, dexamethasone has been shown to exhibit pro-fibrotic effects by augmenting TGF-β-induced α-SMA expression in myofibroblasts [49].

Conclusion

We have successfully established and characterized the different phenotypes that fibroblasts and macrophages acquire in response to different *in vitro* experimental conditions. In the absence of serum, elongated fibroblasts had a low circularity and decreased α-SMA expression; with increasing serum concentration, these cells differentiated into myofibroblasts with high circularity and increased α-SMA expression. Unstimulated macrophages had a high circularity and low CD86 expression; when these cells were stimulated with LPS to acquire a M1 phenotype, they displayed increased CD86 expression and a decreased circularity. We then used our previously established co-culture method to evaluate the effect of M1 macrophages on myofibroblast and myoblast cell numbers; we found that M1 macrophages resulted in myofibroblast, but not myoblast, cell death. The addition of LY294002 could rescue myofibroblast cell numbers: LY294002 prevented myofibroblast cell death by causing a decrease in macrophage numbers; dexamethasone may confer protection by affecting myofibroblast morphology, but the effect on myofibroblast proliferation was not significant. Altogether, these findings highlight the ability of macrophages and fibroblasts to acquire different functional phenotypes depending on the experimental conditions. Importantly, these phenotypes have differential effects on myoblasts during stages of wound repair. The detrimental effect of M1 macrophages on myofibroblasts would negatively affect myogenesis since myofibroblasts are important for promoting myoblast migration and fusion.

Acknowledgements

The work was supported by the South African National Research Foundation, South African Medical Research Council and University of KwaZulu-Natal.

References

1. Bentzinger CF, Wang YX, Dumont NA, Rudnicki MA. Cellular dynamics in the muscle satellite cell niche. *EMBO Rep*, 14(12), 1062-1072 (2013).
2. Cantini M, Giurisato E, Radu C *et al.* Macrophage-secreted myogenic factors: a promising tool for greatly enhancing the proliferative capacity of myoblasts in vitro and in vivo. *Neurol Sci*, 23(4), 189-194 (2002).
3. Sonnet C, Lafuste P, Arnold L *et al.* Human macrophages rescue myoblasts and myotubes from apoptosis through a set of adhesion molecular systems. *J Cell Sci*, 119(Pt 12), 2497-2507 (2006).
4. Saclier M, Cuvellier S, Magnan M, Mounier R, Chazaud B. Monocyte/macrophage interactions with myogenic precursor cells during skeletal muscle regeneration. *FEBS J*, 280(17), 4118-4130 (2013).
5. Deng B, Wehling-Henricks M, Villalta SA, Wang Y, Tidball JG. IL-10 triggers changes in macrophage phenotype that promote muscle growth and regeneration. *J Immunol*, 189(7), 3669-3680 (2012).
6. Arnold L, Henry A, Poron F *et al.* Inflammatory monocytes recruited after skeletal muscle injury switch into antiinflammatory macrophages to support myogenesis. *J Exp Med*, 204(5), 1057-1069 (2007).
7. Desmouliere A, Geinoz A, Gabbiani F, Gabbiani G. Transforming growth factor-beta 1 induces alpha-smooth muscle actin expression in granulation tissue myofibroblasts and in quiescent and growing cultured fibroblasts. *J Cell Biol*, 122(1), 103-111 (1993).
8. Tomasek JJ, Gabbiani G, Hinz B, Chaponnier C, Brown RA. Myofibroblasts and mechano-regulation of connective tissue remodelling. *Nat Rev Mol Cell Biol*, 3(5), 349-363 (2002).
9. Chapman MA, Meza R, Lieber RL. Skeletal muscle fibroblasts in health and disease. *Differentiation*, 92(3), 108-115 (2016).
10. Rao N, Evans S, Stewart D *et al.* Fibroblasts influence muscle progenitor differentiation and alignment in contact independent and dependent manners in organized co-culture devices. *Biomed Microdevices*, 15(1), 161-169 (2013).
11. Bosurgi L, Manfredi AA, Rovere-Querini P. Macrophages in injured skeletal muscle: a perpetuum mobile causing and limiting fibrosis, prompting or restricting resolution and regeneration. *Front Immunol*, 2, 62 (2011).
12. Mann CJ, Perdiguero E, Kharraz Y *et al.* Aberrant repair and fibrosis development in skeletal muscle. *Skelet Muscle*, 1(1), 21 (2011).
13. Villalta SA, Nguyen HX, Deng B, Gotoh T, Tidball JG. Shifts in macrophage phenotypes and macrophage competition for arginine metabolism affect the severity of muscle pathology in muscular dystrophy. *Hum Mol Genet*, 18(3), 482-496 (2009).
14. Loell I, Lundberg IE. Can muscle regeneration fail in chronic inflammation: a weakness in inflammatory myopathies? *J Intern Med*, 269(3), 243-257 (2011).
15. Charge SB, Rudnicki MA. Cellular and molecular regulation of muscle regeneration. *Physiol Rev*, 84(1), 209-238 (2004).
16. Karalaki M, Fili S, Philippou A, Koutsilieris M. Muscle regeneration: cellular and molecular events. *In Vivo*, 23(5), 779-796 (2009).
17. Baoge L, Van Den Steen E, Rimbaut S *et al.* Treatment of skeletal muscle injury: a review. *ISRN Orthop*, 2012, 689012 (2012).
18. Garg K, Corona BT, Walters TJ. Therapeutic strategies for preventing skeletal muscle fibrosis after injury. *Front Pharmacol*, 6, 87 (2015).
19. Tidball JG. Inflammatory processes in muscle injury and repair. *Am J Physiol Regul Integr Comp Physiol*, 288(2), R345-353 (2005).

20. Tidball JG, Villalta SA. Regulatory interactions between muscle and the immune system during muscle regeneration. *Am J Physiol Regul Integr Comp Physiol*, 298(5), R1173-1187 (2010).
21. Ploeger DT, Hosper NA, Schipper M, Koerts JA, de Rond S, Bank RA. Cell plasticity in wound healing: paracrine factors of M1/ M2 polarized macrophages influence the phenotypical state of dermal fibroblasts. *Cell Commun Signal*, 11(1), 29 (2013).
22. Mathew SJ, Hansen JM, Merrell AJ *et al.* Connective tissue fibroblasts and Tcf4 regulate myogenesis. *Development*, 138(2), 371-384 (2011).
23. Murphy MM, Lawson JA, Mathew SJ, Hutcheson DA, Kardon G. Satellite cells, connective tissue fibroblasts and their interactions are crucial for muscle regeneration. *Development*, 138(17), 3625-3637 (2011).
24. Venter C, Niesler C. A triple co-culture method to investigate the effect of macrophages and fibroblasts on myoblast proliferation and migration. *Biotechniques*, 64(2), 52-58 (2018).
25. Venter C, Niesler CU. Cellular alignment and fusion: Quantifying the effect of macrophages and fibroblasts on myoblast terminal differentiation. *Exp Cell Res*, 370(2), 542-550 (2018).
26. Venter C, Niesler CU. Rapid quantification of cellular proliferation and migration using ImageJ. *Biotechniques*, 66(2), 99-102 (2019).
27. Vaughan MB, Howard EW, Tomasek JJ. Transforming growth factor-beta1 promotes the morphological and functional differentiation of the myofibroblast. *Exp Cell Res*, 257(1), 180-189 (2000).
28. Howard EW, Crider BJ, Updike DL *et al.* MMP-2 expression by fibroblasts is suppressed by the myofibroblast phenotype. *Exp Cell Res*, 318(13), 1542-1553 (2012).
29. Hecker L, Jagirdar R, Jin T, Thannickal VJ. Reversible differentiation of myofibroblasts by MyoD. *Exp Cell Res*, 317(13), 1914-1921 (2011).
30. Bencze M, Negroni E, Vallese D *et al.* Proinflammatory macrophages enhance the regenerative capacity of human myoblasts by modifying their kinetics of proliferation and differentiation. *Mol Ther*, 20(11), 2168-2179 (2012).
31. Hinds S, Tyhovych N, Sistrunk C, Terracio L. Improved tissue culture conditions for engineered skeletal muscle sheets. *Sci World J*, 2013, 370151 (2013).
32. Desai VD, Hsia HC, Schwarzbauer JE. Reversible modulation of myofibroblast differentiation in adipose-derived mesenchymal stem cells. *PLoS One*, 9(1), e86865 (2014).
33. Chen BC, Lin WW. Potentiation of lipopolysaccharide-induced IL-6 release by uridine triphosphate in macrophages: cross-interaction with cyclooxygenase-2-dependent prostaglandin E(2) production. *J Biomed Sci*, 6(6), 425-432 (1999).
34. Banjanac M, Munic Kos V, Nujic K *et al.* Anti-inflammatory mechanism of action of azithromycin in LPS-stimulated J774A.1 cells. *Pharmacol Res*, 66(4), 357-362 (2012).
35. Chien HY, Lu CS, Chuang KH, Kao PH, Wu YL. Attenuation of LPS-induced cyclooxygenase-2 and inducible NO synthase expression by lysophosphatidic acid in macrophages. *Innate Immun*, 21(6), 635-646 (2015).
36. Yano H, Uchida M, Saito T, Aoki T, Kremenik MJ, Oyanagi E. Reduction of Real-Time Imaging of M1 Macrophage Chemotaxis toward Damaged Muscle Cells is PI3K-Dependent. *Antioxidants (Basel)*, 7(10) (2018).
37. Erasalo H, Laavola M, Hamalainen M, Leppanen T, Nieminen R, Moilanen E. PI3K inhibitors LY294002 and IC87114 reduce inflammation in carrageenan-induced paw oedema and down-regulate inflammatory gene expression in activated macrophages. *Basic Clin Pharmacol Toxicol*, 116(1), 53-61 (2015).

38. Kim SH, Kim J, Sharma RP. Inhibition of p38 and ERK MAP kinases blocks endotoxin-induced nitric oxide production and differentially modulates cytokine expression. *Pharmacol Res*, 49(5), 433-439 (2004).
39. Shi Q, Cheng L, Liu Z *et al.* The p38 MAPK inhibitor SB203580 differentially modulates LPS-induced interleukin 6 expression in macrophages. *Cent Eur J Immunol*, 40(3), 276-282 (2015).
40. Nieminen R, Lahti A, Jalonen U, Kankaanranta H, Moilanen E. JNK inhibitor SP600125 reduces COX-2 expression by attenuating mRNA in activated murine J774 macrophages. *Int Immunopharmacol*, 6(6), 987-996 (2006).
41. Korhonen R. Dexamethasone Inhibits Inducible Nitric-Oxide Synthase Expression and Nitric Oxide Production by Destabilizing mRNA in Lipopolysaccharide-Treated Macrophages. *Molecular Pharmacology*, 62(3), 698-704 (2002).
42. Miller L, Hunt JS. Regulation of TNF-α Production in Activated Mouse Macrophages by Progesterone. *J Immunol*, 160(10), 5098-5104 (1998).
43. Nascimento FR, Gomes EA, Russo M, Lepique AP. Interferon regulatory factor (IRF)-1 is a master regulator of the cross talk between macrophages and L929 fibrosarcoma cells for nitric oxide dependent tumoricidal activity. *PLoS One*, 10(2), e0117782 (2015).
44. Humphreys DT, Wilson MR. Modes of L929 cell death induced by TNF-alpha and other cytotoxic agents. *Cytokine*, 11(10), 773-782 (1999).
45. Huang SK, White ES, Wettlaufer SH *et al.* Prostaglandin E(2) induces fibroblast apoptosis by modulating multiple survival pathways. *FASEB J*, 23(12), 4317-4326 (2009).
46. Ramalingam A, Hirai A, Thompson EA. Glucocorticoid inhibition of fibroblast proliferation and regulation of the cyclin kinase inhibitor p21Cip1. *Mol Endocrinol*, 11(5), 577-586 (1997).
47. Liu H, Perlman H, Pagliari LJ, Pope RM. Constitutively activated Akt-1 is vital for the survival of human monocyte-differentiated macrophages. Role of Mcl-1, independent of nuclear factor (NF)-kappaB, Bad, or caspase activation. *The Journal of Experimental Medicine*, 16(2), 113-126 (2001).
48. Mendoza-Milla C, Machuca Rodriguez C, Cordova Alarcon E *et al.* NF-kappaB activation but not PI3K/Akt is required for dexamethasone dependent protection against TNF-alpha cytotoxicity in L929 cells. *FEBS Lett*, 579(18), 3947-3952 (2005).
49. Gu L, Zhu YJ, Guo ZJ, Xu XX, Xu WB. Effect of IFN-gamma and dexamethasone on TGF-beta1-induced human fetal lung fibroblast-myofibroblast differentiation. *Acta Pharmacol Sin*, 25(11), 1479-1488 (2004).

Supplementary Information

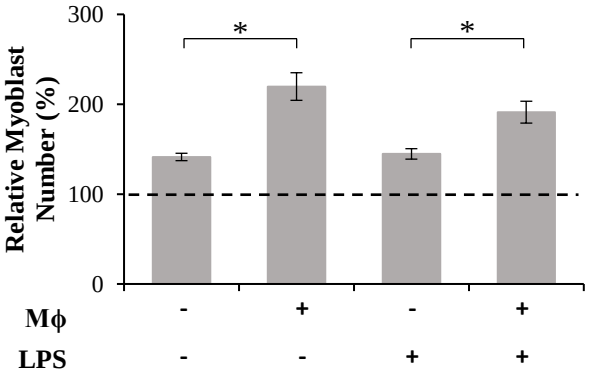

Figure S1: The effect of macrophages on myoblasts. Cells were cultured with or without macrophages (Mϕ; 40 x 10^3) in SFM with or without LPS (0.1 μg/ml) for 24 hours and the relative cell numbers determined. * = $p < 0.05$; N = 4.

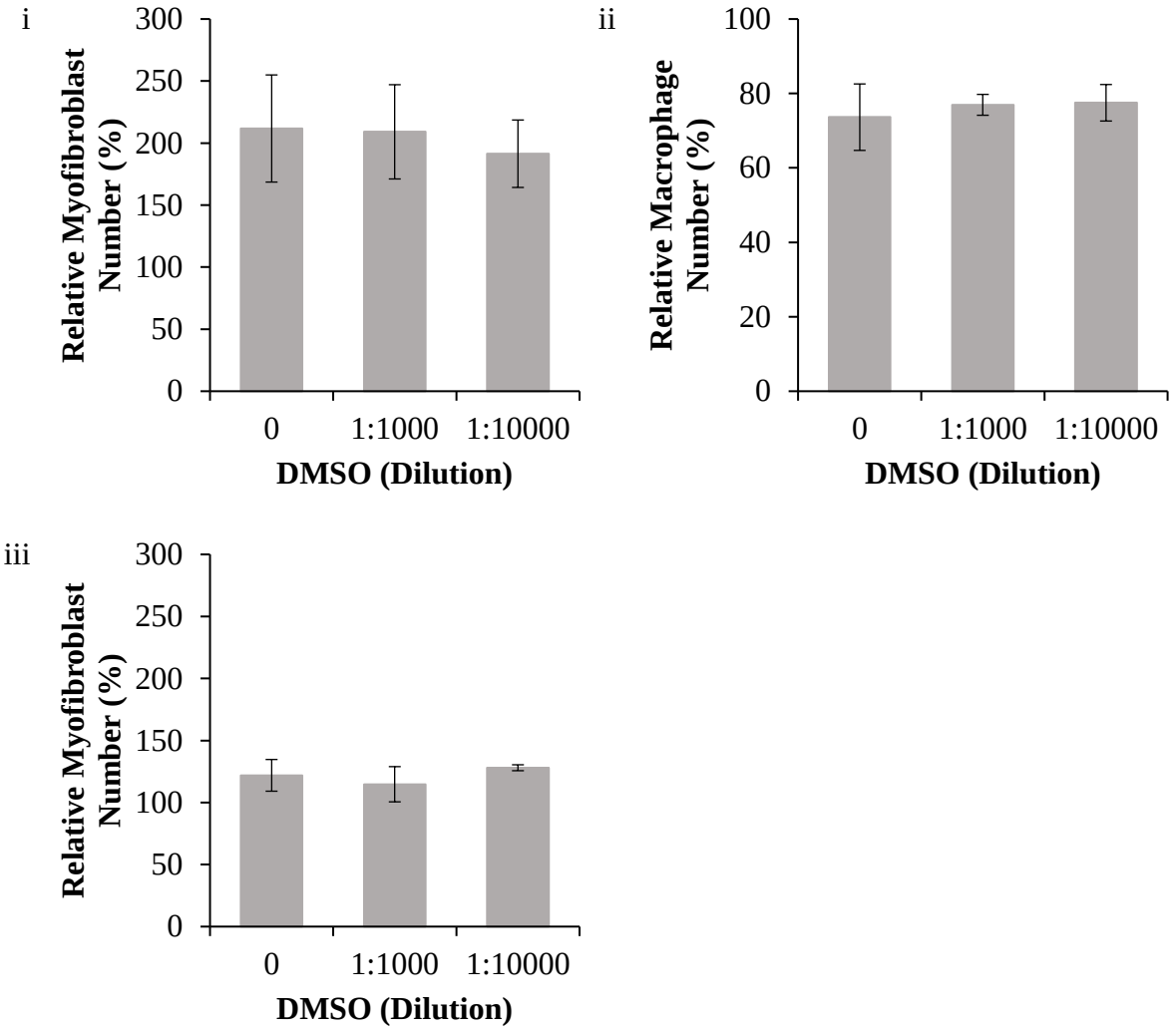

Figure S2: The effect of DMSO on myofibroblasts and macrophages. (i) Myofibroblasts, (ii) macrophages and (iii) myofibroblasts cultured with macrophages (pre-treated with 0.1 μg/ml LPS) were treated with DMSO (1:1000 and 1:10 000) in 2% SCM for 24 hours and the relative cell numbers determined. * = $p < 0.05$; N = 4.

CHAPTER 7: CONCLUSIONS AND RECOMMENDATIONS FOR FURTHER RESEARCH

Myogenesis during wound repair involves the activation of satellite cells to myoblasts, which proliferate, migrate into the wound and subsequently align and fuse into myofibres; this process is regulated by non-myogenic cells, such as macrophages and fibroblasts. Studying myogenesis *in vitro* is dependent on the establishment of muscle models and the assessment of cellular behaviours in response to various experimental conditions. In this thesis, we have developed an *in vitro* co-culture model and analysis tools to investigate muscle regeneration. Our novel co-culture technique, which is simpler and faster to establish than previously used co-culture techniques, also enabled co-culture of at least three different cell types with no physical separation and permitted an array of cellular interactions that would occur in vivo, including direct cell-cell contact. We successfully optimized ImageJ (image analysis software) to identify and quantify both cell number and wound area to assess proliferation and migration, respectively. These methods were faster and more accurate to perform than manual analysis and conventionally used methods. We also optimized the program ct-FIRE to determine the orientation of cells and quantify alignment using an alignment index; this method of alignment analysis was accurate and simpler to perform compared to previously developed methods. Lastly, we used ImageJ's circularity feature as a tool to quantitively describe and assess changes in cellular morphology. Altogether, these methods were applied to investigate the effect of non-myogenic cells on myogenesis as well as communication between the non-myogenic cells.

We first used our novel co-culture model and optimized analysis tools to understand the effects of increasing macrophage and/or fibroblast numbers on the early (proliferation and migration) and late (alignment and fusion) stages of myogenesis. We observed that macrophages promoted the proliferation of myoblasts in a cell density-dependent manner (5 to 80 x 10^3 cells); low macrophage numbers (5 to 40 x 10^3 cells) had no effect on myoblast migration while high macrophage numbers (80 x 10^3 cells) promoted migration. We observed that low fibroblast numbers (20 x 10^3 cells) promoted myoblast proliferation, but this effect was lost when cell numbers were increased further (40 to 80 x 10^3 cells). Additionally, fibroblasts promoted myoblast migration in a cell density-dependent manner (5 to 80 x 10^3 cells). When both macrophages (40 x 10^3 cells) and fibroblasts (40 x 10^3 cells) were co-

cultured with myoblasts (i.e. triple co-culture), we observed that myoblast proliferation continued to be promoted by macrophages, but the positive effect of fibroblasts on myoblast migration was abrogated in the presence of macrophages. We also observed that macrophages (5 to 80 x 10^3 cells) promoted alignment, but inhibited fusion, in a cell density-dependent manner. Fibroblasts, on the other hand, had no significant effect on myoblast alignment but could promote (5 to 10 x 10^3 cells) and inhibit (20 to x 10^3 cells) fusion. In triple co-culture, macrophages (40 x 10^3 cells) continued to promote myoblast alignment and inhibit fusion in the presence of fibroblasts (40 x 10^3 cells).

We initially did not stimulate the macrophages or fibroblasts to acquire specific phenotypes; phenotypic changes may have occurred, however, in response to co-culture conditions. Furthermore, we did not distinguish between the fibroblast and myofibroblast phenotypes in our initial studies, which were performed in serum-free or serum-containing media. We next expanded on our initial studies by intentionally stimulating macrophages to acquire a pro-inflammatory phenotype and myofibroblasts to de-differentiate from fibroblasts. We characterized the phenotypes of these non-myogenic cells using circularity to quantitively assess changes in morphology and confocal microscopy to assess the expression of specific markers (i.e. α-SMA for myofibroblasts and CD86 for M1 macrophages). We found that myofibroblasts had a greater circularity (corresponding with a rounded morphology) and higher levels of α-SMA expression; fibroblasts had a lower circularity (corresponding with an elongated morphology) and decreased α-SMA expression. Unstimulated macrophages had a higher circularity and low CD86 expression; M1 macrophages had a lower circularity with increased levels of CD86.

Our initial results indicated a potential for macrophages to negatively affect fibroblasts and their pro-migratory effect on myoblasts. We expanded on this and found that macrophages stimulated to an M1 phenotype specifically resulted in a decrease on myofibroblast numbers with no negative effects on myoblast numbers. We investigated the mechanism of M1 macrophage-mediated decrease in myofibroblast numbers and found that the iNOS/NO, COX-2/PGE_2, p38 MAPK and JNK pathways were not involved. However, the PI3K inhibitor LY294002 prevented myofibroblast death by M1 macrophages. Furthermore, we showed that LY294002 prevented myofibroblast death by decreasing macrophage numbers. Dexamethasone, on the other hand, directly interacted with myofibroblasts to increase cell circularity, but the implications of this require further investigation.

The findings in this thesis provided novel insights into the involvement of macrophages and fibroblasts during the early and late stages of wound repair. The number of cells in co-culture represented either the expansion (low to high cell numbers) or resolution (high to low cell numbers) of non-myogenic cells as would be observed during the progression of muscle wound repair *in vivo*. We showed that it is important for macrophages to increase in number upon muscle injury to promote myoblast proliferation. The population of macrophages needs to subsequently subside to enable recruited fibroblasts to promote myoblast migration into the wound. However, it is important that macrophages do not completely resolve during the later stages of wound repair to promote myoblast alignment prior to fusion. Fibroblasts are also required to incompletely resolve to promote myoblast fusion. Furthermore, these non-myogenic cells displayed cell density-dependent, and even opposing effects, on myogenesis. This highlights an important consideration when studying myogenesis using *in vitro* co-culture models since most co-culture studies focus on evaluating a set number of cells in co-culture rather than distinct ratios. It is difficult to accurately associate the cell numbers used *in vitro* with the cell numbers that are present *in vivo*. Therefore, cell type ratios present during *in vivo* wound repair require investigation to design wound repair strategies that carefully regulate the timely expansion and resolution of non-myogenic cells.

Our findings also showed that macrophages with a pro-inflammatory phenotype are detrimental to the population of fibroblasts; this would result in aberrant wound repair since the fibroblast population is important for promoting myoblast fusion. The phenotypes that macrophages acquire and their timely transition from the M1 to M2 phenotype during wound repair is therefore important. Furthermore, M1 macrophage-mediated death of myofibroblasts was prevented by inhibiting the PI3K signalling pathway; this resulted in macrophage, but not myofibroblast, death. Therefore, the PI3K pathway is a potential therapeutic target to treat aberrant muscle wound repair in diseases, such as myositis, that is caused by the dysregulated presence of macrophages.

We primarily investigated the effect of the presence of macrophages and/or fibroblasts on myoblast behaviour, but not the mechanism of communication. Our co-culture technique permitted an array of cellular interactions between cell types (i.e. cell-cell, cell-soluble factor and cell-matrix factor), but we did not identify the exact mediators of communication. Therefore, future studies would be aimed at identifying these and determining if direct cell-

cell contact with macrophages and fibroblasts modulates myoblast behaviour by comparing the effects of direct contact vs. secreted factors. In this study, conditioned media from the non-myogenic cells would be collected and serially diluted to represent different cell numbers. Investigating changes in mRNA/protein levels of signalling molecules could also shed light on how non-myogenic cells influence myogenesis. However, analysing specific changes in signalling molecules would be a challenge using our co-culture method; analysis would need to be microscopy-based.

We have demonstrated that non-myogenic cells have different effects on myogenesis depending on their cell density. Future studies would be aimed at determining the optimal ratio of non-myogenic cells to promote myoblast behaviour. We previously showed that 40 x 10^3 macrophages promoted myoblast alignment while 5 x 10^3 fibroblast promoted fusion; a future study would use these cell numbers in triple co-culture to promote myoblast alignment *and* fusion. Myogenesis *in vivo* could also be mimicked *in vitro* by timeously adding and removing non-myogenic cells (to represent their expansion and subsequent resolution in the wound), as well as stimulating them to acquire specific phenotypes, as myoblasts proliferate, migrate, align and fuse into myotubes.

Although we limited our study to macrophages and fibroblasts, other non-myogenic cells (such as endothelial cells) are involved in muscle wound repair and should be evaluated for their role in regulating myogenesis. This can be done in the future by using our co-culture system to include four or more cell types. We also stimulated macrophages to acquire an M1 phenotype and investigated the effect on fibroblasts; however, we have yet to evaluate the effect of M2 macrophages on fibroblasts. Furthermore, our study was limited to murine cell lines and future studies should be aimed at determining if similar results are obtained with more clinically relevant primary human cells.

APPENDIX A: PROTOCOL FOR: RAPID QUANTIFICATION OF CELLULAR PROLIFERATION AND MIGRATION USING IMAGEJ

Protocol Title: Quantification of Adherent Cell Proliferation and Migration Using ImageJ

Reagents

1. Dulbecco's Modified Eagle's Medium (DMEM; Sigma, St Louis, MO, USA)
2. Fetal bovine serum (FBS; Biowest, Riverside, MO, USA)
3. Penicillin/Streptomycin (PenStrep; Lonza, Basel, Switzerland)
4. Phosphate buffered saline (PBS; Merck, Kenilworth, NJ, USA)
5. T75 culture flasks, 12- and 24-well plates (NEST, Wuxi, China)
6. Trypsin-EDTA (Trypsin, Lonza, Basel, Switzerland)
7. Methanol (Radchem, Orland Park, IL, USA)
8. Crystal Violet (Sigma, St Louis, MO, USA)

Recipes

1. Growth Media (GM): Supplement DMEM with FBS (10%) and PenStrep (2%)
2. Crystal Violet Stain: Add 0.2% (m/v) crystal violet powder to 100% methanol

Equipment

1. Innova® CO-170 CO2-incubator (New Brunswick, USA)
2. Olympus CKX41 microscope (Olympus, Tokyo, Japan)
3. Motic 3.0 megapixel camera (Wetzlar, Germany)
4. Computer (Windows, OS or Linux)
5. ImageJ (available at https://imagej.nih.gov/ij/)

Procedure

Cell Culture

1. Culture C2C12 myoblasts in a T75 culture flask with GM at 37°C and 5% CO_2 until 70% confluent.

2. Wash the cells twice with sterile PBS (5 ml), detach with trypsin (2 ml, 10 mins), add GM (2 ml) and count the cells.

Experimentation

Proliferation:

3.1. Plate out cells ($5 – 20 \times 10^3$) into a 24-well plate in GM (500 µl) and incubate (3 hours) to promote adherence.

Attention: The number of cells plated out depends entirely on the researcher's requirements and experimental conditions. Avoid plating out too many cells which cause cell clumps and making analysis difficult.

Hint: Gently swirl and shake the culture plate prior to incubating to ensure even cell distribution.

3.2. Change the media to experimental conditions and incubate (24 hours).

3.3. Remove the media, wash with PBS (500 µl, 5 mins) and stain with crystal violet (500 µl, 15 mins).

3.4. Remove the stain, wash the cells be gently submerging the plate in a water bath until all the stain is removed and leave to completely dry.

3.5. Take images of the cells (3-5 fields of view per replicate for 2-3 replicates) using a camera-attached brightfield microscope (4x objective lens).

Migration:

4.1. Plate out cells (120×10^3) into 12-well plate in GM (1 ml) and incubate (24 hours).

Attention: The number of cells can be varied but aim to achieve a confluency of 90-100% after 24 hours. Plate the cells out into a 12-well and not a 24-well plate to produce wound areas that can be accurately identified by ImageJ.

4.2. Scratch the confluent monolayer with a 200 µl sterile loading tip.

Attention: Perform the scratch directly in the centre of the well to produce wound areas that can be accurately identified by ImageJ.

Hint: Use a ruler as a brace for the loading tip when performing scratches to generate a straight and central wound.

4.3. Wash the cells twice with sterile PBS (500 µl), change to experimental media and incubate (7 hours).

4.4. Take images of the wound area at different time points (0, 3, 5 and 7 hours) with a camera-attached microscope (4x objective lens).

ImageJ Processing

Macro Creation

5.1. Open ImageJ and navigate to *Plugins → New → Macro.*

5.2. In the new window, copy/paste the corresponding code for the following macros.

5.3. Proliferation Macro:

```
//Convert Image to 8-bit
run("8-bit");
//Remove Noise
run("Despeckle");
//Adjust Brightness and Contrast
setMinAndMax(-87, 167);
run("Apply LUT");
//Apply Phansalkar Local Threshold
run("Auto Local Threshold...", "method=Phansalkar radius=15 parameter_1=0 parameter_2=0 white");
setAutoThreshold("Default");
//Watershed
run ("Watershed");
//Count Objects (i.e. Cells)
run("Analyze Particles...", "display clear summarize");
```

5.4. Migration Macro:

```
run("8-bit");
run("Find Edges");
for (i = 0; i < 37; i++)
{run("Smooth");}
setAutoThreshold("MinError");
//run("Threshold...");
run("Analyze Particles...", "size=10000-Infinity show=Outlines display");
```

5.5. Migration Image Processing Macro:

```
run("8-bit");
run("Find Edges");
for (i = 0; i < 37; i++)
{run("Smooth");}
```

5.6. Save each macro (*File → Save As)* separately with the corresponding name followed by ".IJM" (without the inverted commas).

Attention: each macro needs to be saved as a separate file followed with the suffix ".IJM" e.g. Proliferation Macro.IJM

Batch Processing

6.1. On a computer, create two folders named "Original" and "Analyzed" in the file location of your choice (e.g. Desktop).
6.2. Copy the images to be analysed into the *Original* folder.
6.3. In ImageJ, navigate to *Process → Batch → Macro.*
6.4. Click on *Input* and select the *Original* folder; click on *Output* and select the *Analyzed* folder.

Hint: The *Input* and *Output* do not need to be selected every time a batch process is performed unless the names and/or file locations for the *Original* and *Analyzed* folders are changed.

6.5. Click on *Open* and select the macro of choice (e.g. Proliferation Macro or Migration Macro).
6.6. Click on *Process.*

Hint: The images in the *Original* folder can be deleted once the batch process is complete; the analysed images are in the *Analyzed* folder.

6.7. For proliferation, save the "Summary" window. The "Count" column contains the number of cells for each image.
6.8. For migration, save the "Results" window. The "Area" column contains the wound area for each image. If there are two areas for one image, select the area which corresponds with the wound area of the analysed image (in the *Analyzed* folder).

Attention: in the event that ImageJ does not accurately identify the wound area, drag and drop the image into ImageJ, run the Migration Image Processing macro (Plugins → *Macros → Run → Migration Image Processing Macro.IJM*), manually select the wound area (Image → *Adjust → Threshold; uncheck Dark Background; adjust the threshold bars)* and Analyze (Analyze → *Analyze Particles → OK).*

APPENDIX B: PROTOCOL FOR: A TRIPLE CO-CULTURE METHOD TO INVESTIGATE THE EFFECT OF MACROPHAGES AND FIBROBLASTS ON MYOBLAST PROLIFERATION AND MIGRATION

Protocol Title: Triple co-culture of myoblasts, macrophages and fibroblasts

Reagents

1. DMEM with L-glutamine (Sigma, cat. no. D5648-1L)
2. FBS (Gibco, cat. no. 10499-044)
3. PenStrep (Lonza, cat. no. DE17-602E)
4. T75 flasks (Nest, cat. no. 708003)
5. 24-well plates (Nest, cat. no. 702001)
6. Trypsin-EDTA (Lonza, cat. no. BE17-161E)

Recipes

1. Growth Media (GM): Supplement DMEM with FBS (10%) and PenStrep (2%)

Equipment

1. Innova® CO-170 CO2-incubator (New Brunswick, USA)
2. Olympus CKX41 microscope (Olympus, Tokyo, Japan)
3. Motic 3.0 megapixel camera (Wetzlar, Germany)
4. DSC-158T desktop centrifuge

Procedure

Cell Culture

1. Culture J774a.1 macrophages, LMTK fibroblasts and C2C12 myoblasts in separate T75 flasks with GM at 37˚C and 5% CO_2 until 70% confluent.
2. Detach macrophages with a cell scraper, pellet the cells via gentle centrifugation (600 rpm, 10 mins), resuspend in 2 ml GM and count using a hemocytometer.
3. Detach fibroblasts with 2 ml trypsin-EDTA for 10 minutes at 37˚C, add 2 ml GM and count using a hemocytometer.

Co-Culture

4. Pipette 40 x 10^3 macrophages and/or 40 x 10^3 fibroblasts along the outer edge of a 24-well plate.

Attention: Ensure that the volume is not less than 30 µl, but not more than 100 µl. If the volume is less than 30 µl, add more growth media to ensure that the cells will be evenly distributed along the outer edge when swirling. If the volume is too high, concentrate the cells further via centrifugation and resuspend in a lower volume of GM; a higher volume will cause the cells to shift towards the centre of the well.

Hint: The number of cells seeded along the outer edge of the well can be changed depending on the experimenter's needs. However, the higher the number of cells seeded, the more likely they are to move to the centre of the well during experimentation. We have found that the upper limit of the total number of cells to be seeded was ~80 x 10^3 cells.

5. Swirl the culture flask by hand to evenly distribute the cells along the outer edge of the well.

Attention: Ensure you rapidly swirl (do not shake) the entire culture plate by hand in a circular fashion. This will cause the media/cell mixture to be evenly distributed along the outer edge of the well.

6. Incubate for one hour at 37˚C and 5% CO_2 to promote cell adherence.
7. Add myoblasts to the centre of the well

Hint: the number of myoblasts can vary depending on the experimenter's needs. We use 20 x 10^3 myoblasts for proliferation analysis and 50 x 10^3 myoblasts for migration analysis.

8. Add 500 µl GM.
10. Gently move the culture plate to evenly distribute the myoblasts.
11. Incubate for 3 h to promote complete adherence.
12. Remove GM and wash with PBS (x2) and continue with desired experiment.

APPENDIX C: PROTOCOL FOR: CELLULAR ALIGNMENT AND FUSION: QUANTIFYING THE EFFECT OF MACROPHAGES AND FIBROBLASTS ON MYOBLAST TERMINAL DIFFERENTIATION

Protocol Title: Quantifying the alignment of cells with ct-FIRE

Reagents

1. Methanol (Radchem, Orland Park, IL, USA)
2. Fuchsine (Sigma, St Louis, MO, USA)

Recipes

1. Fuchsine Stain: Add 1% (m/v) Fuchsine powder to 100% methanol

Equipment

1. Olympus CKX41 microscope (Olympus, Tokyo, Japan)
2. Motic 3.0 megapixel camera (Wetzlar, Germany)
3. Computer (Windows, OS or Linux)
4. ImageJ (available at https://imagej.nih.gov/ij/)
5. ct-FIRE (available at https://loci.wisc.edu/software/ctfire)

Procedure

Image Capture

1. Stain the cells with Fuchsine stain for 10 mins, remove the dye by submerging in a water bath, and leave to completely dry.

Note: other cytological stains, such as crystal violet, may be used instead of Fuchsine.

2. Capture images with a brightfield microscope using the 10x objective lens.

Attention: it is important to capture images using a high illumination and/or camera exposure to clearly distinguish between cells at a high confluency.

ImageJ Processing

3. Open an image in ImageJ (*File* → *Open*), convert it to grayscale (*Image* → *Type* → *8-bit*), remove image noise (*Process* → *Noise* → *Despeckle*) and apply a mean threshold (*Image*

→ *Adjust* → *Auto Local Threshold: Mean; Uncheck "White objects on black background"*).

Hint: it is possible to simultaneously process several images using the macro recording and batch processing feature in ImageJ, but this is not covered in this protocol.

ct-FIRE Processing

4. Open the processed image in ct-FIRE (*Open File*) and run the program (*Run*).

Attention: ensure that "Angle histogram & values" under Output Options is selected; all other options may be deselected.

Hint: it is possible to simultaneously analyse several images using the batch processing feature by checking *Batch* before selecting the files.

Data Analysis

5. Locate the excel document with the output values (*ctFIREout* → *HistANG_ct-FIRE_ImageName*).
6. Copy the output values to the template under "ct-FIRE Values".

Attention: ct-FIRE output values use a period, and not a comma, to separate decimal points. Ensure that Excel is set up to do the same.

7. Under "Calculate Mode", highlight the largest value under frequency.
8. To calculate the mode average, add the largest value from the frequency column to "Largest Value". Furthermore, select the equation for "Mode AVG" and change the "X" and "Y" to the largest and smallest bin values, respectively.
9. Extend the equation for Alignment Index down to calculate an AI for all ct-FIRE values.
10. The average AI for the image is under "Image AI".

Hint: the template is for one image, but the sheet may be copied multiple times for several images. The AI for all images (for a replicate) may then be averaged.

APPENDIX D: CONFERENCE ABSTRACTS

Conference: Second International Conference on Tissue Engineering and Regenerative Medicine (ICTERM) (2017)

Title: Myogenesis in a dish: Investigating the complexity of skeletal muscle regeneration

Abstract

Skeletal muscle wound repair and regeneration is associated with multiple cell types that each play distinct roles in regulating satellite cell activation and myogenesis. Macrophages secrete a host of inflammatory cytokines that activate and regulate the proliferation of satellite cells, and also modulate their differentiation. Fibroblasts differentiate to myofibroblasts and secrete cytokines and extracellular matrix (ECM) factors that form a scaffold for wound repair. Macrophages and fibroblasts therefore work together with myoblasts to facilitate wound repair. In order to understand the regulation of myogenesis by macrophages and fibroblasts, previous *in vitro* studies have primarily focused on the use of conditioned media or co-culture systems that physically separate the cell populations. The current study developed a simple and inexpensive co-culture method that allows for physical contact between cell types; in addition, a novel method was developed to quantitively assess myoblast alignment prior to fusion. The effect of macrophages and fibroblasts on myoblast proliferation, migration, alignment and fusion was then determined.

J774A.1 macrophages and LMTK fibroblasts were found to promote the proliferation of C2C12 myoblasts in a cell dependent manner; macrophages had a maximal effect at 80 x 10^3 cells, whereas fibroblasts promoted maximum proliferation at 20 x 10^3 cells. Macrophages and fibroblasts both promoted myoblast migration with maximal effects at 80 x 10^3 cells. Co-culturing a combination of macrophages (40 x 10^3) and fibroblasts (40 x 10^3) with myoblasts revealed that fibroblasts did not alter the pro-proliferative effects of macrophages on myoblasts; however, macrophages were able to decrease the pro-migratory effects of fibroblasts on myoblasts.

Analysis of alignment demonstrated that fibroblasts did not significantly affect myoblast/myotube alignment, while macrophages promoted alignment in a cell density-

dependent manner with a maximal effect at 80 x 10^3 cells. Macrophages had no significant effect on myoblast fusion at 5 x 10^3, but increasing the number of cells beyond this significantly decreased myoblast fusion with the lowest percentage fusion at 80 x 10^3 macrophages. Co-culture with 5 or 10 x 10^3 fibroblasts significantly increased myoblast fusion; however, further increases in fibroblast number abrogated this effect.

In conclusion, we have developed a novel co-culture technique that better represents *in vivo* cell interactions by allowing for cell-cell contact and facilitating variable numbers. We show that macrophages are more important for promoting myoblast proliferation, while fibroblasts have a prominent role in promoting myoblast migration. We have also created a novel method to quantify alignment and further go on to show that macrophages play a distinct role in promoting myoblast/myotube alignment prior to fusion, but are required to resolve for successful fusion to occur. Fibroblasts, on the other hand, are required at low, but not high, numbers to promote myoblast fusion.

Conference: First Conference of Biomedical and Natural Sciences and Therapeutics (CoBNeST) (2018)

Title: Myogenesis in a dish: Investigating the complexity of skeletal muscle regeneration

Abstract

Communication between non-myogenic cells, such as macrophages and fibroblasts, and myoblasts is critical for successful skeletal muscle repair by influencing various cell behaviours. To evaluate the relationship between these cell types, we first developed a novel, inexpensive *in vitro* co-culture method for two or more cell types with some degree of cell contact; we the evaluated the effect of macrophages and/or fibroblasts on myoblast proliferation and migration. We found that macrophages and fibroblasts can both promote myoblast proliferation and migration depending on their cell numbers; triple co-culture of macrophages, fibroblasts and myoblasts revealed that macrophages and fibroblasts continued to promote myoblast proliferation, but the presence of macrophages impaired the positive effect of fibroblasts on myoblasts migration. We then developed a method to rapidly determine cell orientation and quantify alignment and used our co-culture technique to determine the effect of macrophages and/or fibroblasts on myoblast alignment and fusion. We

found that increasing numbers of macrophages promoted myoblast/myotube alignment but inhibited fusion; fibroblasts, however, had no effect on alignment but promoted and inhibited fusion at lower and higher numbers, respectively. Triple co-culture of the cells showed that the effect of macrophages on myoblast alignment remains unaltered in the presence of fibroblasts. Altogether, our results show that high numbers of macrophages and fibroblasts are initial important to promote myoblast proliferation and migration, but lower numbers are required later on during terminal differentiation to promote alignment and fusion.

APPENDIX E: PUBLISHED PAPERS IN PRINT

1. Venter and Niesler (2019). Rapid quantification of cellular proliferation and migration using ImageJ. *BioTechniques* 66 (2), 99-102
2. Venter and Niesler (2018). A triple co-culture method to investigate the effect of macrophages and fibroblasts on myoblast proliferation and migration. *BioTechniques* 64, 52-58
3. Venter and Niesler (2018). Cellular alignment and fusion: Quantifying the effect of macrophages and fibroblasts on myoblast terminal differentiation. *Experimental Cell Research* 370 (2), 542-550

Benchmarks

BioTechniques

For reprint orders, please contact: reprints@futuremedicine.com

Rapid quantification of cellular proliferation and migration using ImageJ

C Venter[1] & CU Niesler*,[1]

ABSTRACT

Cellular proliferation and migration are crucial during development, regeneration and disease. Methods to quantify these processes are available; however, many are time consuming and require specialized equipment and costly reagents. Simple cell counts (proliferation analysis) and the scratch assay (migration analysis) are favorable methods due to their simplicity and cost–effectiveness; however, they rely on subjective and labor-intensive manual analysis, resulting in low throughput. We have developed optimized protocols to rapidly and accurately quantify adherent cell number and wound area using ImageJ, an open-source image processing program. Notably, these adaptable protocols facilitate quantification with significantly greater accuracy than manual identification.

METHOD SUMMARY

Optimized automated methods to rapidly quantify proliferation and migration of adherent cells using ImageJ are presented. These methods support high-throughput and deliver enhanced accuracy when compared to manual analysis.

KEYWORDS

adherent cell counts • ImageJ • migration • myoblast • scratch assay • proliferation

[1]*Discipline of Biochemistry, School of Life Sciences, University of KwaZulu-Natal, Private Bag X01, Scottsville 3209, South Africa; *Author for correspondence: niesler@ukzn.ac.za*

BioTechniques 66: 99-102 (February 2019) 10.2144/btn-2018-0132

Cellular proliferation and migration are important processes during tissue development, repair and disease. Following skeletal muscle injury, proliferation and migration of activated muscle stem cells (myoblasts) is crucial to ensure that sufficient progenitor cells reach the wound site and facilitate repair [1]. Myoblast proliferation and migration are regulated by signalling molecules released from the extracellular matrix and resident/infiltrating cells such as macrophages and fibroblasts [2]. Proliferation can be quantified by measuring changes in DNA (via BrdU, ^{3}H-Thymidine), metabolism (via MTT), proliferation-specific proteins (e.g., Ki-67) or simple cell counts (e.g., hemocytometer, TC20™) [3–7]. Migration can be assessed by determining the number of cells that move across a microporous membrane (transwell migration assay) or by measuring the surface area that cells occupy over time after creating a 'cell-free' area (scratch assay) [8–10]. Of these, cell counts and the scratch assay are favorable methods due to their cost-effective and simple nature, with fewer steps and a reduced need for specialized equipment.

ImageJ, a popular opensource image processing program, has previously been used to manually count cells (selecting and tallying individual cells) and assess wound closure (tracing the wound perimeter and calculating percentage closure) [11–13]. These manual approaches are laborious and time-consuming, whereas automated image analyses would facilitate a higher throughput and greater objectivity. In the current study, we utilized the image processing capabilities of ImageJ to develop an optimized batch processing macro for rapid and accurate identification and quantification of adherent cell number and wound area from images captured using a brightfield phase contrast microscope. We demonstrate that these protocols are easier, faster and more objective than alternative methods.

Murine C2C12 myoblasts (ATCC, cat. CRL-1772™, USA) were cultured at 37°C and 5% CO_2 and maintained in growth media (GM) containing Dulbecco's Modified Eagle's Medium (Sigma, cat. D5648, USA) supplemented with 10% (v/v) Fetal Bovine Serum (Gibco, cat. 10500, USA), 2% (v/v) penicillin–streptomycin (LONZA, cat. DE17–602E, Switzerland). Media was changed every 48 h. Results were analyzed using either a paired, two-tailed Student's T-test (for comparison between methods at a single cell number or timepoint; Figure 1B & 2C) or one-way ANOVA (for cell number changes within a method; Figure 1C), and values of $p < 0.05$ considered statistically significant. All data were represented as mean ± SEM.

For proliferation analysis, myoblasts (5, 10, 20, 40, 60, 80 and 100 × 10^3 cells) were cultured in GM (500 μl) in a 24-well plate for 3 h to promote adherence. Media was then removed, and cells stained with 0.2% (w/v) crystal violet (Sigma, cat. C-3886) in methanol (Sigma, cat. 24229) for 15 min; excess stain was subsequently removed by water submergence and the plate left to air dry. Cells were visualized using an Olympus CKX41 microscope (4x objective lens) and images captured (three fields of view per replicate; three replicates) with a Motic 3.0 megapixel camera. Cell number was assessed and compared using three methods: manual cell identification, automated cell identification and the spectrophotometric (crystal violet) assay.

For manual identification, captured images were converted to grayscale in ImageJ (*Image → Type → 8-bit*) (Figure 1Ai), the cells were manually marked out with a red pencil dot (size: 4 px) in Microsoft Paint (Figure Aii), the dots were then automatically identified (*Image → Adjust → Color Threshold (Hue 225 to 255; Dark Background: True)*) and counted (*Analyze → Analyze Particles*) using ImageJ. For automated identification, the images were converted to grayscale, image noise removed (*Process → Noise → Despeckle*), brightness and ▶

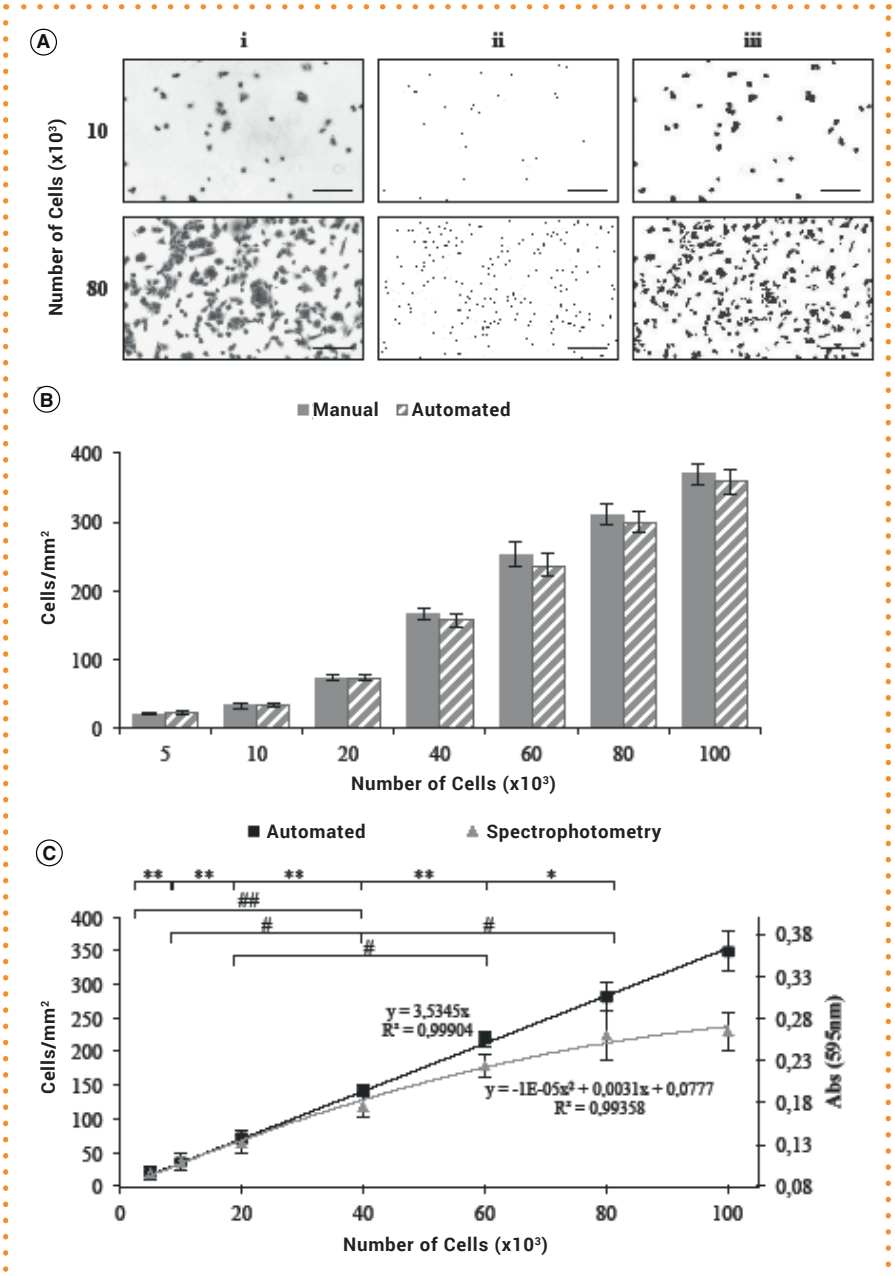

Figure 1. Quantification of cell number: a comparison of manual, automated (ImageJ) and spectrophotometric identification methods. (A) C2C12 myoblasts (10×10^3 and 80×10^3 are shown) were stained with crystal violet and captured with an Olympus CKX41 microscope coupled to a Motic 3.0 megapixel camera: (i) Brightfield images prior to processing, (ii) cells manually marked in Microsoft Paint and subsequently counted, (iii) cells automatically identified using the optimized ImageJ macro and subsequently counted. Scale bar = 200 μm. (B) Standard curve of cell density (cells/mm²) following application of the manual versus the automated ImageJ analysis. (C) Standard curve of cell density (cells/mm²) following application of automated ImageJ analysis versus spectrophotometry.
*$p < 0.05$ and **$p < 0.005$ for automated ImageJ analysis; #$p < 0.05$ and ##$p < 0.005$ for spectrophotometric analysis; n = 4–9.

▶ contrast adjusted (*Image → Adjust → Brightness/Contrast: min = 87; max = 167*), and a Phansalkar threshold (*Image → Adjust → Auto Local Threshold: Phansalkar*) and watershed (*Process → Binary → Watershed*) were finally applied (Figure Aiii). Adjusting the brightness and contrast, and applying the Phansalkar threshold, made the cells more distinguishable from the background, while the watershed step segmented any clustered cells from one another. The identified cells were finally counted using ImageJ. For spectrophotometric analysis, the crystal violet-stained cells were solubilized with 200 μl SDS (1% w/v; Merck, cat. SAAR5823610EM, USA) for 1 h; 100 μl of the solution was then removed and added to a 96-well microplate [14]. The absorbance (595 nm) was read using the FLUOptima micro 96-well plate reader.

For proliferation analysis, myoblasts were manually counted or identified and assessed using ImageJ. ImageJ could automatically identify cells at lower (5×10^3 cells) and higher (100×10^3 cells) numbers, despite the cells being clustered closely together; however, this is likely to become increasingly challenging as confluence is attained. No significant difference was found between automated (ImageJ) versus manual identification, confirming the accuracy of the automated method (Figure 1B). Manual cell identification was also a slow and laborious task compared to automated assessment. We then compared our automated cell number analysis with spectrophotometric analysis of crystal violet-stained cells; the latter assay is a simple, inexpensive method commonly used to quantify cell number (Figure 1C). The standard curve generated using the spectrophotometric assay yielded a polynomial line ($y = -1E\text{-}05x^2 + 0.0031x + 0.0777$; $R^2 = 0.9936$); as the number of plated cells increased, the absorbance (at 595 nm) increased, but plateaued after 60×10^3 cells (~65% confluence), possibly due to crystal violet saturation (Figure 1C). By contrast, the standard curve generated using the automated ImageJ macro resulted in a straight line ($y = 3.5345x$; $R^2 = 0.999$), indicating a directly proportional relationship between the number of cells plated and the number calculated per mm². In addition, each sequential increase in plated cell number was reflected as a significant increase in cell density when utilizing the automated counting method; this was not the case for the polynomial generated from crystal violet absorbance readings (Figure 1C). Therefore, ImageJ was sensitive enough to accurately detect both smaller changes in cell numbers and a wider range of cellular densities than spectrophotometric analysis of crystal violet-stained cells.

For migration analysis, myoblasts (120×10^3) were plated out in GM (1 ml) in

a 12-well plate for 24 h, before a scratch assay was performed as described by Goetsch *et al.* [15]. Briefly, the confluent monolayer of myoblasts was scratched with a sterile 200 μl loading tip to create a linear 'wound' devoid of cells. The cells were then washed twice with sterile PBS and fresh GM (500 μl) was added. The cells were incubated for 7 h and images captured at 0, 3, 5 and 7 h using the camera-attached microscope (4x objective lens; two fields of view per replicate, for two replicates). To measure wound area manually, the edges of the wound were traced using the Motic Images Plus 2.0 ML software [15]. To carry out automated wound area measurements, the captured image was converted to grayscale, the edges found (*Process → Find Edges*) and the image blurred (*Process → Smooth*) multiple times (x37). The *Find Edges* step highlighted sharp changes in intensity with a white outline so that when the image was blurred numerous times, these outlines blurred together; as a result, the areas containing cells were white whereas the wound area (devoid of cells) remained black. A MinError threshold was then applied (*Image → Adjust → Auto Threshold: MinError*) to automatically detect the wound area. If the wound area was not accurately selected, it could be manually thresholded (*Image → Adjust → Threshold*). Once the wound area was identified, it was then quantified (*Analyze → Analyze Particles [size: 10,000 – infinity]*).

The percentage wound closure was calculated and the results generated using the manual versus automated methods were compared (Figure 2). The use of ImageJ to detect wound edges revealed that, when compared with manual assessment, automated analysis was able to accurately define these edges (Figure 2A); in fact, the automated analysis seemed to define the wound edges more accurately than the manual method (Figure 2B). As a result, when the percentage wound closure was assessed, a significant difference between the manual (12.13 ± 0.98%) and automated (7.54 ± 0.76%) method was detected at 3 h post-wounding ($p < 0.05$). This was attributed to the fact that ImageJ could trace the outline of the wound more accurately than the researcher's manual attempt. This was particularly evident during early wound repair when the wound borders were not well defined and, therefore, harder to accurately

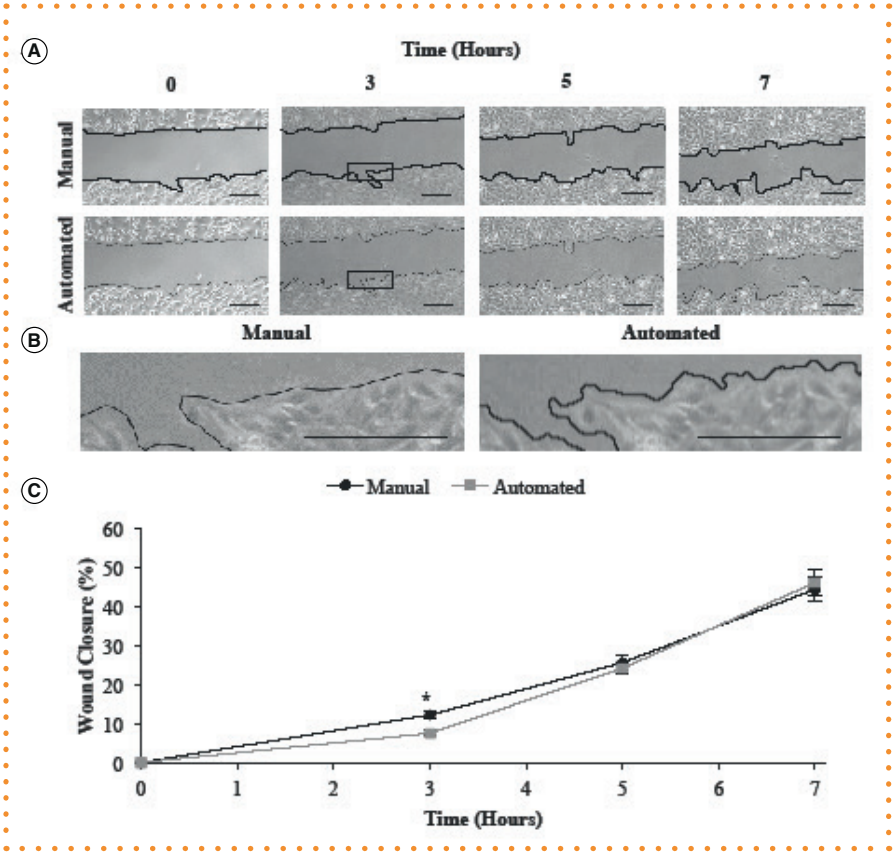

Figure 2. Quantification of wound area: a comparison of manual and automated (ImageJ) identification methods. (A) C2C12 myoblasts (120×10^3) were scratched and images captured with an Olympus CKX41 microscope coupled to a Motic 3.0-megapixel camera (0, 3, 5 and 7 h): manual identification using Motic Images Plus 2.0 ML software to trace the wound edge and automated identification using ImageJ. (B) Zoomed-in images of wound edges following manual and automated identification at 3 h. (C) Percentage wound closure (%) at 3, 5 and 7 h post-injury. *$p < 0.05$; $n = 16$. Scale bar = 200 μm.

trace. In addition to increased sensitivity and accuracy, the application of the ImageJ macro was less laborious and faster than manual analysis.

In summary, we have developed an optimized ImageJ-based automated method for rapid quantification of cell number and migration *in vitro*. ImageJ could automatically identify and accurately quantify cell numbers and wound area; in some cases, the results were superior to those generated via traditional manual or spectrophotometric methods. In addition, our macros generated data faster than previous manual methods. Although programs have previously been developed to count cells (e.g., CellC and CellCounter) or measure wound closure (e.g., TScratch) [16–19], they did not match the flexibility of ImageJ which, as a single program, can be extended to quantify cell number in tissue sections and suspension cultures or adapted to monitor important cellular processes [19]. Finally, the open-source nature of this software permits further optimization depending on user requirements, yielding a superior and versatile method compared with previous protocols.

AUTHOR CONTRIBUTIONS

CV: PhD postgraduate student responsible for the execution of the laboratory work, as well as compilation and revision of the manuscript. CUN: Senior author providing intellectual input and supervision to the student involved. This author also provided the funding for the project and contributed to revisions of multiple drafts of the article.

FINANCIAL & COMPETING INTERESTS DISCLOSURE

The work was supported by the South African National Research Foundation ▶

▶ (Grant CPRR13091035184; 90502) and the University of KwaZulu-Natal. The authors have no other relevant affiliations or financial involvement with any organization or entity with a financial interest in or financial conflict with the subject matter or materials discussed in the manuscript apart from those disclosed.

No writing assistance was utilized in the production of this manuscript.

OPEN ACCESS

SUPPLEMENTARY DATA

A supplementary protocol accompanies this paper. To view the supplementary data that accompany this paper please visit the journal website at: www.future-science.com/doi/suppl/10.2144/btn-2018-0132

REFERENCES

1. Mann CJ, Perdiguero E, Kharraz Y *et al.* Aberrant repair and fibrosis development in skeletal muscle. *Skelet. Muscle* 1(1), 21 (2011).
2. Bosurgi L, Manfredi AA, Rovere-Querini P. Macrophages in injured skeletal muscle: a perpetuum mobile causing and limiting fibrosis, prompting or restricting resolution and regeneration. *Front. Immunol.* 2, 62 (2011).
3. Hughes WL, Bond VP, Brecher G *et al.* Cellular proliferation in the mouse as revealed by the autoradiography with tritiated thymidine. *Proc. Natl Acad. Sci. USA* 44(5), 476–483 (1958).
4. Gratzner HG. Monoclonal antibody to 5-bromo- and 5-iododeoxyuridine: a new reagent for detection of DNA replication. *Science* 29(4571), 474–475 (1982).
5. Mosmann T. Rapid colorimetric assay for cellular growth and survival: Application to proliferation and cytotoxicity assays. *J. Immunol. Meth.* 65(1–2), 55–63 (1983).
6. Scholzen T, Gerdes J. The Ki-67 protein: from the known to the unknown. *J. Cell. Physiol.* 182(3), 311–322 (2000).
7. Boulton RA, Hodgson JF. Assessing cell proliferation: a methodological review. *Clin. Sci. (Lond.)* 88(2), 119–130 (1995).
8. Boyden S. The chemotactic effect of mictures of antibody and antigen on polymorphonuclear leucocytes. *J. Exp. Med.* 115(3), 453–466 (1962).
9. Lampugnani MG. Cell migration into a wounded area ***in vitro***. *Methods. Mol. Biol.* 96, 177–182 (1999).
10. Hulkower KI, Herber RL. Cell migration and invasion assays as tools for drug discovery. *Pharmaceutics* 3(1), 107–124 (2011).
11. Schindelin J, Rueden CT, Hiner MC, Eliceiri KW. The ImageJ ecosystem: an open platform for biomedical image analysis. *Mol. Reprod. Dev.* 82(7–8), 518–529 (2015).
12. De Vos K. Cell counter. (2001). Available at: https://imagej.nih.gov/ij/plugins/cell-counter.html (Accessed 6 September 2018).
13. Goetsch KP, Myburgh KH, Niesler CU. ***In vitro*** myoblast motility models: Investigating migration dynamics for the study of skeletal muscle repair. *J. Muscle. Res. Cell. Motil.* 34(5–6), 333–347 (2013).
14. Feoktistova M, Geserick P, Leverkus M. Crystal violet assay for determining viability of cultured cells. *Cold. Spring. Harb. Protoc.* 2016(4), pdb prot087379 (2016).
15. Goetsch KP, Niesler CU. Optimization of the scratch assay for ***in vitro*** skeletal muscle wound healing analysis. *Anal. Biochem.* 411(1), 158–160 (2011).
16. Selinummi J, Seppala J, Yli-Harja O, Puhakka JA. Software for quantification of labeled bacteria from digital microscope images by automated image analysis. *Biotechniques* 39(6), 859–863 (2005).
17. Li X, Yang H, Huang H, Zhu T. CELLCOUNTER: novel open-source software for counting cell migration and invasion ***in vitro***. *Biomed. Res. Int.* 2014(2014), 6 (2014).
18. Geback T, Schultz MM, Kousmoutsakos P, Detmar M. TScratch: a novel and simple software tool for automated analysis of monolayer wound healing assays. *Biotechniques* 46(4), 265–274 (2009).
19. Abràmoff MD, Magalhães PJ, Ram SJ. Image processing with ImageJ. *J. Biophotonics* 11(7), 36–42 (2004).

A triple co-culture method to investigate the effect of macrophages and fibroblasts on myoblast proliferation and migration

Colin Venter[1], and Carola Niesler[1,*]
[1]*Discipline of Biochemistry, School of Life Sciences, University of KwaZulu-Natal, Private Bag X01, Scottsville 3209, South Africa.*

BioTechniques 64:52-58 (February 2018) doi 10.4155/btn-2017-0100
Keywords: fibroblasts; macrophages; myoblasts; myogenesis; triple co-culture

Supplementary material for this article is available at www.BioTechniques.com/article/btn-2017-0100.

The communication between nonmyogenic cells, such as macrophages and fibroblasts, and myoblasts is crucial for successful skeletal muscle repair. *In vitro* co-culture methods can be used to increase our understanding of these cellular interactions; however, current protocols are restricted to two, often physically separate, cell populations. Here, we demonstrate a novel, inexpensive *in vitro* triple co-culture method that facilitates the co-culture of at least three cell populations with some degree of cell–cell contact. Using this method, we determined the effect of macrophages and fibroblasts on myoblast proliferation and migration. A significant increase in myoblast proliferation and migration was observed following co-culture with either macrophages or fibroblasts. However, triple co-culture of macrophages, fibroblasts, and myoblasts revealed that the presence of macrophages prevented fibroblasts from maintaining this positive effect on myoblast migration. Macrophages, on the other hand, continued to promote myoblast proliferation whether in the presence of fibroblasts or not. Our triple co-culture system highlights the significance of multicellular communication in regulating myoblast proliferation and migration and emphasizes the importance of more complex co-culture systems when investigating myogenesis *in vitro*.

Severe skeletal muscle injury causes damage to myofibers and the surrounding extracellular matrix (ECM) (1). As a result, the damaged muscle undergoes sequential and overlapping stages of wound repair, where several cell types are activated to proliferate and migrate into the wound (2,3). Macrophages and fibroblasts are present during these stages and are critical to the successful completion of the wound healing process (4). Soon after injury, tissue degeneration, characterized by ruptured and necrotizing myofibers, is evident (5,6). This is followed by inflammation, where macrophages residing in the epimysium and perimysium enter the wound to clear cell debris and secrete cytokines to initiate regeneration (2,7). During the regenerative phase, infiltrating tissue fibroblasts are induced to differentiate into contractile myofibroblasts, which display a greater synthetic phenotype than fibroblasts. Myofibroblasts secrete cytokines, growth and extracellular matrix factors, as well as enzymes that assist in remodelling the wound matrix (8–11). This provides a mechanical scaffold for activated satellite cells (myoblasts) to proliferate and move from their niche between the basal lamina and sarcolemma to the area of damage (12). At the wound site, they differentiate into myotubes and fuse with existing skeletal muscle tissue to repair damaged myofibers. The interplay of nonmyogenic cells with activated satellite cells is therefore crucial for myogenesis and successful repair; a cellular imbalance may lead to impaired wound healing and, in the long term, chronic disease due to conditions such as fibrosis (4).

In order to fully understand the complex mechanisms controlling myogenesis, it is important to take into account the relevant cells that regulate this process. There are a number of methods that can be used to achieve this; these include the use of *in vivo*

METHOD SUMMARY

A novel triple co-culture method facilitates the co-culture of macrophages, fibroblasts, and myoblasts. This assay, which permits some cell–cell contact, can be extended to include more than three cell types, and it represents a simple, cost-effective way to probe complex multicellular communication *in vitro*.

approaches, *in vitro* 3D tissue engineered skeletal muscle, or *in vitro* co-culture systems. *In vivo* models are more accurate in reflecting the process of muscle wound repair, but due to the array of interactions that take place, this environment is highly complex, making it difficult to identify individual mechanisms (13). *In vitro* 3D tissue engineered skeletal muscle mimics *in vivo* conditions more closely than *in vitro* monolayer studies, but this approach is more time-consuming in its establishment and requires extensive optimization (14). Co-culture systems make use of two or more cell populations, within the same *in vitro* microenvironment, thereby allowing some degree of interaction for studying intercommunication between different cell types (13). This creates an experimental model that more closely mimics the intercellular communication in the *in vivo* environment and is therefore superior to conventional mono-culture (13,15,16).

Co-culture systems fall into one of two categories. First, those that physically separate the cell populations from one another, typically by using a multi-compartment approach (e.g., transwell plates or "overflow" culture chambers) that allows communication only via soluble factors (Figure 1Ai and ii) (17,18). A disadvantage of this type of method is that cells are not permitted to come in direct contact with one another, as would occur under *in vivo* conditions. Diffusion rates of soluble factors in larger culture volumes (as required in the overflow chamber) are also a consideration; if the rate of diffusion is too low, signalling factors may not be able to reach their targets timeously (13,19). Secondly, there are methods that allow direct interactions between cells (i.e., micropatterning); this is usually achieved by spatially controlling the position of the adhering cell populations within a culture dish (such as that reported by Javaherian et al., 2013, or the co-culture method presented in this paper) (Figure 1A iii and iv) (20). Co-culturing by way of micropatterning involves the creation of a distinct population of cells within a culture dish by selectively controlling the attachment of cells (Figure 1A iii). This can be achieved by creating a nonadhesive area via a physical barrier (using stamps, as seen in (21)) or a chemical barrier (e.g., bovine serum albumin (BSA) (20)). The first population of cells will adhere to the area surrounding the barrier; once the barrier is removed (either by physical removal or by coating the nonadhesive area with an adhesive matrix factor (20)), the second cell population binds in the remaining space (22). This method has the advantage of allowing cells to interact via both secreted factors and cell–cell interactions, but is laborious, requiring additional steps and specialized equipment.

Here, we describe a novel triple co-culture method (Figure 1A iv), where a standard circular well-containing plate can be employed to culture multiple distinct cell populations, allowing for both direct and indirect cellular communication. Using this method, we investigate the regulatory role of macrophages and fibroblasts on myoblast proliferation and migration, and demonstrate the importance of macrophage resolution to facilitate fibroblast-regulated wound repair *in vitro*.

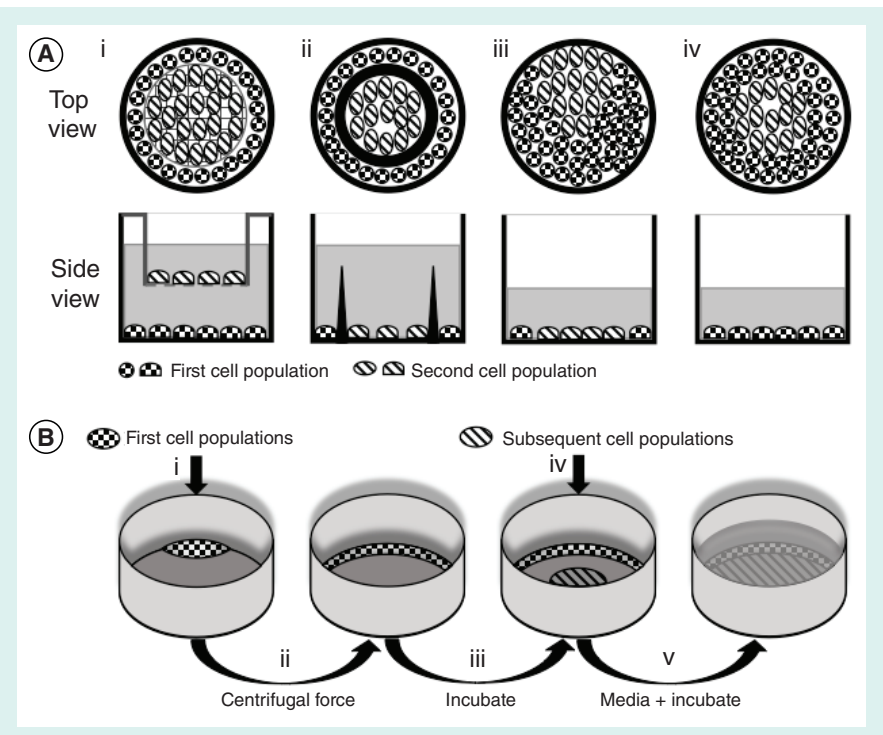

Figure 1: Schematic diagram of co-culture methods and steps. A) Transwell inserts (i); overflow co-culture chamber (ii); micropatterning (iii); and our novel co-culture method (iv). **B)** Steps to establish the novel triple co-culture method: first cell populations are plated at the outer edge of a well (i); the culture plate is then rotated to distribute the cells along the outer edge of the well (ii); cells are incubated for 1 hour to promote adherence (iii); the subsequent cell population is then plated in the center of the well (iv); media is added (v).

Materials and methods

Cell culture

Mouse C2C12 myoblasts (Cat. CRL-1772™, ATCC, VA, USA), LMTK fibroblasts (Cat. CCL-1.3™, ATCC) and J774A.1 macrophages (Cat. TIB-67™, ATCC) were cultured at 37°C and 5% CO_2 and maintained in growth media containing Dulbecco's Modified Eagle's Medium (DMEM; Cat. D5648, Sigma, MO, USA) supplemented with 10% (v/v) fetal bovine serum (Cat. 10500, Gibco, Thermo Fisher Scientific, MA, USA) and 2% (v/v) penicillin–streptomycin (Cat. DE17-602E, Lonza, Basel, Switzerland). Media was changed every 48 h.

Co-culture method

For co-culture of two cell types, either macrophages or fibroblasts (0, 5, 10, 20, 40, or 80 x 10^3 cells) were plated along the outer edge of a dry 24-well plate in a volume of growth media not exceeding 100 µl, but not less than 30 µl (Figure 1B i). For co-culture of three cell types (i.e., "triple" co-culture) 40 x 10^3 macrophages and 40 x 10^3 fibroblasts were combined in 100 µl growth media and plated as above. A centrifugal force was then applied to the plate to ensure that the cells only attached to the outer edge of the well; this was achieved by simply rotating the plate in a circular motion (2 min) by hand, or using a rotational device (20 rpm) set at a 45° angle (Figure 1B ii). Cohesion of the low media volume ensures the cells do not spread towards the center of the well. The cells were then incubated at 37°C and 5% CO_2 for 1 h to promote adherence (Figure 1B iii). Following this, myoblasts were plated in

the center of the well and allowed to adhere to the unoccupied area (Figure 1B iv and v). Proliferation and migration of myoblasts in the center of the well was then analyzed as described below.

Proliferation analysis

To analyze the effect of macrophages and fibroblasts on myoblast proliferation, 20 x 10^3 C2C12 cells were allowed to adhere for 2 h, then washed twice with sterile PBS and cultured in serum-free DMEM (500 µl). Cells were co-cultured for 24 h, washed with PBS and stained with basic Fuchsin (Cat. 47860, Sigma) for 10 min (1% w/v basic Fuchsin dissolved in 100% methanol). Cells were then submerged in water to remove the stain and manually counted following visualization and image capture with an Olympus CKX41 microscope (Olympus Corporation, Tokyo, Japan) and a Motic 3.0 megapixel camera (4x objective; Motic, Kowloon, Hong Kong). Three fields of view per replicate (taken from the center of the well), with three replicates per experiment, were used. C2C12 cells plated in the absence of macrophages or fibroblasts served as a control. Changes in myoblast number were calculated relative to the number of myoblasts initially plated out and expressed as a percentage increase (%).

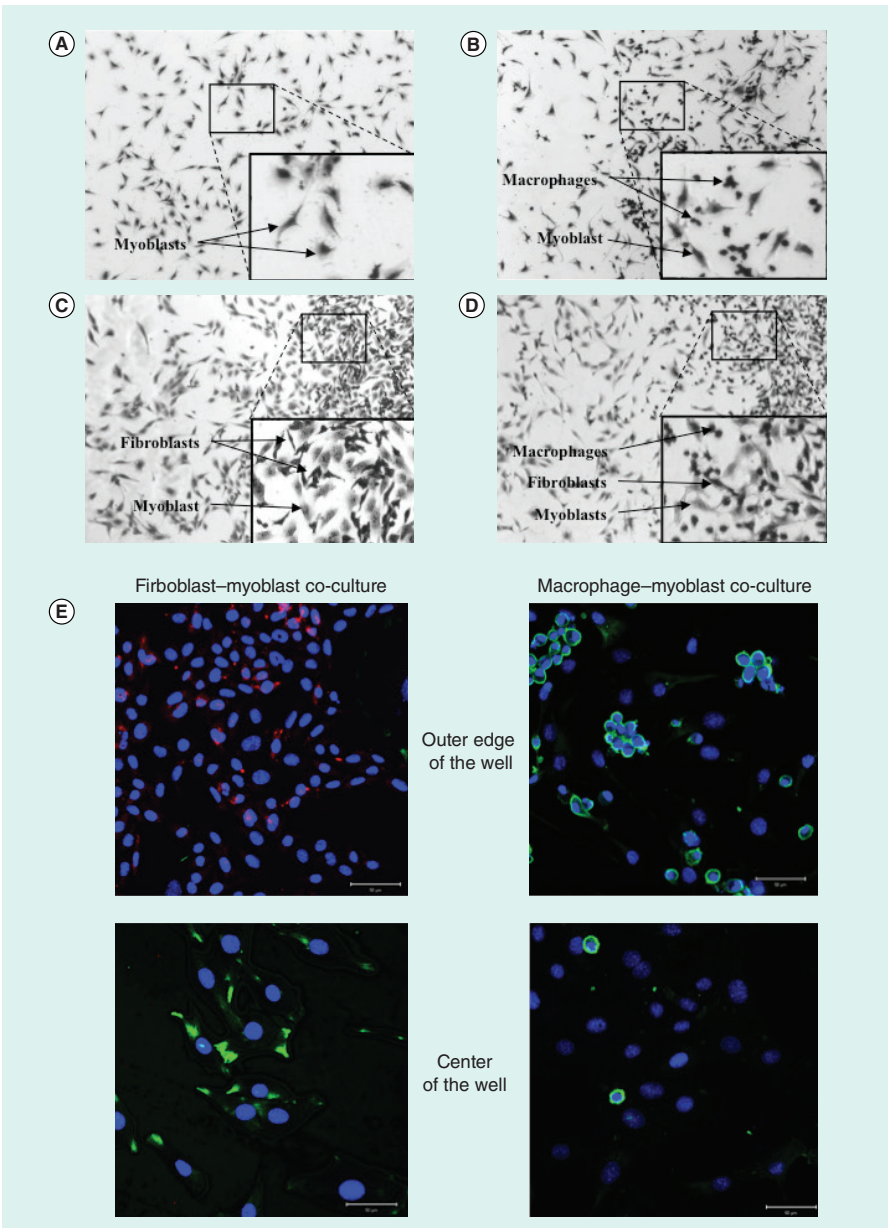

Figure 2: Cell populations in distinct regions of the co-culture plate. A) Myoblasts are at the center of the well, while **B)** macrophages, **C)** fibroblasts, or **D)** macrophages *and* fibroblasts are present predominantly at the outer edge of the culture well (right) with some overlap with myoblasts. **E)** Fibroblast–myoblast co-cultures (left panel) immunostained with both mouse monoclonal anti-TCF-4 (red; fibroblasts) and rabbit polyclonal anti-desmin (green; myoblasts), while macrophage–myoblast co-cultures (right panel) were immunostained with rabbit polyclonal anti-E-cadherin (green; macrophages). Hoeschst (blue) was used as a nuclear stain. Images were captured using a Zeiss 710 confocal microscope with a 25x objective lens. Scale bar = 50µm. Representative images from the outer edge and center of the well are shown.

Migration analysis

For migration analysis, 50 x 10^3 C2C12 myoblasts were allowed to adhere for 24 h before undergoing a scratch assay as described by Goetsch et al. (2011) (23) in serum-free DMEM (500 µl). Briefly, while being careful not to disturb the cells on the outer edge, the confluent monolayer of myoblasts at the center of the well was scratched with a sterile 200 µl loading tip to physically remove myoblasts and create a linear "wound." The remaining cells were washed twice with sterile PBS and 500 µl serum-free DMEM was added. The cells were then incubated for 7 h and images taken at 0 and 7 h using an Olympus CKX41 microscope and a Motic 3.0 megapixel camera (4x objective). The percentage of wound closure was calculated after tracing the wound edges using the Motic Images Plus 2.0 ML software (23).

Immunocytochemistry and confocal microscopy

To immunocytochemically identify cells in co-culture, cells were cultured on glass coverslips as described above. Briefly, macrophages (40 x 10^3) or fibroblasts (40 x 10^3) were plated in growth medium at the edge of the well, followed by myoblasts (20 x 10^3) in the center of the well. The cells were then washed twice with PBS and switched to serum-free DMEM for 24 h to mimic the proliferation time-frame. To analyze the effect of macrophages on fibroblast phenotype, macrophages (40 x 10^3) were plated in growth medium at the edge of the well after which fibroblasts (40 x 10^3) were allowed to adhere in the center of the well. The cells were then washed twice with PBS and switched to serum-free DMEM for 7 h to mimic the migration timeframe.

Cells were then fixed with 4% paraformaldehyde, washed with PBS, blocked at 4ºC with 5% donkey serum (Cat. D9663, Sigma) and incubated at room temperature for 2 h with the following primary antibodies as appropriate: polyclonal rabbit anti-desmin antibody (1:500; Cat. ab15200, Abcam, Cambridge,

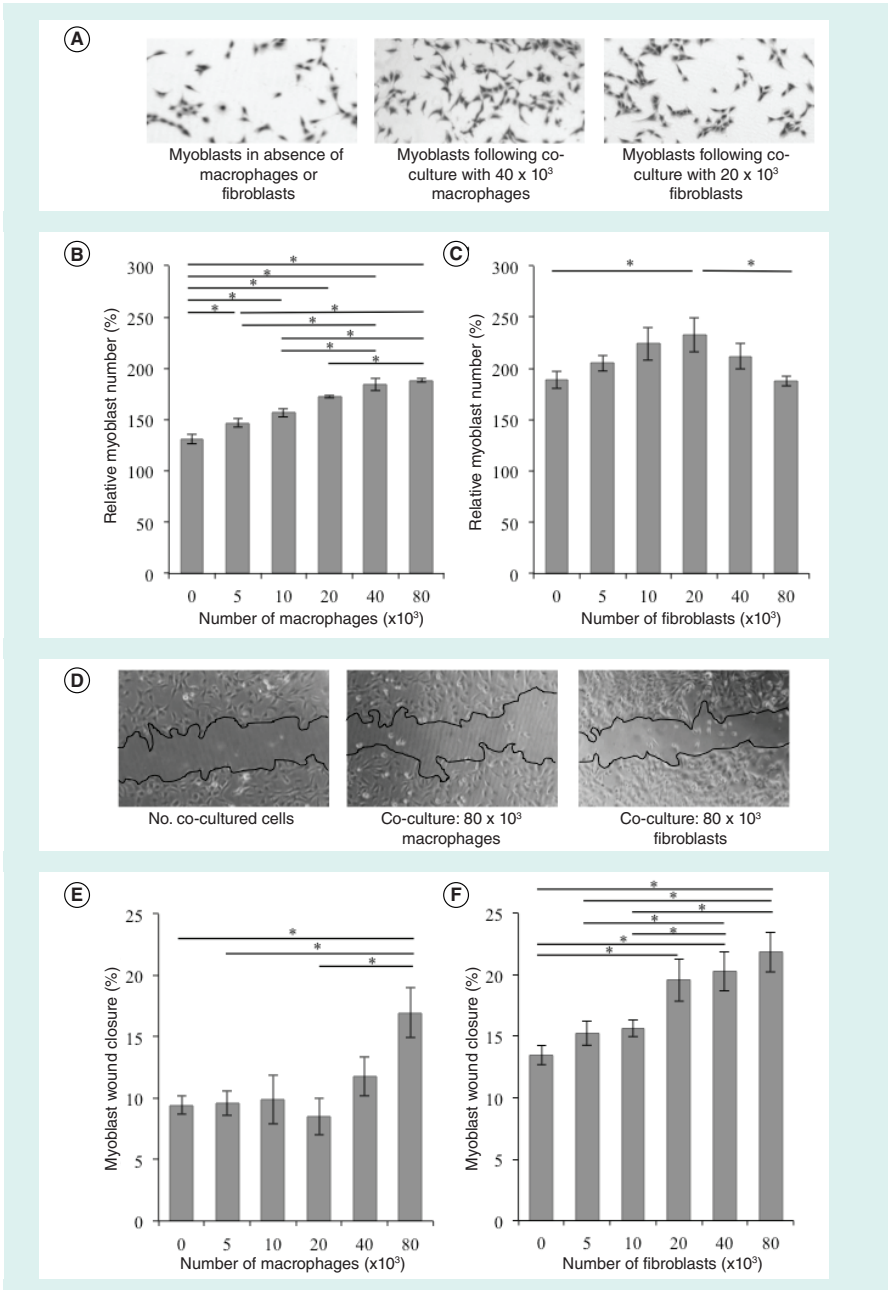

Figure 3: The effect of macrophages or fibroblasts on myoblast proliferation and migration. A) Cells were stained with 1% Fuchsin in methanol. **B)** and **C)** Relative cell number for myoblasts cultured in the presence of increasing numbers of macrophages or fibroblasts, respectively. **D)** The wound area of myoblasts. **E)** and **F)** Percentage wound closure at 7 h for myoblasts cultured in the presence of increasing numbers of macrophages or fibroblasts, respectively. * = $p < 0.05$; B, C and E: n = 6; F: n = 5). Cells were visualized using an Olympus CKX41 microscope and images were captured with a Motic 3.0 megapixel camera (4x objective lens).

UK), monoclonal mouse anti-TCF-4 antibody (1:20; Cat. 05-511, Merck Millipore, MA, USA), polyclonal rabbit anti-E-cadherin (1:40; Cat. sc-7870, Santa Cruz Biotechnology, TX, USA) or monoclonal mouse anti-α-smooth muscle actin (SMA; 1:500; Cat. A2547, Sigma). The cells were then washed with PBS and incubated at room temperature for 1 h in the dark with one of the following appropriate secondary antibodies: Dylight488-conjugated donkey anti-rabbit antibody (1:1000; Cat. 711-485-152, Jackson ImmunoResearch, Newmarket, Suffolk, UK), Dylight594-conjugated donkey anti-mouse antibody (1:1000; Cat. 715-515-151, Jackson ImmunoResearch) or Dylight488-conjugated donkey anti-mouse antibody (1:2000; Cat. 715-485-151, Jackson ImmunoResearch). Hoescht (1:100; stock 10 mg/ml; Cat. B2261, Sigma) was subsequently added for 10 min and coverslips washed with PBS prior to being fixed again with 4% paraformaldehyde (10 mins), washed with PBS, and mounted on glass slides with Mowiol (Cat. 81381, Sigma). The cells were viewed with a Zeiss 710 confocal microscope (Carl Zeiss GmbH, Oberkochen, Germany).

Statistical analysis

Data was determined to be normally distributed; results were analyzed using a parametric paired, two-tailed Student's t-test and values of $p < 0.05$ were considered to be statistically significant compared with the control. All data was represented as mean ± SEM.

Results & discussion

To initially co-culture two cell populations, macrophages were plated at the outer edge of the well, while myoblasts were cultured in the center of the well (Figure 2A & 2B). J774A.1 macrophages are relatively small, circular cells, easily distinguishable from larger, spindle-shaped myoblasts that overlap to an extent with macrophages, allowing for a degree of cell–cell interaction (Figure 2B). This method of co-culture was then successfully repeated using fibroblasts instead of macrophages (Figure 2C). LMTK fibroblasts are larger than J774A.1 macrophages, but smaller than C2C12 myoblasts, and have an elongated shape. To establish the "triple co-culture," macrophages and fibroblasts were both cultured at the outer edge of the well, while myoblasts were cultured at the center of the well (Figure 2D). Fibroblasts and macrophages were clearly identified at the outer edge of the well via expression of TCF-4 and E-cadherin, respectively (Figure 2E); significant numbers of macrophages and fibroblasts were not observed amongst the myoblasts at the center of the well (Figure 2E). Our method was established using a 24-well plate, but it can be adapted to any culture vessel with circular wells. The advantage of this method over others lies in its simplicity and the fact that it can be established quickly without the need for additional, specialized equipment. A further benefit of our system is that it can be expanded to include more than three cell types; this is crucial when one is trying to mimic the *in vivo* environment.

Using our co-culture method, we sought to determine the effect of macrophages and fibroblasts on myoblast proliferation and migration. Co-culture experiments revealed that macrophages and fibroblasts promote the proliferation of myoblasts (Figure 3A). Relative myoblast numbers already showed a small significant increase from 130 ± 4.38% to 146 ± 4.12% (16% increase; $p < 0.05$) when co-cultured for 24 h with 5 x 10^3 macrophages compared with control cultures (Figure 3B). A maximal effect was reached following co-culture with 80 x 10^3 macrophages (188 ± 1.75%; $p < 0.05$; Figure 3B). The presence of fibroblasts also increased the proliferation of myoblasts; however a significant, maximal effect was only achieved in response to 20 x 10^3 fibroblasts; when fibroblast numbers were increased further, this pro-proliferative effect was lost (Figure 3C). In response to 20 x 10^3 fibroblasts, relative myoblast numbers increased significantly from 189 ± 8.31% to 232 ± 16.76% ($p < 0.05$); whereas in response to co-culture with 80 x 10^3 fibroblasts, relative myoblast numbers returned to control levels of 187 ± 7.72% (Figure 3C).

Analysis of myoblast migration revealed that co-culture with 80 x 10^3 macrophages resulted in a significant increase in the percentage of wound closure (17.0 ± 2.04%) compared with the control (9.42 ± 0.75%), 5 x 10^3 (9.58 ± 1.00%) and 20 x 10^3 (8.51 ± 1.52%) macrophages (Figure 3D and 3E; $p < 0.05$). The presence of lower numbers of macrophages had no significant effect on myoblast migration (Figure 3E). When co-cultured with fibroblasts, myoblasts responded by increasing their migration in a cell-density dependent manner (Figure 3D and 3F). Significant effects were already observed in response to 20 x 10^3 fibroblasts (Figure 3F), rather than at only 80 x 10^3 as seen with macrophages (Figure 3E). Following co-culture with 20 x 10^3 cells, myoblast wound closure had increased significantly to 19.57 ± 1.71% with a maximal significant effect observed in response to 80 x 10^3 cells (21.9 ± 1.62%) compared with the control (13.5 ± 0.79%) ($p < 0.05$; Figure 3F). This data suggests that rising fibroblast numbers promote myoblast motility, while macrophages lose their promigratory effect as their numbers decrease.

To determine the combined effect of macrophages and fibroblasts on myoblast proliferation and migration, a triple co-culture experiment was carried out where myoblasts were co-cultured with 40 x 10^3 macrophages and 40 x 10^3 fibroblasts. Total cell numbers exceeding 80 x 10^3 cells caused the fibroblasts and macrophages to move to the center of the well, hence 40 x 10^3 of each cell type was used. Analysis of myoblast proliferation revealed that triple co-culture of myoblasts with both macrophages and fibroblasts did not significantly change myoblast numbers when compared with conditions using macrophages or fibroblasts alone (Figure 4A). The pro-proliferative effect of macrophages on myoblasts was therefore observed both in the absence and presence of fibroblasts. However, when myoblast migration was analyzed, triple co-culture of myoblasts with both macrophages and fibroblasts abrogated the previous significant positive effect of fibroblasts on myoblast migration (Figure 4B). The promigratory effect of fibroblasts on myoblasts was therefore lost in the presence of macrophages. Further immunocytochemistry and confocal microscopy revealed that, whether in the absence or presence of macrophages, fibroblasts expressed αSMA (Figure 4C). It is well known that the presence of serum promotes the myofibroblast phenotype (24); therefore α-SMA expression was expected in these cells. Our results suggest that macrophages do not initiate de-differentiation of myofibroblasts over the 7 h migration period. Interestingly, a decrease in cell number was observed, suggesting perhaps a pro-apoptotic effect of macrophages. This requires further investigation.

Following muscle injury, the inflammatory response is accompanied by an increasing population of macrophages, followed by the migration of resident fibroblasts that are promoted to proliferate and differentiate to myofibroblasts (25–30). Triple co-culture studies using macrophages, fibroblasts and myoblasts revealed that the presence of macrophages negates the promigratory effects of fibroblasts on myoblasts. This supports the premise that although an inflammatory response is crucial for repair, under certain conditions, it can negatively affect repair. The pro-proliferative effect of

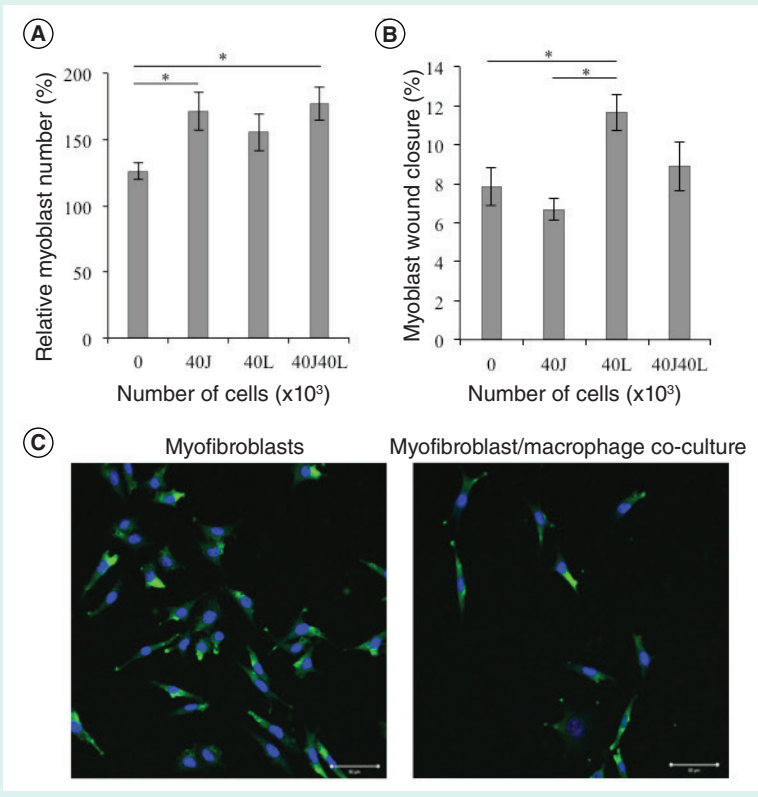

Figure 4: The effect of macrophages and fibroblasts on myoblast proliferation and migration. A) Relative cell number or **B)** percentage of wound closure for myoblasts cultured in the presence of both 40 x 10^3 macrophages and 40 x 10^3 fibroblasts (40J40L). Controls include no macrophages or fibroblasts (0), 40 x 10^3 fibroblasts alone (40L), or 40 x 10^3 macrophages alone (40J). **C)** Myofibroblasts cultured alone (left) or co-cultured with macrophages (right), immunostained with mouse monoclonal anti-α-SMA antibody (green), and stained with Hoescht (blue). Images were captured using a Zeiss 710 confocal microscope .(25x objective). Scale bar = 50μm. *$p < 0.05$; n = 5).

macrophages on myoblasts was however maintained even in the presence of fibroblasts, suggesting less of an influence of fibroblasts on macrophage–myoblast communication.

Previous studies using more than two cell types in co-culture are limited (31); in fact, no previous studies have been performed to determine the combined effect of macrophages and fibroblasts on myoblast proliferation and migration.

A crucial advantage of the current protocol is that it can be expanded to include additional relevant cell types, such as endothelial cells. In addition, the format allows the user to a) determine the phenotype of the participating cells (e.g., M1 vs M2 macrophages or fibroblasts vs myofibroblasts) using immunocytochemistry and b) polarize the co-cultured cells in order to determine whether distinct populations have differential effects on myoblast proliferation and migration. Our results underscore the importance of including cellular complexity in *in vitro* co-culture systems in order to gain a better understanding of how cellular communication regulates regenerative outcomes in skeletal muscle.

In previous *in vitro* studies, the conditioned media of pro-inflammatory M1 macrophages was found to increase the proliferation of myoblasts, while inhibiting migration (32–35). In our study, we used unmanipulated macrophages. This may account for some of the differences seen in our results compared with these previously published studies.

It would be valuable to determine whether any change in macrophage phenotype is observed in response to myoblast injury. *In vivo* studies suggest that ablation of fibroblasts leads to depletion of satellite cells, premature satellite cell differentiation, and results in smaller regenerated myofibers (36). *In vitro* studies have shown that increasing fibroblasts in co-culture also promotes the migration of myoblasts (18) and that fibroblasts protect myoblasts from apoptosis during differentiation, promoting myotube formation (37). This agrees with our current studies showing that the presence of fibroblasts increases myoblast cell numbers and migration.

In summary, our optimized triple co-culture assay has numerous advantages: it is easier, simpler, and cheaper to establish than conventional techniques; it allows for both direct and indirect cellular communication; and it can be expanded in its complexity to include additional cell types such as endothelial cells. Using this model, we confirm that macrophages and fibroblasts are important regulators of myoblast proliferation and migration. We also show for the first time that macrophages can negatively influence the ability of fibroblasts to promote myoblast migration in an *in vitro* wound healing setting. Knowledge generated from this method will further our understanding of the role of cellular interplay in regenerative processes.

Author contributions

Colin Venter executed the laboratory work, as well as compiled and revised the manuscript. Carola Niesler guided the laboratory work, provided the funding, and compiled and revised the manuscript.

Acknowledgements

The work was supported by the South African National Research Foundation (Grant CPRR13091035184; 90502) and the University of KwaZulu-Natal. The authors thank the UKZN Microscopy and Microanalysis Unit (Pietermaritzburg) for their assistance.

Competing interests

The authors declare no competing interests.

References

1. **Kaariainen, M., T. Jarvinen, M. Jarvinen, J. Rantanen, and H. Kalimo.** 2000. Relation between myofibers and connective tissue during muscle injury repair. Scand. J. Med. Sci. Sports *10*:332–337.
2. **Baoge, L., E. Van Den Steen, S. Rimbaut, N. Philips, E. Witvrouw, K.F. Almqvist, G. Vanderstraeten, and L.C. Vanden Bossche.** 2012. Treatment of skeletal muscle injury: a review. ISRN Orthop. 2012: Article ID 689012, 7 pages. doi:10.5402/2012/689012.
3. **Prisk, V. and J. Huard.** 2003. Muscle injuries and repair: the role of prostaglandins and inflammation. Histol. Histopathol. *18*:1243–1256.
4. **Mann, C.J., E. Perdiguero, Y. Kharraz, S. Aguilar, P. Pessina, A.L. Serrano, and P. Munoz-Canoves.** 2011. Aberrant repair and fibrosis development in skeletal muscle. Skelet. Muscle *1*:21.
5. **Ebisui, C., T. Tsujinaka, T. Morimoto, K. Kan, S. Iijima, M. Yano, E. Kominami, K. Tanaka, and M. Monden.** 1995. Interleukin-6 induces proteolysis by activating intracellular proteases (cathepsins B and L, proteasome) in C2C12 myotubes. Clin. Sci. (Lond.) *89*:431–439.
6. **Mbebi, C., D. Hantai, M. Jandrot-Perrus, M.A. Doyennette, and M. Verdiere-Sahuque.** 1999. Protease nexin I expression is up-regulated in human skeletal muscle by injury-related factors. J. Cell Physiol. *179*:305–314.
7. **Brigitte, M., C. Schilte, A. Plonquet, Y. Baba-Amer, A. Henri, C. Charlier, S. Tajbakhsh, M. Albert, et al.** 2010. Muscle resident macrophages control the immune cell reaction in a mouse model of notexin-induced myoinjury. Arthritis Rheum. *62*:268–279.
8. **Chazaub, B., M. Brigitte, H. Yacoub-Youssef, L. Arnold, R. Gherardi, C. Sonnet, P. Lafuste, and F. Chretien.** 2009. Dual and beneficial roles of macrophages during skeletal muscle regeneration. Exerc. Sport Sci. Rev. *37*:18–22.
9. **Sanderson, R.D., J.M. Fitch, T.R. Linsenmayer, and R. Mayne.** 1986. Fibroblasts promote the formation of a continuous basal lamina during myogenesis *in vitro*. J. Cell Biol. *102*:740–747.
10. **Hinz, B.** 2007. Formation and function of the myofibroblast during tissue repair. J. Invest. Dermatol. *127*:526–537.
11. **Turner, N.A. and K.E. Porter.** 2013. Function and fate of myofibroblasts after myocardial infarction. Fibrogenesis Tissue Repair *6*:5.
12. **Thomas, K., A.J. Engler, and G.A. Meyer.** 2015. Extracellular matrix regulation in the muscle satellite cell niche. Connect. Tissue Res. *56*:1–8.
13. **Goers, L., P. Freemont, and K.M. Polizzi.** 2014. Co-culture systems and technologies: taking synthetic biology to the next level. J. R. Soc. Interface *11*:20140065. http://dx.doi.org/10.1098/rsif.2014.0065
14. **Snyman, C., K.P. Goetsch, K.H. Myburgh, and C.U. Niesler.** 2013. Simple silicone chamber system for *in vitro* three-dimensional skeletal muscle tissue formation. Frontiers Physiol. *4*:349. http://doi.org/10.3389/fphys.2013.00349
15. **Bacchus, W. and M. Fussenegger.** 2013. Engineering of synthetic intercellular communication systems. Metab. Eng. *16*:33–41.
16. **Miki, Y., K. Ono, S. Hata, T. Suzuki, H. Kumamoto, and H. Sasano.** 2012. The advantages of co-culture over mono cell culture in simulating *in vivo* environment. J. Steroid Biochem. Mol. Biol. *131*:68–75.
17. **Zhang, C., M.P. Barrios, R.M. Alani, M. Cabodi, and J.Y. Wong.** 2016. A microfluidic transwell to study chemotaxis. Exp Cell Res *342*:159–165.
18. **Goetsch, K.P., C. Snyman, K.H. Myburgh, and C.U. Niesler.** 2015. Simultaneous isolation of enriched myoblasts and fibroblasts for migration analysis within a novel co-culture assay. BioTechniques *58*:25–32.
19. **Goetsch, K.P., K.H. Myburgh, and C.U. Niesler.** 2013. *In vitro* myoblast motility models: investigating migration dynamics for the study of skeletal muscle repair. J. Muscle Res. Cell Motil. *34*:333–347.
20. **Javaherian, S., K.J. Li, and A.P. McGuigan.** 2013. A simple and rapid method for generating patterned co-cultures with stable interfaces. BioTechniques *55*:21–26.
21. **Cho, C.H., J. Park, A.W. Tilles, F. Berthiaume, M. Toner, and M.L. Yarmush.** 2010. Layered patterning of hepatocytes in co-culture systems using microfabricated stencils. BioTechniques *48*:47–52.
22. **D'Arcangelo, E, and A.P. McGuigan.** 2015. Micropatterning strategies to engineer controlled cell and tissue architecture *in vitro*. BioTechniques *58*:13–23.
23. **Goetsch, K.P, and C.U. Niesler.** 2011 Optimisation of the scratch assay for *in vitro* skeletal muscle wound healing analysis, Anal Biochem, *411*:158-160.
24. **Vaughan, M.B., E.W. Howard, and J.J. Tomasek.** 2000. Transforming growth factor-beta1 promotes the morphological and functional differentiation of the myofibroblast. Exp. Cell Res. *257*:180–189.
25. **Iyer, S.S., W.P. Pulskens, J.J. Sadler, L.M. Butter, G.J. Teske, T.K. Ulland, S.C. Eisenbarth, S. Florquin, et al.** 2009. Necrotic cells trigger a sterile inflammatory response through the Nlrp3 inflammasome. Proc. Natl Acad. Sci. USA *106*:20388–20393.
26. **Kharraz, Y., J. Guerra, C.J. Mann, A.L. Serrano, and P. Munoz-Canoves.** 2013. Macrophage plasticity and the role of inflammation in skeletal muscle repair. Mediators Inflamm. *2013*: Article ID 491497, 9 pages, 2013. doi:10.1155/2013/491497
27. **Otis, J.S., S. Niccoli, N. Hawdon, J.L. Sarvas, M.A. Frye, A.J. Chicco, and S.J. Lees.** 2014. Pro-inflammatory mediation of myoblast proliferation. PloS One *9*:e92363.
28. **Maxson, S., E.A. Lopez, D. Yoo, A. Danilkovitch-Miagkova, and M.A. LeRoux.** 2012. Concise review: role of mesenchymal stem cells in wound repair. Stem Cells Transl. Med. *1*:142–149.
29. **Bentzinger, C.F., Y.X. Wang, N.A. Dumont, and M.A. Rudnicki.** 2013. Cellular dynamics in the muscle satellite cell niche. EMBO Rep. *14*:1062–1072.
30. **Landen, N.X., D. Li, and M. Stahle.** 2016. Transition from inflammation to proliferation: a critical step during wound healing. Cell. Mol. Life Sci. *73*:3861–3885.
31. **Hatherell, K., P.O. Couraud, I.A. Romero, B. Weksler, and G.J. Pilkington.** 2011. Development of a three-dimensional, all-human *in vitro* model of the blood–brain barrier using mono-, co-, and tri-cultivation transwell models. J. Neurosci. Methods *199*:223–229.
32. **Wynn, T.A.** 2008. Cellular and molecular mechanisms of fibrosis. J. Pathol. *214*:199–210.
33. **Cornelison, D.D.W.** 2008. Context matters: *in vivo* and *in vitro* influences on muscle satellite cell activity. J. Cell. Biochem. *105*:663–669.
34. **Martinez, F.O. and S. Gordon.** 2014. The M1 and M2 paradigm of macrophage activation: time for reassessment. F1000 Prime Rep. *6*:13.
35. **Ko, M.H., C.Y. Li, C.F. Lee, C.K. Chang, and S.H. Fang.** 2016. Scratch wound closure of myoblasts and myotubes is reduced by inflammatory mediators. Int. Wound J. *13*:680–685.
36. **Murphy, M.M., J.A. Lawson, S.J. Mathew, D.A. Hutcheson, and G. Kardon.** 2011. Satellite cells, connective tissue fibroblasts and their interactions are crucial for muscle regeneration. Devel. *138*:3625–3637.
37. **Zhang, Y., H. Li, Z. Lian, and N. Li.** 2010. Myofibroblasts protect myoblasts from intrinsic apoptosis associated with differentiation via beta1 integrin-PI3K/Akt pathway. Devel. Growth Diff. *52*:725–733.

First draft submitted: 22 September 2017; Accepted for publication: 11 January 2018.
Address correspondence to Carola Niesler, Discipline of Biochemistry, School of Life Sciences, University of KwaZulu-Natal, Private Bag X01, Scottsville 3209, South Africa. Tel.: +33 260 5465; E-mail: niesler@ukzn.ac.za

Experimental Cell Research xxx (xxxx) xxx–xxx

Contents lists available at ScienceDirect

Experimental Cell Research

journal homepage: www.elsevier.com/locate/yexcr

Cellular alignment and fusion: Quantifying the effect of macrophages and fibroblasts on myoblast terminal differentiation

C. Venter, C.U. Niesler*

Discipline of Biochemistry, School of Life Sciences, University of KwaZulu-Natal, Private Bag X01, Scottsville 3209, South Africa

ARTICLE INFO

Keywords:
Cellular alignment
Co-culture
Differentiation
Myoblast
Macrophage
Fibroblast

ABSTRACT

Successful skeletal muscle wound repair requires the alignment and fusion of myoblasts to generate multi-nucleated myofibers. *In vitro*, the accurate quantification of cellular *alignment* remains a challenge. Here we present the application of ImageJ and ct-FIRE to quantify muscle cell orientation by means of an alignment index (AI). Our optimised method, which does not require programming skills, allows the alignment of myoblasts in vitro to be determined independently of a predefined reference point. Using this method, we demonstrate that co-culture of myoblasts with macrophages, but not fibroblasts, promotes myoblast alignment in a cell density-dependent manner. Interestingly, myoblast fusion was significantly *decreased* in response to co-culture with macrophages, while the effect of fibroblasts on fusion was density-dependent. At lower numbers, fibroblasts significantly *increased* myoblast fusion, whereas at higher numbers a significant *decrease* was observed. Finally, triple co-culture revealed that the effect of macrophages on myoblast alignment and fusion is unaltered by the additional presence of fibroblasts. Application of our optimised method has therefore revealed quantitative differences in the roles of macrophages versus fibroblasts during alignment and fusion: while successful myoblast alignment is promoted by increasing macrophage numbers, regenerative fusion coincides with a decreasing macrophage population and initial rise in fibroblast numbers.

1. Introduction

Skeletal muscle represents a heterogenous tissue with multiple cell types that each play distinct and important roles in wound repair [1]. Damage to skeletal muscle results in the disruption of myofibres and the extracellular matrix (ECM) that surrounds them [2]. Myogenesis, the differentiation and fusion of mono-nucleated myoblasts into multi-nucleated myofibers, is a critically important stage of muscle regeneration and serves to restore muscle structure and function [3]. Non-myogenic cell types, such as macrophages and fibroblasts, mediate the behaviour of muscle cells during wound repair by secreting an array of signalling molecules and matrix factors [4,5]. We have previously investigated the regulatory role of these non-myogenic cells on myoblast proliferation and migration. We demonstrated that macrophages promote the proliferation of myoblasts in co-culture, while fibroblasts promote migration, during in vitro wound repair; the latter pro-migratory effect was reduced when myoblasts were co-cultured in the presence of both fibroblasts and macrophages under triple co-culture conditions [6,7].

During the terminal phase of myogenesis, myoblasts align to organize themselves relative to each other and to existing myofibres [8]. This process brings the lipid bilayers in close contact with one another in order for the cells to fuse together to form functional muscle with myotubes orientated in the same direction [8]. Several strategies can be used to promote myotube *alignment,* including topographical patterning (e.g. grooved culture plates [9]), mechanical stimulation (e.g. stretch [10]) or application of magnetic/electrical fields [11,12]. In order to *quantify* the exact effect of these strategies on alignment, one has to identify the cell/nuclear outline or actin cytoskeleton, then determine the orientation of these elements and finally calculate a value that represents the extent of alignment [13]. To achieve this, cells are visually identified in images, their outlines manually selected, and their orientation ascertained by determining the angle of deviation of the longitudinal axis of the cell (in degrees) from the x-axis (set to 0°). This manual process is accurate, but arduous and time-consuming with low throughput [13]. Automated image processing techniques (e.g. Fast Fourier Transform (FFT) and local intensity gradient [14,15]) have previously been used to determine cellular orientation; however, these approaches were designed for determining the orientation of a type of pattern rather than determining the orientation of cells and therefore yield low alignment scores [13].

Xu et al. addressed the challenges of these techniques by developing the Binarization-based Extraction of Alignment Score (BEAS) method to

* Corresponding author.
E-mail address: niesler@ukzn.ac.za (C.U. Niesler).

https://doi.org/10.1016/j.yexcr.2018.07.019
Received 24 May 2018; Received in revised form 9 July 2018; Accepted 10 July 2018

rapidly and accurately quantify the alignment of cells [13]. However, a major challenge with BEAS (and other previous methods) is that the information required to determine cellular orientation is presented as a complex image-processing algorithm, which needs to be computed in MATLAB (a costly computer programming language and computing environment). This implementation is problematic for researchers who have neither programming experience nor access to MATLAB. An easily accessible, automated method to quantify *cellular* orientation was therefore required.

ct-FIRE is a freely available, standalone and fully developed framework designed to determine the orientation of *collagen fibres;* it has not been tested for its ability to determine *cellular* orientation [16]. In order to adapt ct-FIRE to measure cellular orientation, a number of approaches can be used. Data can be organized into 10˚ bins and either represented as a histogram of frequency distribution (however, this gives no indication of the extent of alignment and makes significance testing problematic) or used to calculate the degree of alignment. In the latter method, cells within less than 10˚ of the preferred orientation are considered aligned and the percentage of cells in that particular frequency is then calculated [17,18]. Alternatively, an alignment index (AI), which determines how well cells align in a specified direction can be calculated [18–20]. An AI is generally easier to calculate if there is a set direction to which orientation can be compared (e.g. directional angle of the grooves on a plate or the average direction of the cells in a culture dish). However, under standard myoblast culture conditions, there is often no set direction to which alignment can be compared as the cells align independently of physical properties of culture plate and subsequently self-organize in response to elongating myoblasts during fusion [21].

In the current study, we present a method for determining cellular alignment; this method does not require a pre-defined reference direction. ct-FIRE is first tested for its ability to determine the alignment of elliptical shapes (representing hypothetical cells) compared to linear collagen shapes (for which the programme was developed); the orientation determined by ct-FIRE is compared to actual orientation using the AI (Fig. 1A). We then generate an alignment model, creating data sets with defined standard deviations, which represent hypothetical images of cells aligned to different extents (Fig. 1B). These hypothetical images are then rotated, and an AI calculated using either the *average* (i.e. the mean direction of cell alignment) or *preferred* (i.e. direction in which most cells are aligned) orientation (Fig. 1B). Lastly, we test our method using images of cultured myoblasts, where the image processing capability of ImageJ is first applied to automatically mark the boundaries of cells and ct-FIRE is subsequently used to analyse cellular orientation and calculate an AI (Fig. 1C) [13,16]. Once established, we then apply this protocol to assess the effect of macrophages and fibroblasts on the alignment of myoblasts during fusion. This accessible, optimised method for the analysis of cellular orientation presents a tool for analysis of alignment in vitro. Our results highlight the distinct regulatory role of non-myogenic cells on alignment and fusion during terminal skeletal muscle differentiation.

2. Materials and methods

2.1. Testing ct-FIRE on images of hypothetical cells

The programme ct-FIRE was initially developed to determine the alignment of collagen fibres; these fibres have linear shapes as opposed to elliptical shapes that are classically associated with elongated spindle-shaped cells. Linear and elliptical shapes were therefore created using Microsoft PowerPoint (2016) and orientated at 0˚, 30˚, 60˚, 90˚, 120˚ and 150˚ (Fig. 2); these orientations represent x in the equation below, where N is the total number of orientations [20,22]:

$$\textit{Alignment Index} \quad \left(AI\right) = \frac{1}{N}\sum_{i=1}^{N}(2 \quad [cos(x-y)]^2 \; - 1)$$

ct-FIRE was then tested to determine whether it would be able to measure the orientation of both shapes, generating the value y in the above equation. An AI value of 0 represents no agreement between x and y, while a value of 1 represents a perfect agreement (i.e. x equals y). This evaluated how well the orientation determined by ct-FIRE agrees with the actual orientation.

2.2. Alignment modelling

A set of normally distributed random data (N = 98) around a mean (set to 90) with a specified standard deviation (0, 4, 16, 64) (Supplementary Table 1) was created using the Microsoft Excel (2016) *=NORM.INV (probability; mean; standard deviation)* function with *= RAND()* as the probability (which creates a random factional value: $0 \leq \alpha \leq 1$). The values in this data set represent theoretical directions in which an "image" containing 98 cells are likely to be orientated (the smaller the standard deviation, the greater the extent of alignment, and vice versa). Using this model, a cell orientated at 180˚ has the same alignment as a cell orientated at 0˚. Similarly, 225˚ equals 45˚, 270˚ equals 90˚ and so on. Therefore, 180˚ was subtracted from values $\geq$ 180˚ and added to values $<$ 0˚ in order to represent cell direction exclusively between 0˚ and 180˚. In order to rotate hypothetical images of these cells, every theoretical cell in a data set was shifted by -90˚ or $+37.1$˚ and values $\geq$ 180˚ or $<$ 0˚ adjusted accordingly. For every data set, the *average orientation* (an average of all orientations) and *preferred orientation* (an average of cell orientations in the frequency bin with the largest value) was calculated and used in the same alignment index equation stated earlier, where N is now the total number of cells, x is the *average* OR *preferred orientation* used as a reference point of the data set and y is the orientation of an individual cell within that data set. This equation determines how well a cell aligns along a particular direction (e.g. a fixed point of reference) or along the average/preferred direction of cells within each individual cell in a data set. The alignment index of every cell in a data set was used to calculate an average alignment index (of all the cells in that data set) between 0 and 1, where 0 represents a group of cells that are randomly orientated and 1 represents a population that is perfectly aligned [22]. The AI was first calculated using the *average orientation* (often associated with a defined reference point [17,18,20]) and this was repeated using the *preferred orientation* of the data set, in order to compare the two.

2.3. Cell culture

Mouse C2C12 myoblasts (ATCC, USA, cat. CRL-1772™; passage 10–20), LMTK fibroblasts (ATCC, USA, cat. CCL-1.3™; passage 6–25) and J774A.1 macrophages (ATCC, USA, cat. TIB-67™; passage 70–90) were cultured at 37 ˚C and 5% CO_2 and maintained in growth media (GM) containing Dulbecco's Modified Eagle's Medium (DMEM, Sigma, St Louis, MO, USA, cat. D5648) supplemented with 10% (v/v) Fetal Bovine Serum (FBS, Gibco, USA, cat. 10500) and 2% (v/v) Penicillin-Streptomycin (PenStrep, LONZA, Switzerland, cat. DE17-602E). Media was changed every 48 h.

Co-culture of macrophages and/or fibroblasts with myoblasts was established as described in Venter and Niesler [6]. Briefly, for double co-culture, macrophages or fibroblasts (0, 5, 10, 20, 40 and 80 $\times$ 10^3) were plated on the outer edge of the well of a 24-well culture plate in GM for an hour to promote adherence; C2C12 myoblasts (50 $\times$ 10^3 cells) were then plated and left to adhere in the centre of the same well for 24 h in GM. For triple co-culture, both macrophages (40 $\times$ 10^3) and fibroblasts (40 $\times$ 10^3) were plated on the outer edge and myoblasts plated in the centre as described above. Myoblasts were differentiated for 5 days in differentiation media (DM; 2% FBS in DMEM) with media

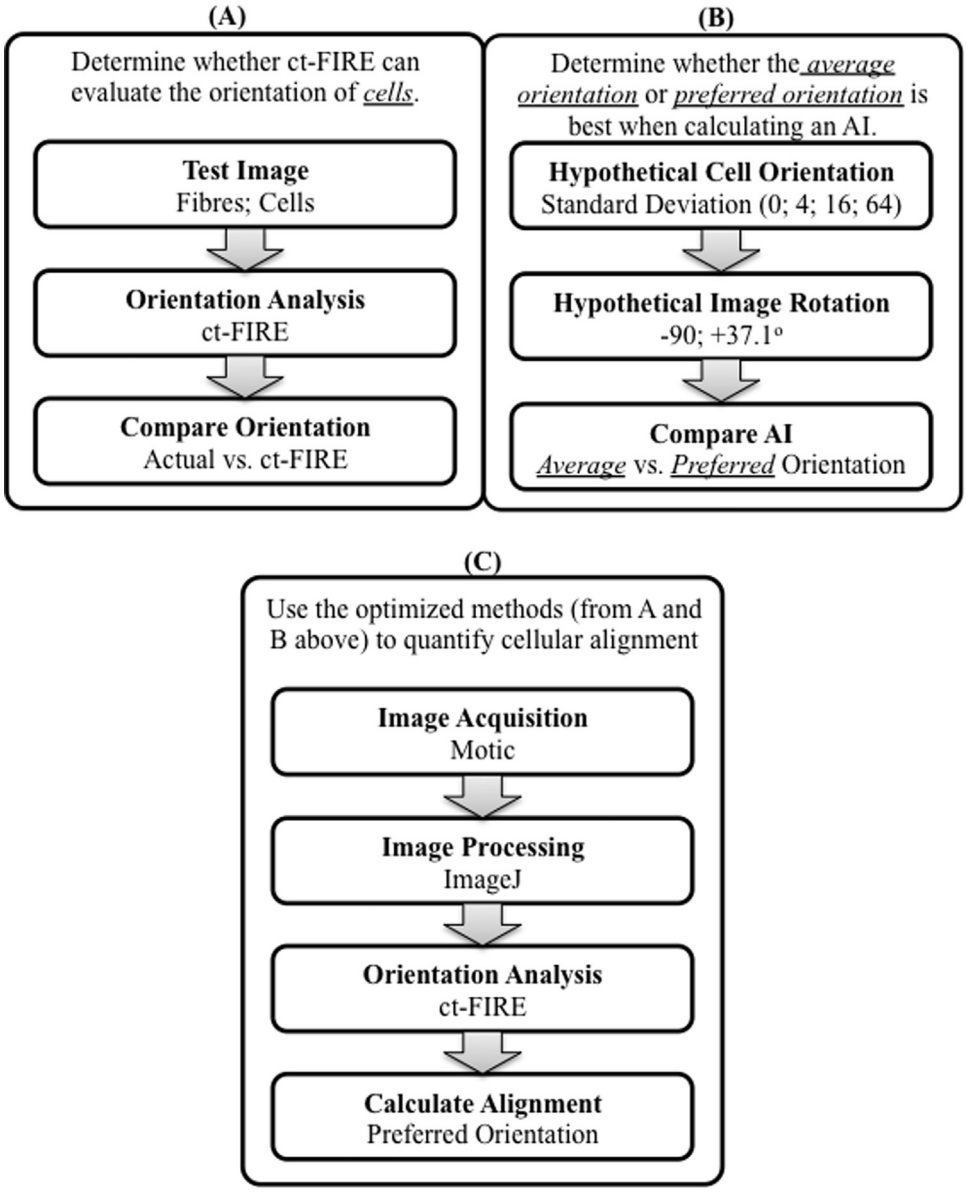

Fig. 1. Overview of methodology development. A) ct-FIRE was tested for its ability to determine the orientation of linear versus elliptical shapes, representing either collagen or cells, respectively. B) A model for alignment was created using Microsoft Excel to represent hypothetical cells that were then rotated at −90° and +37.1°; their alignment was calculated and compared using the *average* orientation versus *preferred orientation*. C) Images of differentiating myoblasts were then acquired, and the AI calculated using the preferred orientation.

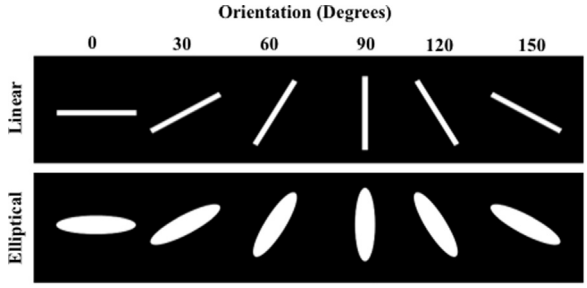

Fig. 2. Representative images of collagen fibres (linear) and cells (elliptical). Hypothetical shapes representing collagen fibres and cells were created using Microsoft PowerPoint orientated at 0°, 30°, 60°, 90°, 120° and 150°.

changed every 2–3 days. After differentiation, the cells were stained with 1% Fuchsin (Sigma, St Louis, MO, USA, cat. 47860) in methanol (15 min), washed three times with distilled water, left to air dry overnight, and evaluated for alignment and fusion.

2.4. Evaluating alignment

Images (5 fields of view; 2 replicates per experiment) of differentiated myoblasts, absent of macrophage or fibroblast clusters, were taken with an Olympus CKX41 microscope and a Motic 3.0 megapixel camera (10× objective lens) (Supplementary Fig. 1A) and processed with ImageJ, using an adaptation of the binarization method described by Xu et al. [13] (Supplementary Fig. 1B). The image was converted to grayscale (*Image → Type → 8-bit*), image noise removed (*Process → Noise → Despeckle*) and a mean threshold applied (*Image → Adjust → Auto Local Threshold: Mean; Uncheck "White objects on black background"*) and further processed with ct-FIRE (Supplementary Fig. 1C). The AI was then calculated using the *preferred* orientation of cells (as described earlier).

2.5. Fusion index

Images (5 fields of view; 2 replicates per experiment) of differentiated C2C12 myoblasts (day 5) were taken with an Olympus CKX41 microscope and a Motic 3.0 megapixel camera (20x objective lens) and the fusion index calculated as follows:

$$\text{Fusion Index}(\%) = (\text{No. of myotube nuclei}(\geq 3 \text{ nuclei})/\text{Total no. nuclei}) \times 100$$

2.6. Statistical analysis

Data was determined to be normally distributed; all results were analysed using a parametric paired, two-tailed Student's T-test and values of $p < 0.05$ were considered to be statistically significant compared to the control. All data was represented as mean ± SEM. Experiments were repeated 3–5 times.

3. Results

3.1. ct-FIRE can determine the orientation of cell-like shapes

ct-FIRE was originally developed to determine the orientation of linear collagen fibres, but its ability to determine the orientation of elliptical cell-like shapes had not been evaluated. The AI's of linear versus elliptical shapes were determined to be 0.9992 versus 0.9999 respectively (Table 1), demonstrating that ct-FIRE is able to determine the orientation of both shapes with a very high degree of accuracy (maximum AI = 1). No significant difference in AI calculation between linear and elliptical shapes were observed. This demonstrates that ct-FIRE can be used to accurately determine the orientation of elliptical shaped objects, such as cells.

3.2. Calculation of cellular alignment should use preferred rather than average orientation

The rotation a hypothetical image of aligned cells (orientated at 90°) by −90° or +37.1° (Fig. 3) does not change *how* they are aligned, but merely shifts the *direction* in which they are aligned (0° or 127.1°, respectively). The data set in Supplementary Table 1 represents either a population of hypothetical cells that are perfectly aligned (SD = 0), somewhat aligned (SD = 4 or 16) or unaligned and randomly orientated (SD = 64).

The alignment index (AI), for each data set representing a hypothetical image of cells (Table 2) with different degrees of alignment (SD = 0, 4, 16 and 64) was then compared, following calculation, using the *average orientation* and *preferred orientation;* the significance within SD's was subsequently tested between 90° and either 0° or 127.71° orientations. When comparing the AI generated for cells orientated at 90° and 127.71° using the *average orientation*, there was no significant difference irrespective of the SD (Table 2). When comparing cells orientated at 90° with those oriented 0°, there was significant difference for SD's 4, 16 and 64. For instance, for SD = 4, the AI was 0.98 at 90° when using the *average orientation* which was significantly different when compared with −0.94 at 0° (Table 2). There was no significant difference between 90° versus 0° and 90° versus 127.1° for any of the standard deviations when using the *preferred orientation*. This suggests that using the *average orientation* as a point of reference to calculate the AI of cells will yield inaccurate results when an image is orthogonally rotated; using the preferred orientation yields the same AI regardless of which direction an image may be rotated.

Table 1
Comparison of the alignment index for hypothetical linear and elliptical shapes. An alignment index (AI) was calculated to determine how well the orientation of the linear and elliptical shapes, as determined by ct-FIRE, agrees with the actual known orientation.

Shape	Linear	Elliptical
Mean	0,9992	0,9999
SD	0,0005	0,0002

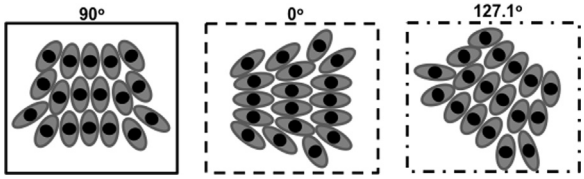

Fig. 3. Model of Alignment. A) Schematic to show that a group of cells can be orientated in any direction (90°, 0° or 127.1°) and still have the same degree of alignment. B) Graph representing the frequency distribution of hypothetical cells, where data sets were created between 0° and 180° with different standard deviations (SD = 0, 4, 16 and 64) using Microsoft Excel to represent cells orientated between 0° and 180° with different degrees of alignment.

Table 2
Comparison of the alignment index of data sets with different standard deviations, calculated using the *average* vs. the *preferred orientation*. Data sets with increasing standard deviations (and orientated about 90°) were created using Microsoft Excel. These data sets represent hypothetical cells aligned to different extents. Hypothetical cells were shifted to 0° and 127.1° and the alignment index calculated compared to the *average* and the *preferred orientation*. * = $p < 0.05$ compared to the alignment index (AI) at 90°.

	Alignment index (AI)					
	Average orientation			Preferred orientation		
SD	**90°**	**0°**	**127.1°**	**90°**	**0°**	**127.1°**
0	1	1	1	1	1	1
4	0,98	−0,94*	0,98	0,98	0,98	0,98
16	0,87	−0,85*	0,88	0,85	0,85	0,86
64	0,16	−0,15*	0,02	0,14	0,14	0,15

3.3. Macrophages inhibit fusion, but promote alignment of myoblasts in a density-dependent manner

Once we had determined that the *preferred orientation* was more appropriate in determining cellular AI's, we went on to evaluate the effect of macrophages on myoblast alignment. Visual analysis of co-culture of macrophages with myoblasts (Fig. 4) suggested that macrophages had differing effects on alignment versus fusion (Fig. 4A). Following calculation, it was evident that the myoblast AI was significantly increased in response to 5×10^3 macrophages (0.21 ± 0.02; $p < 0.05$) and continued to increase in a cell density-dependent manner reaching a maximum effect at 80×10^3 cells (0.46 ± 0.03; $p < 0.05$), compared to the control (0.14 ± 0.02) (Fig. 4B). Co-culture with macrophages, however, was observed to negatively impact fusion (Fig. 4C), with 20×10^3 macrophages causing a significant decrease in the fusion at day 5 (14.88 ± 0.75%; $p < 0.05$) compared to the control (19.55 ± 0.15%). Macrophages continued to negatively affect myoblast fusion in a density-dependent manner with 80×10^3 macrophages having the greatest significant effect (6.08 ± 0.49%; $p < 0.05$) compared to the control.

3.4. Fibroblasts do not significantly alter myoblast alignment, but have differential effects on fusion

Co-culturing fibroblasts with myoblasts resulted in no observable difference in alignment; it appears though that lower fibroblast numbers were associated with larger myotubes, while co-cultures with higher fibroblast numbers displayed smaller myotubes (Fig. 5A).

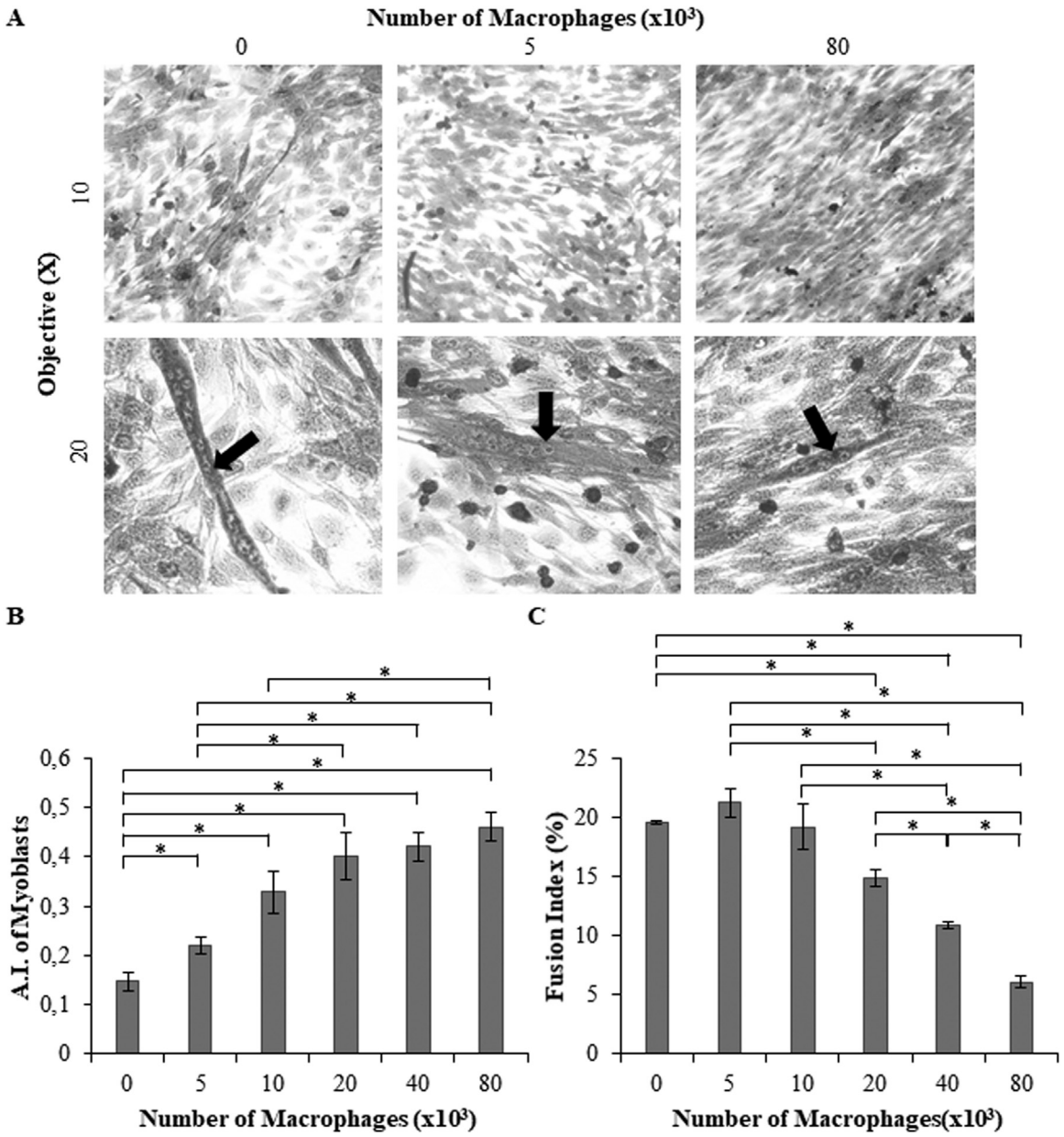

Fig. 4. The effect of macrophages on the alignment and fusion of myoblasts. Macrophages (0 (control), 5, 10, 20, 40 and 80 × 10^3) were co-cultured with differentiating myoblasts for 5 days, stained with Fuchsin and viewed using an Olympus CKX41 microscope A) Images of myoblasts co-cultured with increasing numbers of macrophages (0, 5 and 80 × 10^3) captured with a Motic 3.0 megapixel camera; arrows indicate differentiated myotubes. B) Cell orientation and alignment index (AI) evaluated using ct-FIRE. C: Fusion index (%). * = $p < 0.05$; Alignment: N = 4; Fusion: N = 3.

Quantification of AI revealed no significant increase in myoblast alignment in response to these non-myogenic cells; indeed, AI values did not exceed 0.27 under any conditions (Fig. 5B). However, a significant increase in the fusion index was observed in response to 5 × 10^3 fibroblasts (42.28 ± 3.47%; $p < 0.05$) in comparison with the control (24.23 ± 1.93%) (Fig. 5C). When further increasing the number of fibroblasts, this positive effect was slowly lost until in fact, at 80 × 10^3 fibroblasts, a significant decrease in fusion is observed (12.62 ± 0.75%; $p < 0.05$) compared to control (Fig. 5C).

3.5. Macrophages continue to promote myoblast alignment and inhibit fusion in the presence of fibroblasts

In order to determine the effect of an inflammatory *and* fibrotic environment on myoblast differentiation, triple co-cultures of macrophages and fibroblasts with myoblasts were carried out (Fig. 6). Analysis of myoblast alignment showed that macrophages (40 × 10^3) on their own continued to significantly promote the alignment of myoblasts (0.45 ± 0.03) compared to the control (0.05 ± 0.01; $p < 0.05$), while fibroblasts (40 × 10^3) had no significant effect (Fig. 6A). Co-culture of macrophages (40 × 10^3) with myoblasts continued to have a negative effect on myoblast fusion (6.37 ± 0.87%; $p < 0.5$) compared to the control (12.90 ± 1.00%), while fibroblasts (40 × 10^3) continued to have no significant effect on myoblast fusion (Fig. 6B). When macrophages and fibroblasts were co-cultured together with myoblasts, macrophages maintained both their positive effect on myoblast alignment (0.38 ± 0.03; $p < 0.05$; Fig. 6A) and their negative effect on myoblast fusion (7.51 ± 0.51; $p < 0.05$; Fig. 6B) compared to the control.

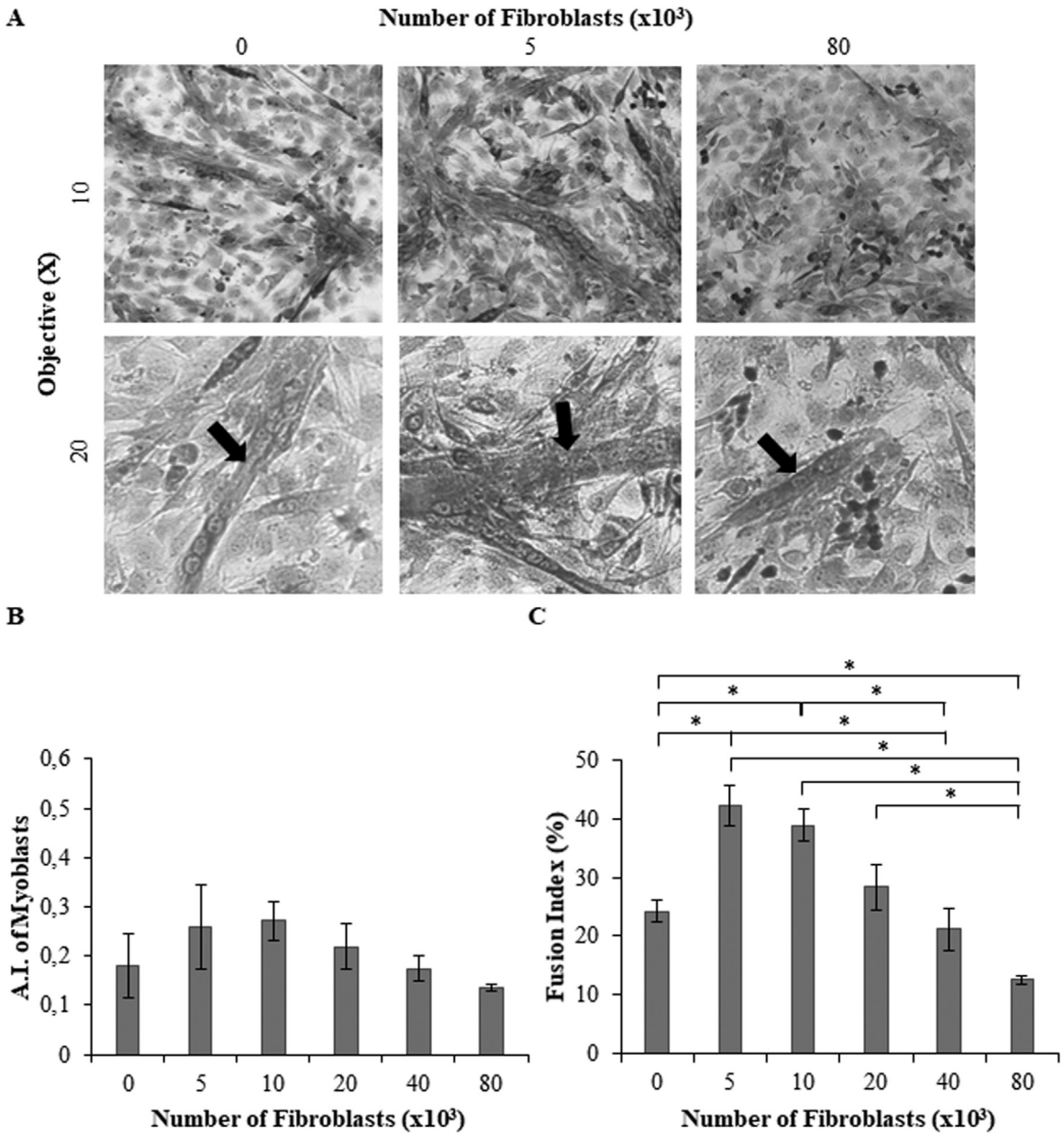

Fig. 5. The effect of fibroblasts on the alignment and fusion of myoblasts. Fibroblasts (0, 5, 10, 20, 40 and 80 × 10^3) were co-cultured with differentiating myoblasts for 5 days, stained with Fuchsin and viewed using an Olympus CKX41 microscope. A) Images of myoblasts co-cultured with increasing numbers of fibroblasts (0, 5 and 80 × 10^3) captured with a Motic 3.0 megapixel camera; arrows indicate differentiated myotubes. B) Cell orientation and alignment index (AI) evaluated using ct-FIRE. C) Fusion index (%). * = $p < 0.05$; Alignment: N = 3; Fusion: N = 3.

4. Discussion

Skeletal muscle has the remarkable ability to repair itself post-injury. In order for this process to occur, satellite cells become activated, migrate into the wound, align with one another as well as existing muscle, and differentiate to form multi-nucleated myotubes [23]. Alignment is an important step during myogenesis, because it orientates the muscle cells in a similar direction and brings lipid membranes together; this allows the cells to fuse and form multinucleated myofibres with parallel longitudinal axes [8,24]. Muscle cells that are cultured in vitro maintain their ability to align and can do so without a predefined template [21].

A number of previous studies have used physical templates, such as grooves in a culture well, to improve myoblast alignment in vitro and promote fusion [9,19,21,25,26]. The alignment of these cells was quantified by determining their orientation relative to these grooves, which were set as the reference. Cells orientated in the direction of these grooves were classified as perfectly aligned (AI = 1), whereas those that were randomly orientated around the reference point were deemed unaligned (AI = 0) [13,22]. A problem however arises when cells are able to align in the absence of a template; under these circumstances there is no point of reference for assessment of AI. We therefore sought to develop a method to address this shortcoming.

Random data sets with a range of standard deviations were created in order to represent cells aligned to different degrees. The smaller the standard deviation within this set, the better the alignment; conversely, the higher the standard deviation, the greater the random orientation. The overall alignment of all the "cells" in the image can be determined by either calculating the mean (referred to as the "*average orientation*") or the mode (referred to as the "*preferred orientation*") of the data set. Rotating this image (irrespective of the standard deviation) should not change the AI, because it merely shifts the direction in which all the

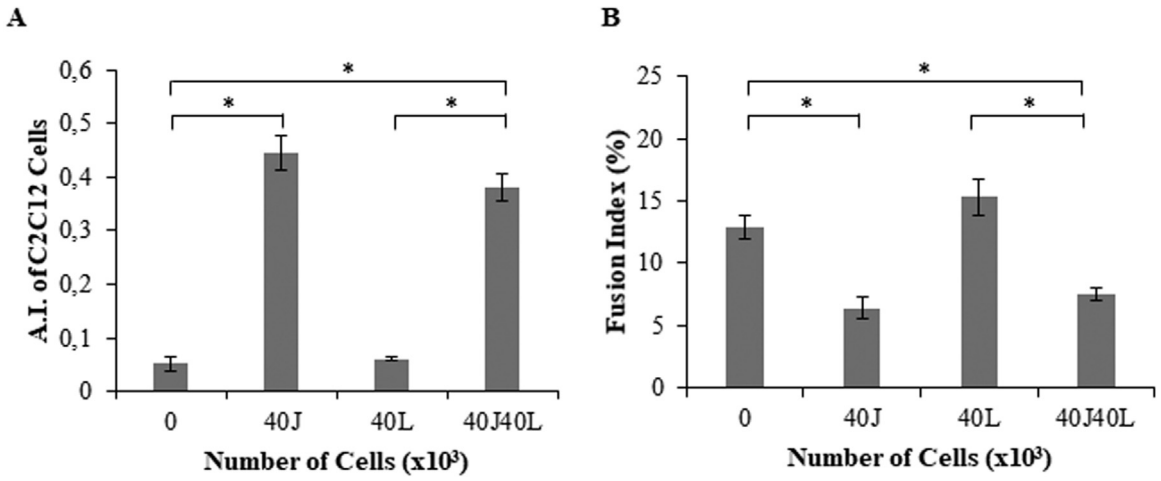

Fig. 6. The effect of macrophages and fibroblasts on the alignment and fusion of myoblasts. Macrophages (40J; 40 × 10^3 cells), fibroblasts (40L; 40 × 10^3 cells) or both macrophages and fibroblasts (40J40L; 40 × 10^3 cells, each) were co-cultured with differentiating myoblasts for 5 days. A) Alignment index (AI). B) Fusion index (%). * = $p < 0.05$; Alignment: N = 5; Fusion: N = 5.

"cells" are all distributed. When the AI was calculated using the *average orientation,* it did not however remain the same when the data set was shifted; on the other hand, when the *preferred orientation* was used, the AI remained the same no matter what direction the data set was shifted. For this reason, we subsequently used the *preferred orientation* in all subsequent calculations.

The orientation of each individual cell can be manually determined by measuring the angle at which it lies relative to another cell [13]. However, this becomes unfeasible when dealing with high numbers of cells. There are few available programs that can perform automated alignment assessment without the need for programming skills. ct-FIRE, software originally designed to determine the orientation of collagen fibres (in essence, straight lines) is one such program [16]. In order to test and compare its ability to determine the orientation of elliptical cell-like shapes, images of straight lines (akin to "collagen") and ellipsis (akin to "cells") were created, orientated in known directions. ct-FIRE was then employed to determine the orientation of these shapes; the measured orientation was then evaluated to determine how well it matched the actual alignment. It was determined that ct-FIRE could not only precisely determine the orientation of *straight* lines as it was intended, but could also be used to measure alignment of *elliptical* cell-like shapes. A limitation of ct-FIRE is that it was not specifically designed to determine cellular orientation; future cellular studies could possibly reveal areas requiring optimization in its application. It is important to note that other automated techniques, such as the Fast Fourier Transform (FFT), the gradient orientation method and the Binarization-based Extraction of Alignment Score (BEAS) method, also have limited abilities when determining cellular orientations [13]. ct-FIRE is therefore an appropriate tool for the calculation of cellular AI in vitro.

Next, we sought to use our established method to determine the effect of macrophages and fibroblasts on myoblast alignment during fusion. Pro-inflammatory macrophages are prevalent in the early stages of wound repair and are important for clearing necrotic debris and apoptotic cells [27,28]. These macrophages are also known to secrete a host of pro-inflammatory signalling molecules that stimulate myoblast proliferation, but delay differentiation [29–33]. Anti-inflammatory macrophages, on the other hand, are typically present in the later, regenerative stages of myogenesis and have been shown to promote myoblast differentiation and fusion [29–31]. In our study, macrophages were not activated prior to co-culture; however, given their in vitro environment, they would most likely display an anti-inflammatory profile. We demonstrate, for the first time, that macrophages significantly improve the *alignment* of myoblasts during differentiation. Co-culture with as few as 5 × 10^3 macrophages and up to 80 × 10^3 macrophages resulted in significantly increased myoblast alignment. Subsequent analysis of fusion suggests that, while the lower macrophage number has no effect on fusion, higher numbers significantly decrease it. Myoblast elongation and alignment have previously been shown to assist in facilitating end-to-end cellular contact, enabling subsequent fusion [34]. Interestingly, while myoblasts cultured on ultrafine grooved surfaces aligned and fused in the direction of the grooves, early differentiating cells were observed to form aggregates not aligned with the groove axis [34]. In other studies, impairment of elongation and alignment has been associated with a decrease in fusion, further supporting a direct correlation between these processes [35,36]. The opposing effect of macrophages on myoblast alignment versus fusion seen in our study is therefore highly intriguing as it suggests an inverse correlation under these conditions; this requires further investigation. Finally, additional triple co-culture studies showed that this effect of macrophages on myoblasts differentiation was not altered by the presence of fibroblasts. This suggests that, whether in the presence or absence of fibroblasts, macrophages are important in the early stages of myogenesis in order to correctly orientate and align the cells while their resolution may be crucial during terminal differentiation.

Fibroblasts are important in muscle regeneration because they are known secretors of ECM scaffold components, such as collagen I and III [37,38]. Fibroblasts, upon in vivo muscle injury, differentiate to form the ECM-secreting "myofibroblasts" [37,39]; in vitro, the myofibroblast phenotype is commonly generated in response to serum [40]. As with macrophages, an extended presence of myofibroblasts may lead to aberrant muscle regeneration [5]. In our study, fibroblasts co-cultured with myoblasts, had no significant effect on alignment. Evaluating the effect of myofibroblasts on myoblast fusion, revealed that low numbers of myofibroblasts (5 × 10^3) significantly promoted fusion. However, as the number of myofibroblasts increased, fusion decreased in a cell density-dependent manner to the point where at the highest numbers, fibroblasts significantly lowered myoblast fusion in comparison to control. Our data suggests that while fibroblasts may not be central regulators of myoblast alignment, their effect on fusion is significant, but highly dependent on their density. Previously published studies investigating the role of fibroblasts on myoblast alignment and fusion in vitro are few. Some suggest that fibroblasts promote myoblast fusion, however these have not investigated alignment [41,42]. One study showed qualitatively that fibroblasts promote alignment, but *inhibit* fusion, when *in direct contact* with myoblasts [43]. This contradictory data emphasizes the need for greater understanding of the regulation of myoblast alignment and fusion by non-myogenic cells.

In summary, we have optimised a protocol for the quantification of

cellular alignment, which can calculate the alignment index of a population of cells in the absence of a predefined reference template. Evaluating the effect of macrophages and fibroblasts on myoblast alignment during differentiation, we showed that macrophages had opposing effects on myoblast alignment versus fusion, promoting and inhibiting these processes, respectively. Furthermore, while fibroblasts had no significant effect on myoblast alignment, they could either promote or inhibit fusion depending on their density. Finally, the presence of fibroblasts did not alter the effect of macrophages on myoblast differentiation. This accessible alignment analysis tool can now be used to provide further insight into the regulation of cellular orientation during myogenesis and other processes.

Acknowledgements

The work was supported by the South African National Research Foundation (Grant CPRR13091035184; 90502).

Appendix A. Supplementary material

Supplementary data associated with this article can be found in the online version at doi:10.1016/j.yexcr.2018.07.019.

References

[1] L.C. Ceafalan, B.O. Popescu, M.E. Hinescu, Cellular players in skeletal muscle regeneration, BioMed. Res. Int. 2014 (2014) 21, https://doi.org/10.1155/2014/957014.

[2] M. Kaariainen, T. Jarvinen, M. Jarvinen, J. Rantanen, H. Kalimo, Relation between myofibers and connective tissue during muscle injury repair, Scand. J. Med. Sci. Sports 10 (2000) 332–337, https://doi.org/10.1034/j.1600-0838.2000.010006332.x.

[3] S.A. Villalta, H.X. Nguyen, B. Deng, T. Gotoh, J.G. Tidball, Shifts in macrophage phenotypes and macrophage competition for arginine metabolism affect the severity of muscle pathology in muscular dystrophy, Hum. Mol. Genet. 18 (2009) 482–496, https://doi.org/10.1093/hmg/ddn376.

[4] L. Bosurgi, A.A. Manfredi, P. Rovere-Querini, Macrophages in injured skeletal muscle: a perpetuum mobile causing and limiting fibrosis, prompting or restricting resolution and regeneration, Front. Immunol. 2 (2011) 62, https://doi.org/10.3389/fimmu.2011.00062.

[5] C.J. Mann, E. Perdiguero, Y. Kharraz, S. Aguilar, P. Pessina, A.L. Serrano, P. Munoz-Canoves, Aberrant repair and fibrosis development in skeletal muscle, Skelet. Muscle 1 (2011) 21, https://doi.org/10.1186/2044-5040-1-21.

[6] C. Venter, C.U. Niesler, A triple co-culture method to investigate the effect of macrophages and fibroblasts on myoblast proliferation and migration, BioTechniques 64 (2018) 52–59, https://doi.org/10.2144/btn-2017-0100.

[7] K.P. Goetsch, C. Snyman, K.H. Myburgh, C.U. Niesler, Simultaneous isolation of enriched myoblasts and fibroblasts for migration analysis within a novel co-culture assay, BioTechniques 58 (2015) 25–32, https://doi.org/10.2144/000114246.

[8] K. Rochlin, S. Yu, S. Roy, M.K. Baylies, Myoblast fusion: when it takes more to make one, Dev. Biol. 341 (2010) 66–83, https://doi.org/10.1016/j.ydbio.2009.10.024.

[9] P.Y. Wang, H.T. Yu, W.B. Tsai, Modulation of alignment and differentiation of skeletal myoblasts by submicron ridges/grooves surface structure, Biotechnol. Bioeng. 106 (2010) 285–294, https://doi.org/10.1002/bit.22697.

[10] W.W. Ahmed, T. Wolfram, A.M. Goldyn, K. Bruellhoff, B.A. Rioja, M. Moller, J.P. Spatz, T.A. Saif, J. Groll, R. Kemkemer, Myoblast morphology and organization on biochemically micro-patterned hydrogel coatings under cyclic mechanical strain, Biomaterials 31 (2010) 250–258, https://doi.org/10.1016/j.biomaterials.2009.09.047.

[11] D. Coletti, L. Teodori, M.C. Albertini, M. Rocchi, A. Pristera, M. Fini, M. Molinaro, S. Adamo, Static magnetic fields enhance skeletal muscle differentiation in vitro by improving myoblast alignment, Cytometry A 71 (2007) 846–856, https://doi.org/10.1002/cyto.a.20447.

[12] T. Tanaka, N. Hattori-Aramaki, A. Sunohara, K. Okabe, Y. Sakamoto, H. Ochiai, R. Hayashi, K. Kishi, Alignment of skeletal muscle cells cultured in collagen gel by mechanical and electrical stimulation, Int. J. Tissue Eng. 2014 (2014) 1–5, https://doi.org/10.1155/2014/621529.

[13] F. Xu, T. Beyazoglu, E. Hefner, U.A. Gurkan, U. Demirci, Automated and adaptable quantification of cellular alignment from microscopic images for tissue engineering applications, Tissue Eng. Part C Methods 17 (2011) 641–649, https://doi.org/10.1089/ten.tec.2011.0038.

[14] Z. Tonar, S. Nemecek, R. Holota, J. Kocová, V. Treska, J. Molacek, T. Kohouteck, S. Hadravska, Microscopic image analysis of elastin network in samples of normal, atherosclerotic and aneurysmatic abdominal aorta and its biomechanical implications, J. Appl. Biomed. 1 (2003) 149–159.

[15] B.B. Chaudhuri, P. Kundu, N. Sarkar, Detection of gradation of oriented texture, Pattern Recog. Lett. 14 (1992) 147–153, https://doi.org/10.1016/0167-8655(93)90088-U.

[16] J.S. Bredfeldt, Y. Liu, C.A. Pehlke, M.W. Conklin, J.M. Szulczewski, D.R. Inman, P.J. Keely, R.D. Nowak, T.R. Mackie, K.W. Eliceiri, Computational segmentation of collagen fibers from second-harmonic generation images of breast cancer, J. Biomed. Opt. 19 (2014) 16007, https://doi.org/10.1117/1.JBO.19.1.016007.

[17] H. Aubin, J.W. Nichol, C.B. Hutson, H. Bae, A.L. Sieminski, D.M. Cropek, P. Akhyari, A. Khademhosseini, Directed 3D cell alignment and elongation in microengineered hydrogels, Biomaterials 31 (2010) 6941–6951, https://doi.org/10.1016/j.biomaterials.2010.05.056.

[18] V. Hosseini, S. Ahadian, S. Ostrovidov, G. Camci-Unal, S. Chen, H. Kaji, M. Ramalingam, A. Khademhosseini, Engineered contractile skeletal muscle tissue on a microgrooved methacrylated gelatin substrate, Tissue Eng. Part A 18 (2012) 2453–2465, https://doi.org/10.1089/ten.TEA.2012.0181.

[19] T. Peterbauer, S. Yakunin, J. Siegel, S. Hering, M. Fahrner, C. Romanin, J. Heitz, Dynamics of spreading and alignment of cells cultured in vitro on a grooved polymer surface, J. Nanomater. 2011 (2011) 1–10, https://doi.org/10.1155/2011/413079.

[20] M. Sun, A.B. Bloom, M.H. Zaman, Rapid quantification of 3D collagen fiber alignment and fiber intersection correlations with high sensitivity, PLoS One 10 (2015) e0131814, https://doi.org/10.1371/journal.pone.0131814.

[21] M. Junkin, S.L. Leung, S. Whitman, C.C. Gregorio, P.K. Wong, Cellular self-organization by autocatalytic alignment feedback, J. Cell Sci. 124 (2011) 4213–4220, https://doi.org/10.1242/jcs.088898.

[22] Y. Pang, X. Wang, D. Lee, H.P. Greisler, Dynamic quantitative visualization of single cell alignment and migration and matrix remodeling in 3-D collagen hydrogels under mechanical force, Biomaterials 32 (2011) 3776–3783, https://doi.org/10.1016/j.biomaterials.2011.02.003.

[23] A. Musaro, The basis of muscle regeneration, Adv. Biol. 2014 (2014) 16, https://doi.org/10.1155/2014/612471.

[24] G. Cossu, S. Biressi, Satellite cells, myoblasts and other occasional myogenic progenitors: possible origin, phenotypic features and role in muscle regeneration, Sem. Cell Dev. Biol. 16 (2005) 623–631, https://doi.org/10.1016/j.semcdb.2005.07.003.

[25] P. Bajaj, B. Reddy Jr, L. Millet, C. Wei, P. Zorlutuna, G. Bao, R. Bashir, Patterning the differentiation of C2C12 skeletal myoblasts, Integr. Biol. 3 (2011) 897–909, https://doi.org/10.1039/c1ib00058f.

[26] S. Ostrovidov, V. Hosseini, S. Ahadian, T. Fujie, S.P. Parthiban, M. Ramalingam, H. Bae, H. Kaji, A. Khademhosseini, Skeletal muscle tissue engineering: methods to form skeletal myotubes and their applications, Tissue Eng. Part B Rev. 20 (2014) 403–436, https://doi.org/10.1089/ten.TEB.2013.0534.

[27] Y. Kharraz, J. Guerra, C.J. Mann, A.L. Serrano, P. Munoz-Canoves, Macrophage plasticity and the role of inflammation in skeletal muscle repair, Mediat. Inflamm. 2013 (2013) 491497, https://doi.org/10.1155/2013/491497.

[28] E. Rigamonti, P. Zordan, C. Sciorati, P. Rovere-Querini, S. Bruneli, Macrophage plasticity in skeletal muscle repair, BioMed. Res. Int. l 2014 (2014) 660629, https://doi.org/10.1155/2014/560629.

[29] M. Bencze, E. Negroni, D. Vallese, H. Yacoub-Youssef, S. Chaouch, A. Wolff, A. Aamiri, J.P. Di Santo, B. Chazaud, G. Butler-Browne, W. Savino, V. Mouly, I. Riederer, Proinflammatory macrophages enhance the regenerative capacity of human myoblasts by modifying their kinetics of proliferation and differentiation, Mol. Ther. 20 (2012) 2168–2179, https://doi.org/10.1038/mt.2012.189.

[30] L. Arnold, A. Henry, F. Poron, Y. Baba-Amer, N. van Rooijen, A. Plonquet, R.K. Gherardi, B. Chazaud, Inflammatory monocytes recruited after skeletal muscle injury switch into anti-inflammatory macrophages to support myogenesis, J. Exp. Med. 204 (2007) 1057–1069, https://doi.org/10.1084/jem.20070075.

[31] B. Chazaud, M. Brigitte, H. Yacoub-Youssef, L. Arnold, R. Gherardi, C. Sonnet, P. Lafuste, F. Chretien, Dual and beneficial roles of macrophages during skeletal muscle regeneration, Ex. Sport Sci. Rev. 37 (2009) 18–22, https://doi.org/10.1097/JES.0b013e318190ebdb.

[32] J.S. Otis, S. Niccoli, N. Hawdon, J.L. Sarvas, M.A. Frye, A.J. Chicco, S.J. Lees, Pro-inflammatory mediation of myoblast proliferation, PLoS One 9 (2014) e92363, https://doi.org/10.1371/journal.pone.0092363.

[33] M. Cantini, E. Giurisato, C. Radu, S. Tiozzo, F. Pampinella, D. Senigaglia, G. Zaniolo, F. Mazzoleni, L. Vitiello, Macrophage-secreted myogenic factors: a promising tool for greatly enhancing the proliferative capacity of myoblasts in vitro and in vivo, Neurol. Sci. 23 (2002) 189–194, https://doi.org/10.1007/s100720200060.

[34] P. Clark, G.A. Dunn, A. Knibbs, M. Peckham, Alignment of myoblasts on ultrafine gratings inhibits fusion in vitro, Int. J. Biochem. Cell Biol. 34 (2002) 816–825, https://doi.org/10.1016/S1357-2725(01)00180-7.

[35] M. Fortier, F. Comunale, J. Kucharczak, A. Blangy, S. Charrasse, C. Gauthier-Rouviere, RhoE controls myoblast alignment prior fusion through RhoA and ROCK, Cell Death Differ. 15 (2008) 1221–1231, https://doi.org/10.1038/cdd.2008.34.

[36] N.T. Swailes, M. Colegrave, P.J. Knight, M. Peckham, Non-muscle myosins 2A and 2B drive changes in cell morphology that occur as myoblasts align and fuse, J. Cell Sci. 119 (2006) 3561–3570, https://doi.org/10.1242/jcs.03096.

[37] J. Baum, H.S. Duffy, Fibroblasts and myofibroblasts: what are we talking about? J. Cardiovasc. Pharm. 57 (2011) 376–379, https://doi.org/10.1097/FJC.0b013e3182116e39.

[38] I.A. Darby, B. Laverdet, F. Bonte, A. Desmouliere, Fibroblasts and myofibroblasts in wound healing, Clin. Cosmet. Investig. Dermatol. 7 (2014) 301–311, https://doi.org/10.2147/CCID.S50046.

[39] J.M. Lemons, X.J. Feng, B.D. Bennett, A. Legesse-Miller, E.L. Johnson, I. Raitman, E.A. Pollina, H.A. Rabitz, J.D. Rabinowitz, H.A. Coller, Quiescent fibroblasts exhibit high metabolic activity, PLoS Biol. 8 (2010) e1000514, https://doi.org/10.1371/journal.pbio.1000514.

[40] E.W. Howard, B.J. Crider, D.L. Updike, E.C. Bullen, E.E. Parks, C.J. Haaksma, D.M. Sherry, J.J. Tomasek, MMP-2 expression by fibroblasts is suppressed by the

myofibroblast phenotype, Exp. Cell Res. 318 (2012) 1542–1553, https://doi.org/10.1016/j.yexcr.2012.03.007.
[41] M. Hicks, T. Cao, P. Standley, NHDF fibroblasts enhance C2C12 skeletal muscle myoblast differentiation: requirement for interleukin-6 (IL6), FASEB J. 25 (2011), https://doi.org/10.1096/fasebj.25.1_supplement.1113.3.
[42] Y. Zhang, H. Li, Z. Lian, N. Li, Normal fibroblasts promote myodifferentiation of myoblasts from sex-linked dwarf chicken via up-regulation of β1 integrin, Cell Biol. Int. 34 (2010) 1119–1127, https://doi.org/10.1042/CBI20090351.
[43] N. Rao, S. Evans, D. Stewart, K.H. Spencer, F. Sheikh, E.E. Hui, K.L. Christman, Fibroblasts influence muscle progenitor differentiation and alignment in contact independent and dependent manners in organized co-culture devices, Biomed. Microdevices 15 (2013) 161–169, https://doi.org/10.1007/s10544-012-9709-9.